UiT The Arctic University of Norway

Department of Arctic and Marine Biology

Thermal properties of arctic fox fur and the effect of fur lice infestation.

Anna Galina Henriksson

Master's thesis in Biology BIO-3950, November 2023

Faculty of Biosciences, Fisheries and Economics

Department of Arctic and Marine Biology

Thermal properties of arctic fox fur and the effect of fur lice infestation.

Anna Galina Henriksson

Master's thesis in BIO-3950,

Arctic chronobiology and physiology

November 2023

Supervisors

Main supervisor: Professor Lars Folkow, UiT – The Arctic University of Norway

Co-supervisor: Dr. Rebecca Davidson, Norwegian Veterinary Institute

Co-supervisor: Dr. Eva Fuglei, Norwegian Polar Institute

Cover photo: Anna Galina Henriksson

Photograph of an arctic fox on Svalbard

Acknowledgements

I extend my sincere gratitude to my supervisors, Lars Folkow, Eva Fuglei, and Rebecca Davidson, for their unwavering guidance, both in the laboratory and during fieldwork. Their dedicated efforts significantly contributed to the success of this project.

Special thanks are due to UiT's BFE technical and maritime services engineers Hans Dybvik and Reidar Kaase. Their commitment and invaluable assistance in constructing the thermal camera field setup were indispensable. I am deeply appreciative of everything they taught me, and this project would not have been possible without their support.

I would also like to acknowledge the crucial contribution of Presisjons Teknikk AS and Henrik Swärd, who generously lent me the thermal camera. Their support was essential for the successful execution of the pilot study.

Ass. Professor Hassan Khawaja from the Faculty of Engineering Science and Technology, UiT, deserves my thanks for lending me the FLIR camera and providing valuable advice on technical aspects. Our insightful discussions greatly enriched my understanding of this field of technology.

Heartfelt appreciation goes to Stein Tore Pedersen and Martine Nyhagen from the Norwegian Polar Institute. Their practical assistance and guidance were indispensable during the fieldwork on Svalbard, and I am very grateful for the time we spent there doing fieldwork. I am also grateful to Taxidermist Thor Inge Knudsen for skinning the arctic foxes and providing valuable advice on pelt treatment. Additionally, I extend my thanks to the Norwegian Research Council for the Arctic Field Grant that funded the Svalbard fieldwork.

Sara, Sari, and Sigrid deserve my gratitude for sharing in the ups and downs of thesis writing.

Thank you Freke and Karianne Sand (Freke's human) for the help with testing the IR camera.

Also, warm thanks to Fjällräven for all the insulation.

Finally, my deepest gratitude goes to my partner, Duncan Butler, for your unwavering support and encouragement throughout this thesis. I look forward to repaying the kindness with countless dinners and cups of tea as you embark on your future studies.

Abstract

In 2019, a new species of sucking louse was observed in arctic foxes (*Vulpes lagopus*) on Svalbard and Northern Canada. Abnormal patterns of fur loss, inconsistent with normal moult, were observed across the neck, shoulders and back, raising concerns as to how the animals would cope with damaged fur during the cold Arctic winter. This study investigates the impact of these lice on Svalbard arctic foxes, focussing on louse prevalence, fur condition and thermal properties. A total of 23 fur samples from 17 arctic foxes were used to estimate louse prevalence, abundance and fur damage compared to thermal properties. Louse density was determined by dissolving skin biopsies and counting lice visually. The thermal properties were determined by establishing a steady heat flow through a system of a standard conductor and a fur sample and measuring the temperature at each interface.

The prevalence was lower (44%) compared to the prevalence estimated (70%) from the previous trapping season (2021-2022). Conductivity values ranged from 0.0304 – 0.0869 W/m°C and conductance from 0.974 to 2.94 W/m^2°C. These values broadly agree with previous studies.

No linear relationship was found between louse density and fur state, suggesting an underlying louse population dynamic. While no linear correlation was found between louse density and thermal conductivity of the fur or fur damage and conductivity, a significant ($p < 0.05$) relationship was found between louse density, fur damage and thermal conductance, implying that infested arctic foxes, as hypothesised, experience excess heat loss compared to non-infested foxes, and that this heat loss is due to a loss of fur rather than a change in the internal structure of the coat.

A pilot study tested the potential use of thermal imaging in the detection and monitoring of fur loss and lice infestation in wild arctic foxes. The initial results showed promise, but the system requires further refinement before large scale field trials. An image of an arctic fox was captured with evidence of fur loss.

Table of Contents

List of tables

List of figures

1 Introduction

1.1 The arctic fox: introduction and overview

The arctic fox (*Vulpes lagopus)* is a small canid endemic to the Arctic, exhibiting a circumpolar distribution. They exhibit genetically fixed colour morphs (white and blue, the blue being brown or charcoal coloured all year round) and are the only canid that changes colour during the winter (Audet, Robbins & Larivière, 2002). They exclusively occupy the tundra biome, spanning a diverse range of habitats including arctic coastlines, alpine inlands tundra and vegetated shrubby landscapes (Berteaux et al., 2017).

The arctic fox displays remarkable adaptability and may be found across a vast geographical expanse in all kinds of tundra habitats such as the arctic tundra of Eurasia and North America, the sub-arctic mountain tundra of Fennoscandia and on the larger arctic and subarctic islands of Greenland, Iceland, and Svalbard as well as arctic archipelagos of Siberia, Canada and the Bering strait (Angerbjörn & Tannerfeldt, 2014; Fuglei & Ims, 2008). In particular, Svalbard harbours the population on which this study focusses on.

Arctic foxes exhibit exceptional mobility, extending their range beyond the confines of terrestrial lands and their typical southern range. Arctic foxes have been observed venturing as far as the North pole, they were observed travelling across the sea ice distribution. Historical records by the early arctic explorer Fridtjof Nansen in 1897 reported observations of arctic foxes venturing across the sea ice far from land (Nansen, 1897). Further, they have been observed as far south as the boreal forest belt (Audet, Robbins & Larivière, 2002; Macpherson, 1969). Their broad range of geographical areas illustrates their ability to live across a very board range of habitats.

1.1.1 Ecological adaptations and resource utilization

The arctic fox is considered an opportunistic scavenger and predator, effective in utilizing any food source available (Prestrud, 1991). Two ecotypes, the “lemming” and the “coastal”, have previously been described by Braestrup (1941).

The lemming ecotype is the most widespread, mainly found in the tundra biome, it feeds primarily on lemmings (*Lemmus* spp. and *Dicrostonyx* spp.) but also prey on voles, hares and

even reindeer (Elmhagen et al., 2000). The lemming ecotype is heavily dependent on the lemming population density which fluctuations cycles every 3-5 years (Macpherson, 1969; Stenseth & Ims, 1993).

The coastal ecotype is not as widespread and is found mainly on arctic and sub-arctic islands such as Greenland, Iceland, and Svalbard, where lemmings don't exist. Their prey mostly originates from the marine environment and consists of sea birds and marine mammals, fish, and carcasses at hand. The terrestrial portion of prey on Svalbard is mainly carcasses of Svalbard reindeer (*Rangifer tarandus platyrhynchus*) and their calves, as well as Svalbard rock ptarmigans (*Lagopus muta hyperborea*) and pink-footed geese (*Anser brachyrhynchus*)(Nater et al., 2021). The availability of food has been shown to influence the reproduction in arctic foxes and the litter sizes. The coastal ecotypes are known to breed most years with relatively small litters, linked to the relatively stable and predictable food supply from the marine environment (Angerbjörn, Hersteinsson & Tannerfeldt, 2004; Eide et al., 2012). Meanwhile the lemming biome arctic foxes exhibit a more cyclic demographic, following the lemming population fluctuations, characterized by very large litters when lemming density is high, and few close to none when density is low (Macpherson, 1969; Tannerfeldt & Angerbjörn, 1996).

1.1.2 Arctic fox trapping: historical and contemporary practises on Svalbard

The arctic fox has captured the fascination of people throughout history, owing to its alluring beauty and in particular its prized pelt - an item which many trappers have committed long winters to gathering, in exchange for handsome profits. A century ago, the demand for pelts accommodated trapping on a larger scale, however in the past few decades hunting has seen a decline. On Svalbard, trapping has been carried out for centuries and has a deep-rooted cultural significance in the region (Fuglei, Meldrum & Ehrich, 2013). Historically, the common practice by trappers was to overwinter in isolated cabins so as to time their efforts to harvest arctic foxes with the superior fur quality exhibited during the cold winter months (Arlov, 2003). By the time of the Second World War, trapping of arctic foxes on Svalbard had already declined. New regulations were introduced in 1997 for animal harvesting on Svalbard, which included reporting obligations and further reductions in bag size. Additionally, trapping was limited to residents only from that point onwards (The Governor of Svalbard, 2022). Today, a few dedicated trappers

continue to overwinter in isolated huts. A large proportion of the trapping occurs in the areas of Nordenskiöld Land and Isfjorden. Here, however the majority are recreational hunters and do not make a living from trapping. The annual catch of arctic foxes may vary between 40 and 300 animals per season, but no clear long-term trend in trapping has been observed. The trapping practice is closely monitored by the Governor of Svalbard (Sysselmesteren) to whom the reporting of hunting became mandatory in 1997. All trapping on Svalbard is subject to the Svalbard Environmental Protection act, which seeks to preserve the environment on Svalbard by regulating the harvest to preserve the size and demographic structure of the population (The Governor of Svalbard, 2022). These reports have provided the Norwegian Polar Institute with valuable samples and data on arctic foxes, which are used continuously in ongoing research monitoring and research, including in this study.

The arctic fox's adaptions to the extreme Arctic environment have also been extensively focused on in research as they serve as a perfect case study of extreme animal physiology, as well as playing a vital role in arctic ecosystems (Berteaux et al., 2017; Macpherson, 1969).

1.2 Thermoregulation and adaptations of arctic animals: a comprehensive overview

The arctic region harbours large populations of mammals and birds. It is one of the most punishing environments on Earth characterized by very cold temperatures, prolonged periods of darkness, large amounts of snowfall, and strong winds. Resident non-migrating homeothermic animals must therefore deal with low temperatures and for long periods of time, upholding a temperature gradient as high as 80-90°C between the body core and the external environment (Scholander et al., 1950c; Underwood, 1971). To successfully maintain a stable and constant body temperature in cold environments a homeothermic organism needs to manage a balance between the heat produced and that dissipating from the body. There are three main ways that animals can lose heat: by conduction/convection, by evaporation, and by radiation (Blix, 2005). Heat loss through conduction is mainly determined by the temperature gradient between the animal's body and its environment, as well as the surface area over which heat may be exchanged. Convection can affect conductive heat loss and may substantially increase it if wind is present and causes warm air built up within the fur to be stirred/mixed. Animals can also lose

heat to the environment through evaporative heat loss via breathing, which is a process that involves the evaporation of water from the respiratory system. Additionally, animals can lose (and gain) heat via infrared radiation. The rate of this radiative heat loss of an object can be considered proportional to the temperature difference between the object and the environment, if this difference is sufficiently small; otherwise, it is described by a modified form of the Stefan-Boltzmann Law, which states that the rate of heat loss is proportional to the fourth power of the absolute temperature (Blix, 2005).

Scholander et al. (1950a) highlight three main avenues by which an arctic animal can adapt to the low temperatures of the arctic: by a change in metabolism (increasing heat production to match heat loss), by reducing the thermal conductance of insulation, and by reducing the temperature difference between the body and the environment.

One important factor when considering thermal biology is the thermal neutral zone (TNZ) of an animal, it refers to the range of temperatures at which the metabolic rate is unchanged. The lower critical temperature (T_{lc}) is, the lower edge of the TNZ and is the temperature at which an animal needs to increase its metabolic rate to produce more heat and maintain a stable internal temperature (Hill, Wyse & Anderson, 2016). The rate of metabolic increase and T_{lc} vary a lot between animals and T_{lc} is an indicator of total body insulation. When compared to animals from lower latitudes, arctic animals have a lower T_{lc} and a slower metabolic rate increase (Scholander et al., 1950a). Several studies have attempted to determine the T_{lc} in arctic foxes, Scholander et al. (1950b) suggested T_{lc} to be below -40°C and Underwood (1971) concluded the T_{lc} to be lower than -35°C. Meanwhile, a more recent study by (Fuglesteg et al., 2006) calculated the T_{lc} to be -7°C. This shows that there are large discrepancies with regard to calculated T_{lc} values for arctic foxes, most likely attributed to very different experimental designs and handling of animals.

What is certain, however, is that given the harsh conditions of the arctic environments, the arctic fox has evolved a variety of adaptation to maintain a heat balance and to conserve energy to survive in the cold.

The next sections will summarize the behavioural, physiological, and morphological adaptations arctic foxes have evolved and developed to earn the title of one of the smallest mammals living in the arctic environment.

1.2.1 Behavioural adaptations

Many animals, including the arctic fox, respond to cold temperature with behavioural traits in order to reduce heat loss (Blix, 2005). Arctic foxes are known to curl up into a ball when exposed to extreme cold and windy conditions. This position involves drawing their front and back legs in towards the trunk and tucking in their head, using the fluffy tale as a mattress and placing the nose by the root of the tail, resembling the shape of a sphere (Follmann, 1978). By curling up, the arctic fox reduces its surface-to-volume ratio and exposes the thickest part of its fur coat, particularly the fur on the dorsal neck and anterior trunk, to the environment, while also hiding areas of the body with less thick insulation (Underwood, 1971). Despite the heat production remaining the same, the curled-up position can create a temperature gradient of up to 52.5°C between the inside of the arctic fox curl and the external environment, making it an effective way to reduce heat loss (Follmann, 1978).

Another behavioural response exhibited by arctic foxes is seeking shelter in snow lairs or dens, which helps to avoid wind and cold temperatures and reduces both conductive and radiative heat loss. This is because the temperature gradient between the arctic fox and the environment is reduced – by taking shelter in a comparatively warm environment. However, there is limited knowledge about how often and to what extent arctic foxes use this strategy (Blix, 2005; Prestrud, 1991).

1.2.2 Physiological adaptations

1.2.2.1 Counter current vascular heat exchange & vasomotor control

While the legs of the arctic fox are not as well insulated as other parts of the body (see section 1.2.3.1), the fox has adapted to combat heat loss from these extremities through a counter-current heat exchange system in the legs (Irving & Krog, 1955). This system reduces heat loss through a special morphological arrangement of blood vessels, allowing warm arterial blood to pass in close proximity to venous blood vessels, transferring heat from warm to cold blood while

traveling in opposite directions. As a result, warm blood is carried back to the core while the paw may reach temperatures close to ambient without losing much heat on the way (Henshaw, Underwood & Casey, 1972; Hill, Wyse & Anderson, 2016).

Arctic foxes have another specialized vascular system to help regulate their body temperature in response to the cold. Blood flow to the skin may also be regulated through vasomotor control, which decreases blood flow to the skin and reduces heat loss. Conversely, vasodilation can assist in heat dissipation when overheating. Its an important adaptation allowing the arctic fox to regulate its body temperature in response to changes in the environment.

1.2.2.2 Regulation of moult and moulting patterns

The timing of the moult is controlled by physiological mechanisms entrained by the diurnal photoperiod as the main external cue. This allows the animal to initiate its moult at a time optimal to match the condition of the environment (Zimova et al., 2018). However, climate change poses some problems to this process as milder winters and less snow create a desynchrony between the moult and the environment. A recent study by Laporte-Devylder et al. (2023) shows that arctic foxes are capable of modulating the timing of their moult in response to snow cover and temperature variations, demonstrating their plasticity in adapting to changing environmental conditions.

Arctic foxes have adapted to the seasonal variations in their environment, which range from freezing, snow-covered winters to milder, snowless summers. One of the ways in which they have adapted is by moulting seasonally and being dichromatic. This process is vital for maintaining a thermal balance and staying camouflaged year-round. During the winter, the fox's fur changes to a thick, white coat that provides insulation and camouflage in snowy environments. In the summer, the fur changes to a brown-grey coloration that blends in with the tundra landscape (although it is important to note that arctic foxes appear in two distinct colour morphs: the white morph, as described, and a ”blue” morph that remains dark-coloured in both summer and winter). These adaptations allow the fox to survive and thrive in the harsh arctic environment (Laporte-Devylder et al., 2023). The moult in arctic foxes typically progresses in a predictable, if patchy, manner, with shedding starting gently around the eyes and face, over the

dorsal-lumbar region, and then progressing to the flanks and legs in large patches. The tail is usually the last part to change (Laporte‐Devylder et al., 2023; Zimova et al., 2018).

A more detailed explanation of winter fur and its thermal properties is included in morphological adaptations in section 1.2.3.

1.2.3 Morphological adaptations

The praised and appreciated features of the arctic fox are actually morphological adaptations to the arctic environment. As a relatively small canid of the arctic, the arctic fox has a large surface-to-volume ratio, which means it is subject to a relatively large rate of heat loss. This characteristic is considered disadvantageous from a thermoregulatory point of view (Berteaux et al., 2017; Blix, 2005). However, the arctic fox has developed several adaptations to reduce its surface area and aid heat retention, including small round ears, a short snout, proportionally shorter legs, and a rounded body shape (Macpherson, 1969). One of the most important morphological adaptations of the arctic fox is the fur, which provides the main defence against the cold (Irving & Krog, 1955). In the next section, the characteristics of arctic fox fur will be described in more detail, including its thickness, composition, and its insulative properties.

1.2.3.1 Fur thickness and composition

The fur of the Arctic fox exhibits significant seasonal variation, with winter fur being nearly twice as long as summer fur. The majority of the fur (70%) consists of a fine undercoat, with the rest made up of longer, protective guard hairs. Overall, the fur provides excellent insulation (Hersteinsson & Macdonald, 1992; Underwood, 1971). Site-specific differences in fur depth between seasons have been observed, with areas that are more readily exposed to the cold and snow in a resting position (such as that described in section 1.2.1) exhibiting a larger increase in fur depth from summer to winter than areas less exposed to the cold, such as the distal areas of the legs and the face. Of particular note are the pads of the feet, which exhibit a 210% increase in fur depth from summer to winter. (Underwood, 1971; Underwood & Reynolds, 1980).

The thermal properties of both winter and summer arctic fox fur have been studied in detail, demonstrating its excellent protection against the cold. Scholander et al. (1950c) conducted a study in which the fur insulation (a measure of a material ability to resists the flow of heat) of various animals of different sizes were measured alongside the thickness of the fur. This study found a linear relationship between fur depth and insulative effect, up to the fur depth of the arctic fox which had the highest measured insulation (see Figure 1). Larger animals' fur depth would thereafter continue increase, however the insulative properties were like if not lower than that of the arctic fox.

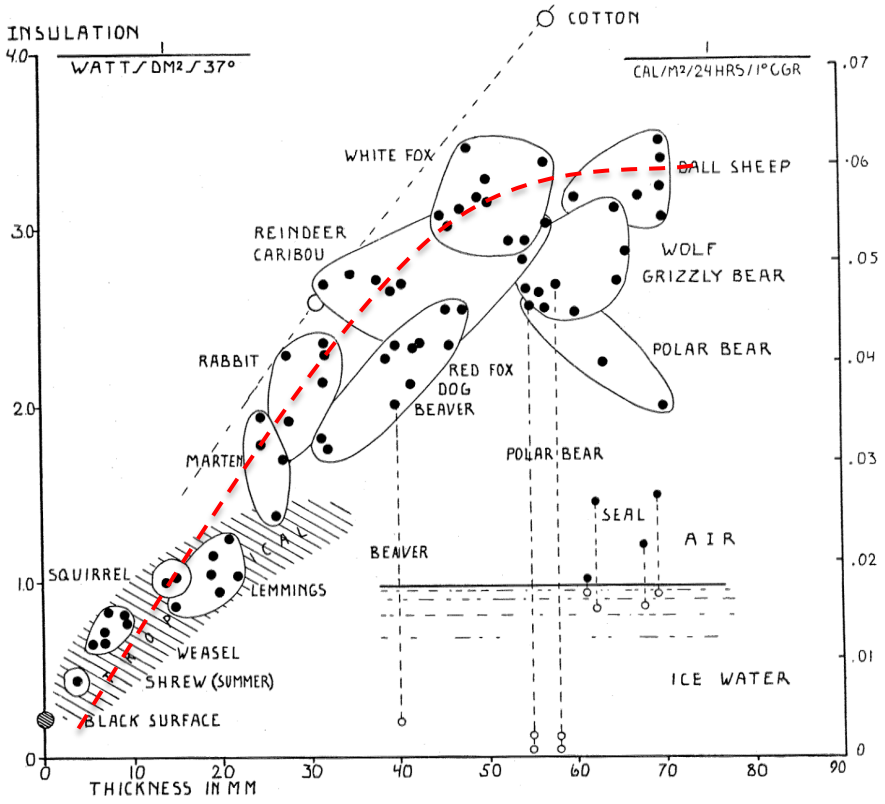

Figure 1 Scholander's plot of insulation in relation to winter fur thickness in arctic animals. The red line indicates the linear relationship between insulation and fur depth up until the arctic foxes, after which an increase in fur depth does not correspond to an increase in insulation. Figure from Scholander et al. (1950c) but with modification.

Several previous studies have determined the insulative properties of the arctic fox's fur, with conductivity and conductance being common measures used to describe it. These measures refer to the fur's ability to conduct heat. They are closely related and often confused, but there is an important distinction.

Thermal conductivity (K) is an inherent property of a material, that describes how well the material conducts heat.It is commonly expressed in W/m°C (or W/m K). It is a property of the material itself, and is independent of size, shape, or thickness.

Thermal conductance (C), on the other hand, is the result of thermal conductivity combined with the thickness of the material. It is expressed in units of W/°C (or W/K), or can be defined over some area, giving it the units of W/°Cm^2. It is the latter definition that is commonly used when considering animal furs, and this is the definition used in this study. Conductance is a measure of the heat flow through an object, rather than a material, and is dependent on thickness. (Kvadsheim, Folkow & Blix, 1994).

The distinction between thermal conductivity and thermal conductance can be illustrated using a wool blanket analogy: The conductivity of the blanket is simply the conductivity of wool, while the conductance would be determined by the thickness of the blanket and the conductivity combined. If the blanket was twice as thick, its conductance would halve, but its conductivity would not change, as the material, wool, has not changed.

Results from previous studies have produced different values for the thermal conductivity of arctic fox fur. Scholander et al. (1950a) calculated the thermal conductivity to be between 0.038-0.051 W/m°C, while Fuglesteg et al. (2006) calculated somewhat higher values between 0.059-0.080 W/m°C. The latter study compared the conductivity of winter fur to summer fur and found no difference, but the average thermal conductance of winter fur was reported to be 1.24 W/m2°C, while summer fur had more than double the conductance of winter fur. These discrepancies in conductivity between studies may be due to differences in experimental design and methodology.

1.3 Parasites in the Arctic: the fur lice

In 2019, in both Svalbard, Norway and Nunavut, Canada separately, abnormal patterns of seasonal fur loss were noted on arctic foxes (Buhler et al., 2021). The fur loss was seen to deviate significantly from the normally very predictable seasonal shedding pattern which occurs as part of springtime moulting (as described in 1.2.2.2). Following closer examination, it was discovered that foxes with abnormal fur loss patterns were infected by lice (Buhler et al., 2021). Buhler et al. (2023) compared lice from arctic foxes on Svalbard and Nunavut and concluded that they were morphologically and genetically identical to one another.

Fur lice are an example of ectoparasite (*ecto* from Ancient Greek ektós, "outside" + parasite), a taxonomically diverse group of organisms of which the majority are invertebrate and belong to the phylum *Arthropoda*. These parasites live and feed externally on a host by embedding themselves to superficial layers of the skin (Durden, 2019; Hopla, Durden & Keirans, 1994).

The two most common groups of lice to cause pediculosis (infestation in fur/hair) in canines are mallophagan (chewing lice) and anopluran (sucking lice) (Durden, 2019; Hanssen et al., 1999). Mallophaga feed on skin debris and sebaceous secretion. Anoplura have highly modified mouth parts specialized to pierce skin to access the hosts blood and tissue fluids (Wall & Shearer, 2001). The lice observed in the arctic foxes, and studied in this thesis, are an example of anoplura (Buhler et al., 2023).

It was initially suggested that the lice observed in the arctic foxes could be *Linognathus setosus*, (*L.setosus)* a common species of sucking louse found on canines, because they were observed to be morphologically similar (Buhler et al., 2021). Despite the morphological similarity to *L.setosus*, the newly discovered lice proved to be genetically different, from *L.setosus* in domestic canines, with less than 90% genetic similarity, suggesting them to be an undescribed species (Buhler et al., 2023).

As well as a morphological similarity, the newly observed lice also exhibit behavioural similarities with *L. setosus*, and similar host symptoms are seen. An *L.setosus* infestation, in domestic dogs, typically exhibits clear predilection sites, namely the ears, head, neck and back

(Gunnarsson, Christensson & Palmér, 2005). Signs of infestation often include pruritus (itchiness), with heavy scratching, excoriations and self-wounding damaging the skin which can lead to alopecia (Englar, 2019). Arctic foxes infested with the newly observed lice have been noted to exhibit similar symptoms, and the lice seem to share the same predilection sites (Buhler et al., 2023; Gunnarsson, Christensson & Palmér, 2005).

As a potentially new species, little else is known of the new lice. Considering their similarities to *L.setosus,* however, some information on this species is included here.

L.setosus is highly species specific in nature. It exclusively infests canids such as domestic dogs (Saari, Näreaho & Nikander, 2018). The entire lifecycle takes place within the fur of the host and if separated from the host a louse may only survive for a few days. In cold climates this period is even shorter (Saari, Näreaho & Nikander, 2018; Wall & Shearer, 2001) *L. setosus* is more common in Northern and colder regions, as the climate is less hospitable to competing fleas and ticks (Hanssen et al., 1999; Kohler-Aanesen et al., 2017). The lice are typically transmitted by direct contact between host individuals (Durden, 2019; Saari, Näreaho & Nikander, 2018)

The life cycle of *L.setosus* consists of 3 stages: eggs, nymphs, and adults, and these three stages are also observed in the newly observed lice. In *L. Setosus,* eggs are cemented to the shaft of the fur with a glue-like substance secreted by the adult female. The eggs hatch within 10-15 days of laying. The nymphs, which resemble the adults, but are smaller, moult several times in the two weeks following hatching, before becoming adults. The length of time from egg to adult is 20-40 days (Saari, Näreaho & Nikander, 2018; Wall & Shearer, 2001).

1.4 Infrared thermography

1.4.1 Theory

All objects with a temperature emit electromagnetic radiation across a spectrum of wavelengths. This emission has a very predictable peak wavelength that varies with temperature. Measuring the wavelength of the peak thermal emission therefore provides a reliable metric by which to measure an object's temperature. For biological systems, this temperature is comparatively low,

and the peak emission is therefore typically found in the longwave infrared (LWIR) section of the spectrum (Tattersall, 2016).

This process assumes a thermal emission close to that of a black body – a theoretical ideal emitter. In reality, objects do not emit as black bodies, and their similarity to a black body is measured by their *emissivity*. This is defined as the ratio of an objects thermal emitted power to that of a black body at the same temperature and is used to scale the temperature measured by thermography. In biological systems, this is taken to be between 0.95- 0.98 – i.e., close to black body emission(Best & Fowler, 1981; Hammel, 1956). Estimated emissivity for fur and feather is 0.96 (Tattersall, 2016).

1.4.2 Application of infrared thermography

Infrared thermal camera (IRT) technology is an increasingly commonly used tool in animal biology such as in wildlife sciences as well as in veterinary diagnostics fields. It has it use in many applications, to study insulation in endotherms, to study anatomical, physiological and behavioural adaptations to hot and bold environments in both captive and wild animals and to estimate metabolic heat loss (McCafferty et al., 2011; McCafferty et al., 2021; Szafrańska et al., 2020). In addition it has long been a tool in veterinary medicine as well as animal husbandry as well to detect and map out local inflammation(Avni-Magen et al., 2017), detect infections of diseases (Dunbar & MacCarthy, 2006), and detect and study ectoparasites parasites in animals (Arenas et al., 2002; Cortivo et al., 2016).

A previous study by Cross et al. (2016) combined the two fields of physiology and veterinary science when studying energetic costs and of sarcoptic mange (*Sarcoptes scabies*) that has induced hair loss in wild wolves through the use in infrared technology. Sarcoptic mange is not an uncommon infestation in animals and has a near global distribution with a wide range of hosts (Escobar et al., 2022), one of which includes arctic foxes. Though to date sarcoptic mange has not been detected on Svalbard, there are cases of outbreaks in mainland Norway occasionally causing substantial fur loss (Miljødirektoratet, 2022). While external parasites on wild animals have been studied using infrared thermography, none have been made on arctic foxes using IRT in relation to fur loss caused by an ectoparasite, such as the fur lice.

1.5 Significance, research questions and hypotheses

The Arctic fox holds a position of significance in both scientific research and the cultural history of Svalbard, as laid out in section 1.1.2. As an apex predator on Svalbard, it plays a vital role in shaping local ecosystems(Fuglei & Ims, 2008).

Historically, and as discussed in section 1.1.2, trapping of arctic foxes has been a central activity conducted by many on Svalbard, and to date, it holds a deep-rooted cultural significance in the region. The Norwegian Polar institute has closely monitored the arctic fox population since 1997 by recording breeding activity in dens, and Nater et al. (2021) have concluded that the population vary between years, but is stable and are balanced by a climate related increase in terrestrial food items and a reduction in marine recourses. Trapping had a negative effect on the population due to an increase in number of trapping areas and number of traps per area around 2008-2009, but after a reduction in the number of areas and traps, this effect disappeared. However, how the newly discovered lice may influence this stability is unknown.

The effects of a fur lice infestation on an arctic fox's general health or on its ability to stay warm in the cold and harsh climate they inhabit are not well known, and comprehensive studies on the prevalence of infested arctic foxes, the level of those infestations, and the effect of an infestation of the thermal properties of a fox's fur are needed.

Addressing the knowledge gap concerning this newly discovered issue affecting the arctic foxes is essential for future research and effective management of the arctic fox population on Svalbard.

The overall aim of this master's thesis is to investigate the potential effects of lice on arctic foxes. This is achieved through three research questions and one pilot study.

Research question 1: What is the prevalence of lice infestation in the Svalbard arctic fox population and what is the abundance of lice in the pelts of infested arctic foxes?

Based on information of prevalence of lice from previous trapping seasons, I hypothesised that lice prevalence would be high, and that infested foxes would show a range of lice abundancies.

Research question 2: Does lice abundance in the pelt correlate to the condition of the fur?

I hypothesised that greater lice infestation on arctic fox pelts would correlate with worse fur condition (higher damage score).

Research question 3: How do observed fur damages and lice infestation affect the insulative properties of the fur?

It was hypothesised that fur lice infestation would cause fur damage which would lead to a reduction in the insulative properties, primarily by altering fur physical structure and thereby increasing thermal conductivity and/or conductance.

Research question 4: A pilot study to assess the feasibility of using thermal cameras in natural settings to identify heat loss in wild free living arctic foxes potentially infested by lice.

I hypothesised that abnormal fur loss in arctic foxes would exhibit higher heat loss, which would be identified as areas of higher temperature in the thermal images, as compared to a healthy fox of the same moulting stage.

The method, results and discussion for the pilot study are detailed in the appendix, section 5.1.

2 Methods

This section compromises the following parts: Firstly, the methods for the collection and examination of arctic foxes caught during the 2022-2023 trapping season is described, this includes the inspection of fur to identify pelts to be included in the study and the collection of demographics and biometric data, including lice density and a fur damage score. Following this, the procedures of how the thermal properties of the pelts were investigated are outlined.

2.1 Research animals

The arctic foxes used for this study originate from the wild population on Svalbard, mainly from the areas of Nordenskiöld Land and Isfjorden (77-79° N, 13-18° E). Arctic foxes are trapped on an annual basis in the period November 1st to March 15th. This trapping is an activity only permitted to the permanent residents of Svalbard. In the trapping season of 2019-2020, 10% of the 116 arctic foxes trapped were found to be infested with lice. In the following season of 2020-2021, 12.5% of the arctic foxes trapped (n=24) were infested. The trapping season of 2021-2022 was saw a substantial increase in lice prevalence to more than 70% of trapped foxes infested. As a result, all furs infected with lice were collected for research on this issue (and the trappers compensated), as opposed to previous years when the infested furs were returned to the trappers. Trappers with permits were distributed cross 25 hunting areas where arctic foxes may be trapped during the annual trapping season. Twenty-three of these are located on Nordenskiöld land (**Figure 2**) and two south of Ny-Ålesund.

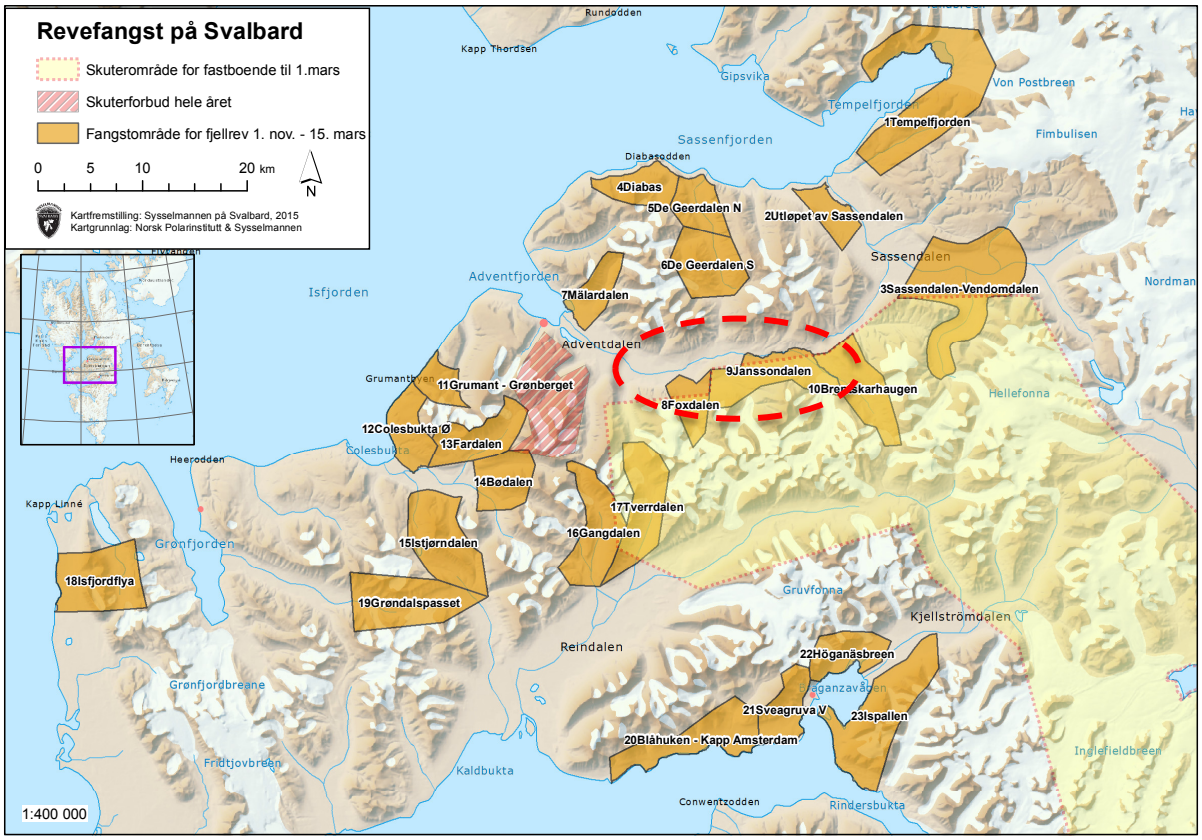

Figure 2 Overview map of the trapping areas on Nordenskiøldland, produced by the Governor of Svalbard. The orange shading illustrates the 23 areas in which trapping is allowed between the 1st of November to the 15th of March. Dashed red circle show the study area of the infrared camera pilot study (section 2.6)

Throughout the trapping season of 2022-2023 all trapped arctic foxes were delivered to the Norwegian Polar Institute headquarters (routine following the guidelines provided by the Governor of Svalbard (2023)). Once an arctic fox is delivered, prior to any handling of the animal, it is stored in a super-freezer with a temperature of -80°C for 7 days. This is done to eliminate the potential for infection with the zoonotic parasite *Echinococcus multilocularis*, thereby reducing the biohazard risk for those handling the fox carcasses. After this process, the carcasses were stored in a freezer at -20°C until the end of the trapping period.

The foxes were weighed using a spring gauge (Pesola Macro-Line spring scale, 5 kg capacity, 50g division; hung from the ceiling) and the sex and estimates of age recorded.

2.2 Fur inspection & selection

Before the fur inspection, fur selection and skinning commenced, the carcasses were removed from the freezer and thawed at room temperature (20°C) for approximately 48 hours.

The initial inspection of the fur was conducted before skinning. This was conducted by Rebecca Davidson, a veterinary parasitologist from the Norwegian Veterinary Institute, by visual examination under bright light conditions, without the use of magnification. This was done by the same person throughout to ensure homogeneity in the method and dataset. Starting at the eyes, a curved anatomical forceps was used to carefully part the fur and expose the skin along the length of the upper and lower eyelids. The same procedure was then repeated but on the rostral half of the upper lip on both sides and across the bridge of the nose. The examination then continued, using both fingers and anatomical forceps to part the hair, exposing the skin and hair roots (Figure 3). Starting at the top of the head, the examination continued between the ears and dorsally down the neck, shoulders, thorax, and pelvis to the base of the tail looking for any sign of lice (adult or juvenile individuals, eggs, and/or faeces) in the fur and on the skin.

Figure 3. Image of lice inspection in action on an arctic fox, parting the fur on the dorsal shoulder area using both curved anatomical forceps and fingers to expose the root of the fur and skin.

If no lice were observed, the examination was terminated, and the animal recorded as having no detected lice, the fox was skinned, and the skin returned to the trapper. One louse-free fur was kept as a control fur for the thermal investigations.

If lice were detected the examination was extended to include all four legs and the whole ventral side of the animal to map the distribution of lice across the whole body (although this data was recorded for use in another research project and was not used in this study). Observations and findings were recorded on paper accompanied by sketches depicting the extent of lice infestation and any other changes to the fur (colour change, density, length, hair loss etc.). Lice infection level was assessed as low (few individuals noted in a couple of locations); moderate (more than 2 adult individuals observed per field of view in more than 2 locations); high (several lice (>4) observed in each field of view at multiple locations), this arbitrary division was defined to ensure that the identification of lice infection level was coherent throughout the inspection. In some

instances, high fur density caused difficulties to see the skin, in these cases if dark/black dusting was present in the lower layers of the fur it was then examined more thoroughly to detect the presence of lice or louse eggs.

In total, 16 foxes were identified as having some level of lice infestation and were included in the study. Twenty foxes were found to be non-infested and were returned to the trappers, save one fox, from which two control pelts were taken (see section 2.2.1 for details on fur preparation).

Each animal's body measurements were taken using a flexible tape. The length was taken from the top of the nose to the base of the tale. The circumference of the neck, chest (by the deepest point) and abdomen (cranial to the hindlimb) were measured and recorded on the paper sheet.

Lastly, before an individual was handed over for skinning, it was photographed, regardless of the presence or absence of lice. Animals were photographed laying on the floor in right and left lateral positions, as well as from a dorsal viewpoint, along with a measuring ruler for scale, to document fur condition. A Sony a7iii mirrorless camera with a f/2.8 28-70mm Tamron lens mounted on a Manfrotto tripod (Manfrotto 502ah with fluid head) was used. Additional photographs of particular areas with fur changes were taken where necessary. Subsequently, a professional taxidermist skinned the animal.

All skinning of the animals was done by the professional taxidermist Thor Inge Knudsen from Agder Utstopping, Kristiansand, Norway.

The skinned carcasses were next evaluated to determine body condition. Visible subcutaneous fat was evaluated on a scale from 0 to 4 as described by Andersen et al. (2015) by visually inspecting the fat deposit on the body

Each skin with lice (as well as the control fur) was placed in a double plastic bag, to prevent cross-contamination with the other furs, and labelled with a plastic ID label before being sealed and placed in a Zarges box kept at -20°C freezer until transport to Tromsø. The box was transported by air flight to Tromsø and imported (Norwegian Food Safety Authority authorisation for the import of animal by-products for diagnostic, educational or research

purposes, licence number 202/23). The furs were then stored frozen (-20°C) at the Norwegian Veterinary Institute, awaiting further analysis.

2.2.1 Fur preparations.

In order to conduct the thermal tests, fur samples (hereafter referred to as pelts) were extracted from the fox furs. The furs were removed from the freezer and allowed to thaw overnight at room temperature (20°C) at the Norwegian Veterinary Institute in Tromsø. Prior to the extraction of the pelts, each fox fur was re-examined thoroughly by collaborating veterinarians from the Norwegian Veterinary Institute in Tromsø, Rebecca Davidson and Line Olsen. Plastic templates were made to standardise the size of the pelts and the cuts made around the edge of these templates. The fox pelt was placed fur side down on a clean table and square section measuring 0.215m by 0.215m was removed from the dorsal cervico-scapular region (hereafter referred to as front pelt) This measurement was dictated by the equipment used to measure the thermal properties, which requires a pelt of 0.2m by 0.2m. The fur was carefully cut using a scalpel along the edge of the plastic template. Whenever feasible, two samples were extracted from a single individual: one front pelt and a second pelt from the lower dorsal/lumbar region (hereafter referred to as back pelt), as illustrated in **Figure 4**. The choice of sampling two pelts from one individual was based on the size of the fox fur. Two pelts were extracted if the fur was big enough to extract two 0.215m by 0.215m squares.

Upon extraction, the fur samples were immediately placed in 2L plastic bread bags , each labelled with an identification tag. The bags were then transported to the freezer at the UiT animal facility and stored there in preparation for the conductivity experiments.

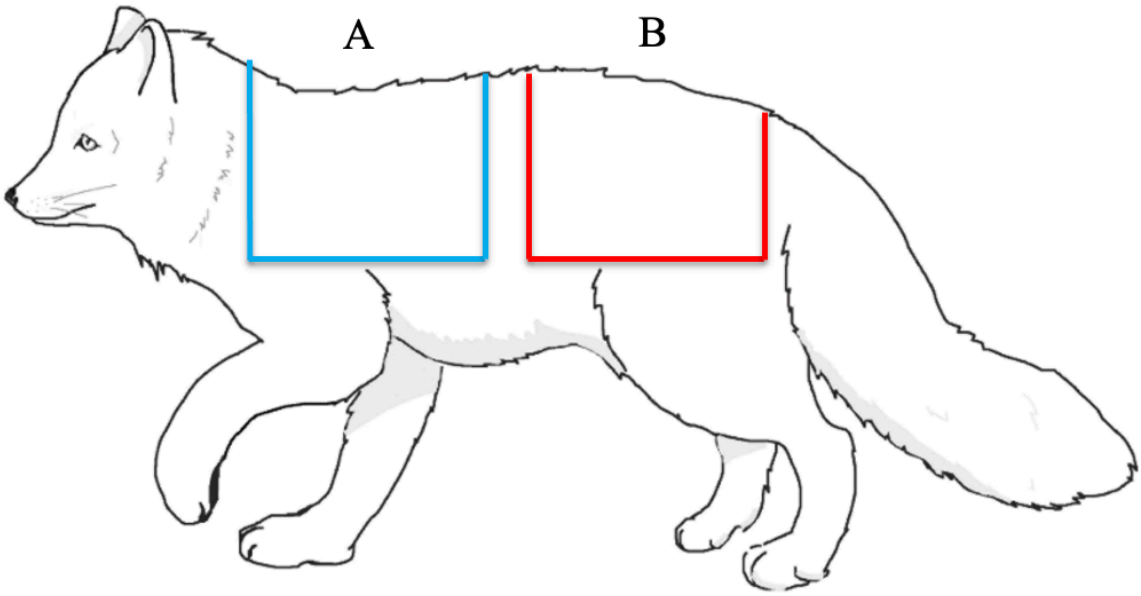

Figure 4. Illustration of extracted pelt positions, front (A) and back (B) pelts.

2.3 Louse density estimation

The detection and quantification of lice infestation in arctic foxes followed recommended procedures for the detection of skin parasites (arthropods). A common method to detect lice is based upon the close inspection of the hair (Deplazes et al., 2016).

After the measurements of thermal properties (section 2.5) a total of 4 skin biopsies (3 cm by 3 cm) were collected from the 20cm-by-20cm fur sample used in the conductivity measurements. Again, a plastic template was made to ensure uniformity of size when cutting the skin. The fur sample was conceptually divided into four quadrants (10cm by 10cm), and from each quadrant the biopsies were extracted from the innermost corner(**Figure 5**, making sure they were spatially proximate to the centre with 3-4cm from each other. The biopsies were cut out from the subcutaneous side using a scalpel blade.

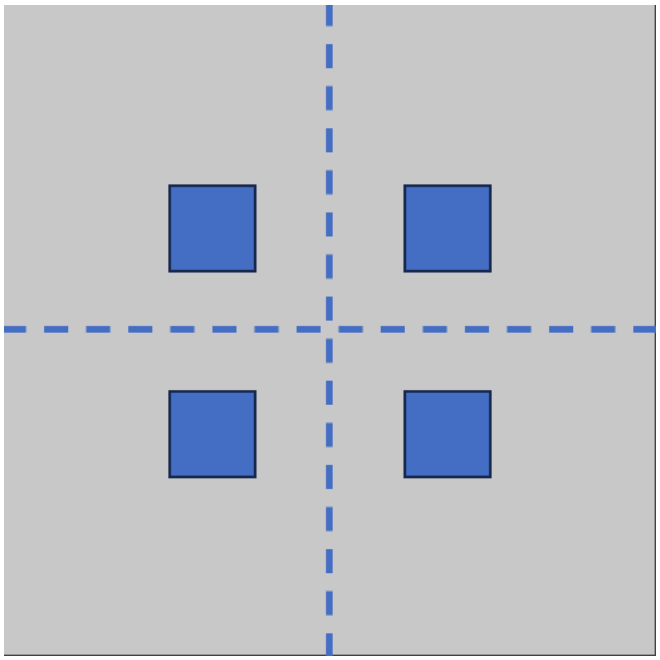

Figure 5 Illustration of biopsies extraction sites. The pelt(grey) and the sites from which the 4 biopsies were extracted from (blue squares). The blue dotted lines show the midlines of the pelt.

To isolate the lice for counting, square grided petri dishes (8.8mm by 8.8mm, 6 by 6 square grid), one for each fur biopsy, were filled with 20 ml of 10% potassium hydroxide (KOH) solution (Norwegian Veterinary Institute, product code 30.087.03) using a 50ml beaker to measure the volume. Potassium hydroxide was used as this dissolves keratin, lipids and proteins in the fur and skin, but leaves chitin containing structures, including lice, unaffected (Tiffin et al., 2020). Each fur biopsy was placed in its dish with the fur side facing down. To remove any trapped air between the hairs and the skin a pair of metal forceps were used to carefully submerge the fur and skin. Petri dishes were covered with a fitted lid and placed under a fume hood at room temperature (20°C) for 24 hours to dissolve the skin and fur. The biopsy samples inside the petri dishes were carefully agitated by swirling the contents in a circular motion at least once during the 24-hour period.

After 24 hours the biopsies were removed and prepared for lice abundance estimation. Using a forceps, the skin was carefully lifted and shaken. A microscope slide needle was used to dislodge

any remains of the top layer of the skin back into the petri dish. The skin biopsies were saved for later examination in a separate container. The contents of the petri-dish were examined using a stereomicroscope (Leica MZ9.5) under magnification 10. The total number of lice adults, nymphs and eggs were recorded using a mechanical counter, and the final result recorded on the paper records. The skin biopsies were then examined using overhead light in the stereomicroscope to identify and count any lice or eggs which remained attached to the skin.

2.4 Fur damage score

A fur damage scoring procedure was created to assess the extent of damage observed on pelts. Initially inspired by a scoring system developed by Berg et al. (2009) for lemur coat and tail conditions, the method was substantially modified and tailored to address the specific context of arctic fox fur damage caused by lice. The method was developed to account for the most prominent observed effects the infestation of lice in a pelt often exhibits, namely fur loss, thinning of the coat, patchiness, and colour change.

Due to the fact that damage was not evenly distributed across a pelt, e.g., one pelt could exhibit severely damage fur in one area, while also having areas without any damage, the surface area of the damage was included in the scoring system.

The procedure consists of two scores:

The first score, “local damage”, ranges from 0 to 5, and focuses on solely on the pelt’s worst observed damage, taking no account of its extent across the pelt.

The second score, “area of damage”, measures the arial extent of damaged or affected fur across the pelt. This score provides a surface area measurement (in cm2) of the damaged area.

The final damage score was calculated my multiplying Score 1 with Score 2.

2.4.1 Score 1: Local damage score

A comprehensive evaluation of the fur damage was developed to assess the condition of arctic fox fur by focusing on various key aspects. This included fur depth, colour change, the presence

and distribution of guard hairs, the condition of the downy undercoat and the degree of exposure (visibility) of the skin under the fur.

The system categorizes the fur damage into six different levels, the lowest being “Pristine” (level 0) and “Severe damage” (level 5) being the highest. The levels and severity of each aspect for each level are as follows:

0 – Pristine: The fur is in perfect condition, similar to pelts with no lice. It is entirely white, with no visible signs of shortened or thinned fur upon visual and physical inspection. Unable to see the skin through the fur.

1 – Minimal loss: The pelt has indications of fur loss or fur thinning but is in generally good condition. Guard hairs are present throughout and no, or only a very faint, indication of colour change is present. The fur for the most part looks dense and fluffy and still not able to see the skin through the fur.

2 –Light damage: Fur loss and/or thinning is noticeable. The guard hairs exhibit an even but thinning distribution. There are indications of colour change, as well as overall fur thinning making it easier to see down into the fur’s layers, although the skin still is not visible.

3 – Moderate damage: The fur shows prominent fur loss. Fur may have a lightly thinned undercoat exhibiting a sheared appearance. Guard hairs are missing and/or are sparsely distributed, resulting in uneven, or less dense, coverage. Changes in colour are evident. It is only just possible to see through the coat along the fibres down to the undercoat.

4 – Significant damage: Fur is sheared and deteriorated. It has less than half the normal depth. Guard hairs are scarcely distributed or missing in large quantities. Colour change is highly noticeable. It is possible to see far down into the fur and the skin just visible. The downy undercoat is exposed and/or damaged and reduced.

5 – Severe damage: The fur is ragged, and the depth is dramatically reduced, down to half, or less, of the normal depth of a winter pelt. Colour change is noticeable and may be dramatic. The

bases of the hairs are visible, the downy undercoat is in rough condition or missing and it may be possible to see exposed skin.

2.4.2 Score 2: Area of damage

The area of damage was measured using the photo editing software Adobe photoshop (v.23.5.1). Images of intact pelt samples were imported to photoshop and batch processed using automatic lens correction to adjust for lens distortion. The images were then cropped to include only the pelt, and then saved individually as new .jpeg files.

The Images of the pelts were individually analysed to estimate the area of damage. Using the analysis tools in Photoshop, a custom measuring scale was created which automatically calibrated the pixels of the images in a marked area to the refence length within an image of a known length.

The area of damaged or affected fur was selected using the quick selection tool in Photoshop which allows for irregular shapes within the image to be selected (see **Figure 6**). Alongside this the surface area selection procedure, the physical pelt under investigation was examined to ensure the surface area was not over or underestimated. This second physical screening also allowed for the local damage score (Score 1) to be accurately applied.

Once the extent of the damage had been marked, the programme automatically displayed the area in cm^2 of the shaded area.

Figure 6 Area of damage example (Animal ID 25). This image is an excerpt from Photoshop, and it illustrates the process of estimating fur damage extent. The black and white lined area symbolizes the area selected as damaged.

2.5 Thermal conductivity of fur

Before experiments, the cut pelts (front and back as illustrated in **Figure 4**) were thawed. If experiments started in the morning pelts would be thawed overnight in a refrigerator of 0°C to be ready for use in the morning. If experiments would start later in the day pelts would be thawed at room temperature for a duration of three hours before finalizing the preparations and beginning

the experiment. After thawing, any pelts that were found wet, soiled, or stained by blood underwent a meticulous cleaning process using cold running tap water with low pressure. This was in accordance with the instructions given by the taxidermist who skinned the foxes. To prevent the potential loss of lice and eggs, the wash water was filtered through a 200mm by 50mm test sieve (Retsch®, Germany) with grating constant 180 μm. Residue collected in the sieve was transferred to a square-grided petri dish for subsequent lice counting following the same lice-count protocol (see section 2.3).

The pelts were then dried using a standard hairdryer and a medium-fine comb to arrange the fur for optimal insulation. Fur thickness was measured as described by Underwood (1971): in fur simulating maximum piloerection, at 21 predetermined sites (see **Figure 7**) across the fur using a calliper: The calliper was carefully placed vertically into the fur down to the surface of the skin. The top slider was then shifted down to mark the depth of the dense fur, determined while keeping the line of sight parallel to the surface. Longer guard hairs with sparse distribution were excluded from the measurements. Final calculations of fur depth mean used the central seven measurement sites, 7, 8, 9, 11, 13, 14, 15.

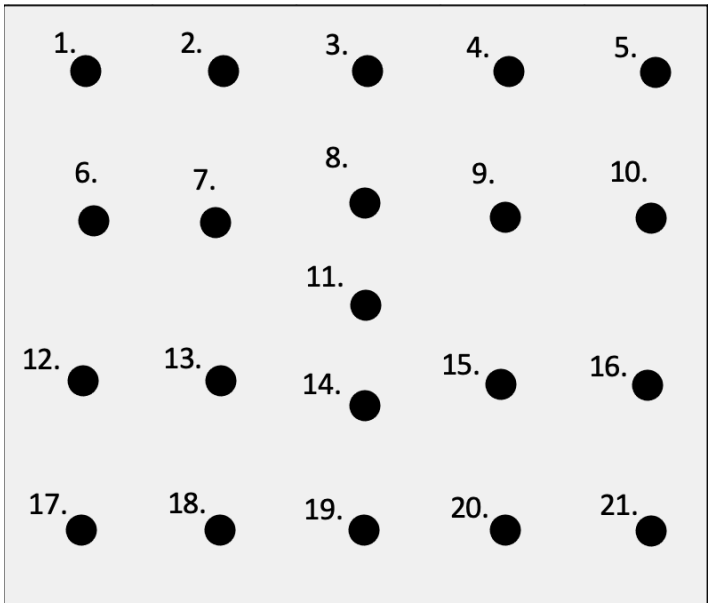

Figure 7. Illustration of the 21 sites fur depth was measured.

2.5.1 Measurement of thermal conductivity

The thermal conductivity of the arctic fox furs was measured using equipment developed and detailed by Kvadsheim, Folkow & Blix (1994) (illustrated in **Figure 8**), referred to as a k-meter.

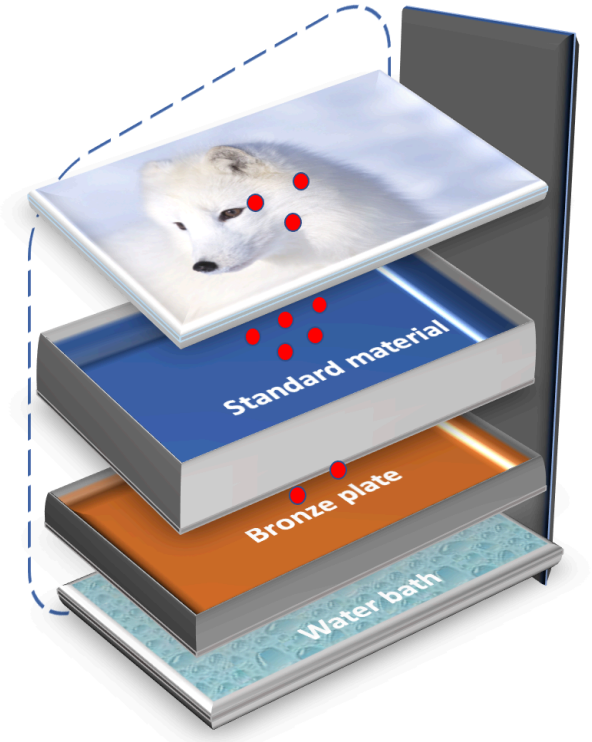

Figure 8 Simplified illustration of the conductivity measurement device (k-meter). Red dots symbolize the placement of thermocouples.

Simply put, this equipment consists of a heat source with constant temperature and a standard material of known conductivity. The fundamental principal revolves around creating a steady-state heat flow through the two conductors (the standard material, and the material under investigation. In this case, an arctic fox pelt).

A solid bronze block measuring 0.2m by 0.2m and 0.055m in thickness was partially immersed in water. An electrical heater (T-643, Heto, Bierod, Denmark) with a connected thermostat was set to 40°C to maintain a water temperature within the range of 35-39°C. Atop of the bronze block, a 0.2m by 0.2m polyethylene high density-1000 plate (Pehd-1000) with a thickness of

0.0315m is positioned. This served as the standard material with a known conductivity value of 0.365 $Wm^{-1}°C^{-1}$(Kvadsheim, Folkow & Blix, 1994). Fur samples, measuring of 0.215m by 0.215m, were carefully positioned onto the Pehd-1000 plate (the standard material), a scalpel blade was used to produce small holes for the attachment of the fur. The fur was stretched onto the standard material and clamped down with an aluminium frame held with bolts, see **Figure 9**.

Figure 9. Photograph of an arctic fox pelt mounted in the conductivity measurement device. Pelt is clamped down and mounted onto the standard material by threading the eight holes made in the pelt using a scalpel blade, over eight plastic screws and attaching the aluminium frame tightly using bolts. A black insulative sealing strip can be seen along the edge of the frame.

An insulated frame of 0.14m expanded polyurethane, covered with PVC (Polyvinyl chloride) on all sides, was tightly placed on top of the bronze block, Pehd-1000 and pelt. Despite the insulating frame, heat leakage was still identified from the edges of the sample using a thermal

imaging camera (FLIR T1030SC, FOL36 lens, 1024 x 768 resolution, spectral range 7.5-14 μm). Therefore, a thin insulative sealing strip (Sealing strip in neoprene, Biltema) was glued on (using Super glue, 3g, Biltema) along the edge of the Pehd-1000 block and the insulative frame to further reduce possibility for heat to escape between the two (**Figure 9**). Subsequently, the whole device was enclosed within a 20 m^3 climate chamber (Model 24/50 DU, Weiss Tecknik, Gissen, Germany; accurate to ±1°C in time and ±2°C in space). The climate chamber maintained a stable, controlled and precisely measured air temperature (although this temperature was difficult to accurately set, and so ranged from -6°C to 0°C between experiments) throughout the experiments. Air temperature was a critical factor when establishing a consistent heat flow through the conductivity device.

Temperatures were measured and recorded using eleven thin (soldering point < 1mm in diameter) quick-responding copper-constantan thermocouples (TT-T-36-SLE, Omega Engineering Inc., Stanford, CT, USA). The thermocouples were connected via a temperature-compensated connector to an AD (analogue-digital) signal converter (ADInstruments, PL3516 Power Lab 16/35 Data Acquisition Systems) translating millivolt (mV) signals to digital format. Data points were sampled at a frequency of 1Hz. The AD signal converter was connected via a high-speed USB (2.0) to a laptop computer (HP ProBook with Windows 10) with ADInstruments software LabChart (v.8.05) for real-time monitoring of signal measurements during data acquisition. The placement of the eleven thermocouples used was as follows: two at the interface between bronze block and the standard material, five between the standard material and the skin, three within the fur near the surface(, and one measuring the ambient temperature at a distance of 30 cm above the device. The thermocouples positioned within the fur were affixed to a metal nail (2 cm length) with plastic cable clips (size 3-5mm, Biltema) threaded and glued onto (Super glue, 3g, Biltema) a thin wooden probe, placed either 40mm or 15 mm away from the tip (**Figure 10**). The probes (one for each thermocouple) were oriented vertically with the tip touching the skin's surface.

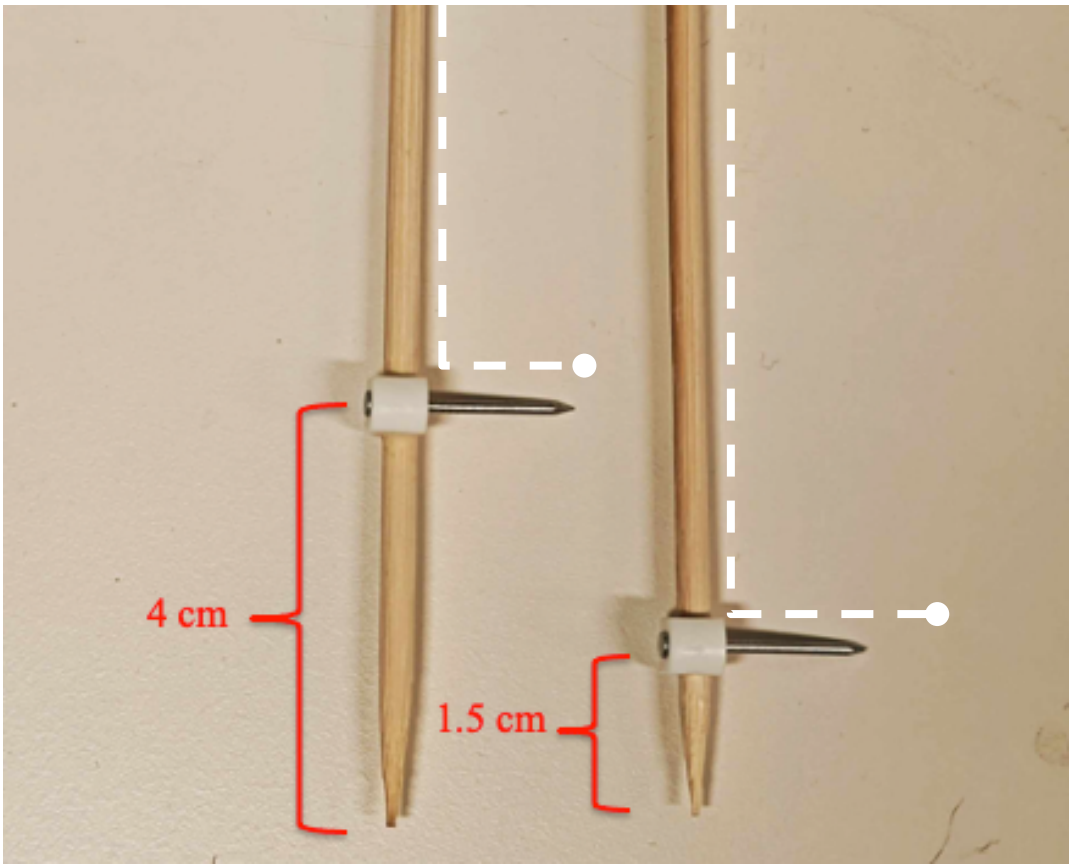

Figure 10 Photo of the thermocouple mounting on a wooden probe with a cable tie to which the thermocouple was affixed to using tape. White-dotted structure symbolises the thermocouple placement.

Every thermocouple placed within the setup was individually marked by number (1-11). In order to maintain an accurate temperature gradient, an axial fan (Ebm-papst, model 3314, 92x92x38mm, with a 16V AC(alternating current) adapter) was positioned 30 cm away from the conductivity apparatus. This fan generated a weak horizontal airflow across the top of the insulative frame, preventing any potential build-up of warm air above the fur (but not strong enough to cause fur to move and compromise the insulative capacity), thereby establishing an accurate and consistent temperature gradient from the bronze plate via the Pehd100 plate and the fur, to the surrounding air.

2.5.2 Calibration of instruments

To ensure that the temperatures measured by the thermocouples were as accurate as possible, all 11 channels were calibrated at regular intervals, after every 5-6 pelts measured. This was to account for any potential calibration drift over time. Calibration was performed using two different reference temperatures: 0°C maintained within a dry-well cooling chamber (Model 5115, Hart scientific, UT, USA), and 36.5°C achieved in a temperature-controlled warm calibration bath (water bath) regulated by a thermostat (Model 6025 Hart scientific, UT, USA), a built-in certified mercury thermometer provided precise temperature readings with 0.1°C resolution.

During calibration the voltage output of the 11 thermocouples were recorded for 2 minutes at each temperature point, with data acquisition occurring at a frequency of 1Hz. The calibration raw data were stored in a designated file and subsequently transferred to an excel file (Microsoft Excel, Version 16.74) for further analysis.

For each thermocouple channel, a mean voltage was computed for each calibration temperature (0°C and 36.5°C). Using the mean voltage value and the associated reference temperature, and assuming linearity, a linear regression equation was employed to calculate the slope and intercept for each of the 11 channels:

$$y = ax + \mathrm{b} \tag{1}$$

Where y is the calibrated temperature value at any given point, x denotes the uncalibrated voltage extracted from the recorded data, a is the slope of the regression, indicating the change in y for each unit change in x, while b represents the intercept, denoting the value of y when x equals zero.

The constants a and b were calculated as:

$$a = \frac{y_2 - y_1}{x_2 - x_1} \quad (2)$$

$$b = \frac{(x_2 \cdot y_1) - (x_1 \cdot y_2)}{x_2 - x_1} \quad (3)$$

Where the known reference values are y_2 and y_1, 36.5°C and 0°C respectively, x_2 and x_1 being the recorded voltage mean value of those points.

This process was repeated for each calibration event throughout the experiment.

2.5.3 Experimental protocol

Before starting the experiment, the water bath was preheated and, when necessary, water was added to maintain a suitable water level. Pre-heating of the climate chamber system had to be performed 3 hours prior to the start of cooling the room to 0°C. Once the set up was ready, the fur was mounted as described in section 2.5.1. A thin layer of silicon grease was spread on to the standard material (Pehd-1000 block) to ensure that no air was trapped between the Pehd-1000 block and the skin before the pelt was clamped down. The system was left to stabilize, to reach a steady state temperature at all thermocouple locations, which took between 5 to 15 hours depending on the fur. The heat source and ambient temperatures were kept constant throughout the experiment. Once steady state temperatures were obtained, defined as less than 0.1°C change in all temperatures in one hour (Kvadsheim & Aarseth, 2002), the thermocouple measurements were noted.

2.5.3.1 Infrared Thermometry and Thermal Imaging Procedure

In conjunction with thermocouple measurements of fur surface temperature, infrared technology was used. This was done to test the reliability of such methods against the standard thermocouple

method, and to provide another means of measuring temperature in instances where the thermocouple may have been unreliable, for instance in pelts with severe fur loss.

Once the fur had a stable heat flow (steady state) the surface thermocouples placed inside the fur were carefully removed to allow infrared measurements to be taken. The temperatures of 23 predetermined sites (see **Figure 11**) were measured across the pelt, using an infrared thermometer (Testo 854, using the close focus optics, spectral range 8-14 µm), while no other changes to the set up were done. Final calculations used the IR thermometer mean of the central nine measurement sites, 7, 8, 9, 11, 12, 13, 15, 16, and 17.

Finally, a FLIR (T1030SC with a FOL36 lens, 1024 x 768 resolution, spectral range 7.5-14 µm) thermal imaging camera was used to capture a thermal image, with the photographic angle perpendicular to the pelt – i.e. taken from directly above – and at 0.60m distance from the pelt (see **Figure 12**).

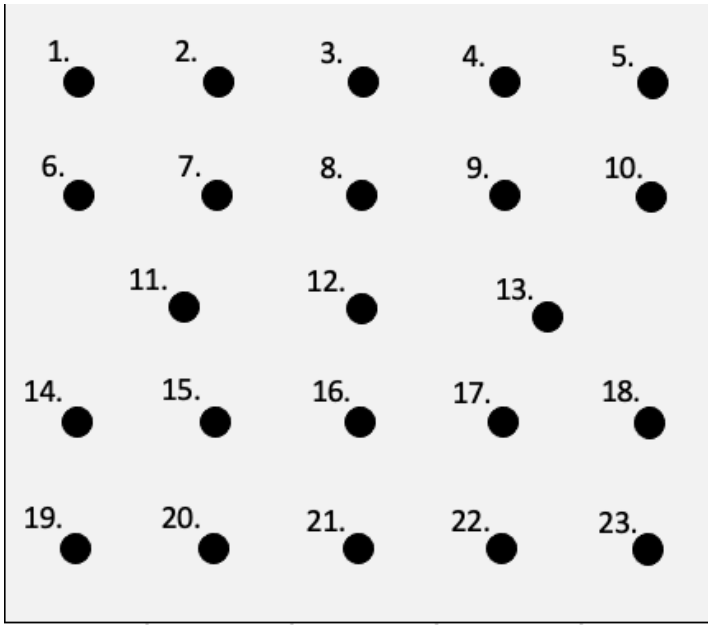

Figure 11 Illustration of the 23 sites infrared thermometer temperatures were measured.

2.5.4 Data extraction

Data from the recording file for each of the conductivity experiments was extracted from LabChart (v.8.05). A 4-minute time segment of the experiment was chosen, following the attainment of a steady state, but preceding the removal of the surface thermocouples, for the IR measurement. This was to ensure that the thermocouple-based and IR sets of data were as close in time as possible.

The extracted data was exported into an Excel datasheet. Mean mV values and standard deviation for each channel were calculated, relying on 240 data points, corresponding to one measurement per second over the four-minute interval.

The mean mV for each channel were converted into temperature values (°C), and the linear calibrations with coherent constants calculated, as described in section 2.5.2, using the calibration data closest in time to each experiment.

2.5.5 Analysis of FLIR infrared thermal images

All IR images taken using the FLIR T1030SC camera were analysed using the licence free FLIR analysis program (FLIR Thermal Studio, v.1.9.70). The measuring square had a known size, 0.2 by 0.2m, giving an area of 0.04m^2. A central square of 0.008m^2 (9cm by 9cm) was marked in the same region where the IR thermometer and thermocouples had been placed, see **Figure 12**. Emissivity was set to be 0.96 in accordance with Tattersall (2016). Additional parameters that were manually adjusted for were distance and atmospheric temperature (climate chamber room temperature measured by thermocouples).

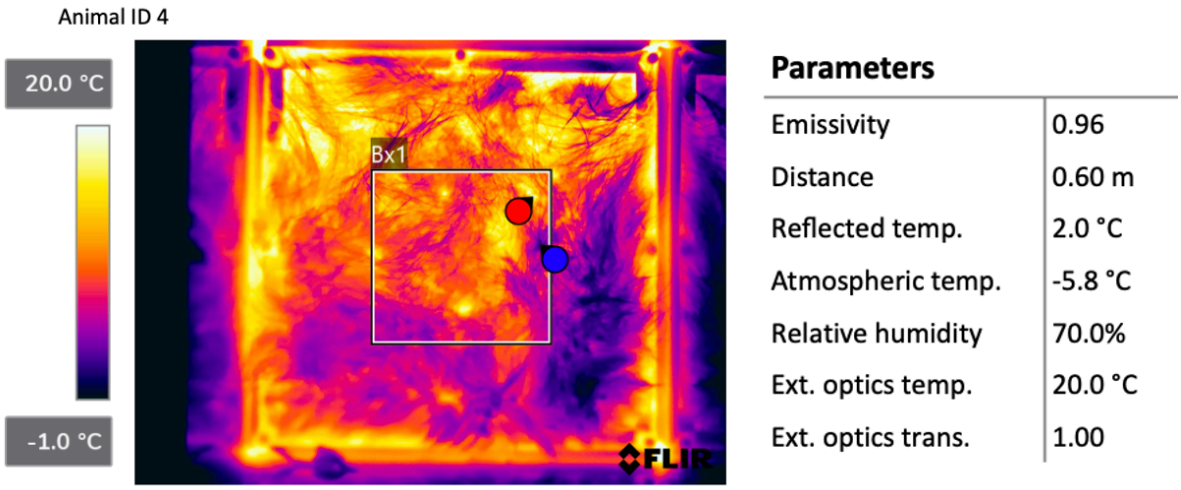

Figure 12. Example of a thermal image of an arctic fox pelt (animal ID 4) at steady state heat flow. Temperature colour scale is shown on the left. A 0.008m^2 square (Bx1) is marked in the centre of the fur, the blue marker indicates the coldest temperature (1°C) within the square and the red indicates the warmest temperature (19.9 °C), average temperature of Bx1 was 9.1°C.

2.5.6 Conductivity and conductance calculations

In 1822 JBJ Fourier derived an equation describing the heat transfer across a plane as follows:

$$Q = \frac{k \cdot A \cdot \Delta T}{d} \quad (4)$$

Where Q represents the heat flow through the plane (Wm^{-2}), k is the thermal conductivity (W/ m°C), A is the surface area of the sample (m^2), ΔT is the difference in temperature across a (°C) and d is the thickness if the sample (m).

By incorporating a standard material with a known conductivity alongside the sample of interest in a serial system, it is possible to apply Fourier's equation for heat flow by combining the equations of the two conductors (the standard material with known conductivity and the fur with unknown conductivity). The heat flow (Q) remains uniform across both conductors in a stable heated system that has attained a steady state at a constant ambient temperature. Consequently, one can solve for the one unknown variable, (k), representing the sample's thermal conductivity:

$$Q = \frac{k \cdot A \cdot \Delta T}{d}$$

$$Q_{standard} = Q_{sample}$$

$$\frac{k_{std} \cdot A \cdot \Delta T_{std}}{d_{std}} = \frac{k_{samp} \cdot A \cdot \Delta T_{samp}}{d_{samp}}$$

$$k_{samp} = \frac{k_{std} \cdot \Delta T_{std} \cdot d_{samp}}{d_{std} \cdot \Delta T_{samp}}$$

(5)

Where k_{samp} is the thermal conductivity of the sample (W/m°C), ΔT_{samp} is the difference in temperature gradient across the sample (°C), d_{samp} is the thickness of the sample (m), k_{std} is the thermal conductivity of the standard material (W/m°C), ΔT_{std} is the difference in temperature across the standard material (°C) and d_{std} is the thickness of the standard material (m).

Tree conductivity values were calculated using equation 5. K_{TC}, which used the difference in temperature across the sample , ΔT_{samp}, based on thermocouples only. K_{IRM}, which used IR thermometer temperatures (see 2.5.3.1) to replace the in-fur thermocouple temperature for ΔT_{samp} , and K_{IRC} which used IR thermometer temperatures (see 2.5.5) to replace the in-fur thermocouple temperature for ΔT_{samp}.

The thermal conductance of the fur was then calculated using equation 6, from the definition of thermal conductance:

$$C_{fur} = Q/\Delta T$$

(6)

Where Q is the heat flow calculated using equation 4 for the standard material, as

$Q_{standard} = Q_{sample}$, and ΔT is the temperature difference across the entire fur sample from under skin to ambient room temperature.

2.6 Data analysis

Statistical analyses were carried out using the integrated development environment (IDE) RStudio (Rstudio PBC. Version 2023.09.1+494). A significance level of $p<0.05$ was selected for all analyses. See appendix 5.3 for R code examples of the use of all models.

Differences between front and back pelts

To evaluate whether both front and back pelts could be used as one dataset, it was necessary to analyse the differences in measured parameters in front and back. This is discussed throughout section 0, Results.

Paired t-test on the difference in conductivity, conductance, fur depth, D-score, and louse density between front and back pelts of the same individuals was conducted. A Welch's two sample t-test was performed. This test was chosen as it is suitable when sample sizes and variances are unequal.

Correlation

A Pearson correlation analysis was performed between fur depth and damage score. This analysis is detailed in section 3.

Linear models

To find and establish whether a response variable could be predicted using various predictor variables, an ordinary least squares (OLS) regression was used when modelling front pelt parameters. Additionally, linear mixed models (LMM) were used when including front and back furs, these models can handle hierarchical or nested data structures using the lmer function from the lme4 package in R (Bates et al., 2014). The model accounts for a random variation effect to accommodate for the variation between animals and within animals (by addressing the dependant data structure of front and back pelts for the same individua) and assumes a Gaussian distribution. Multiple and adjusted R-squared values are not automatically provided due to there being both mixed and random effects, introducing complexity in the model and challenging traditional R-square computing such as used in OLS models. Therefore, additional calculations

were performed (see R-squared GLMM code in appendix 5.3) to retrieve a measure of goodness-of-fit for the LMM (Nakagawa & Schielzeth, 2013). Two types of r-squared values, namely, marginal R-squared (fixed predictors account for the variation in the response variable while ignoring the random effects), and conditional R-squared (both the fixed and random effects are accounted for), were calculated.

The response variables plotted in the model were conductivity (based on temperatures measured only using thermocouples, (K_{TC}) and conductance (C). The predictor variables were damage score (D-score), fur depth (cm), fat index and louse density (total lice/cm^2) . Individual residual diagnostic plots with a large influence and leverage on the model were then excluded from the model to test whether the ultimate outcome and conclusions differed.

Measure of agreement

A measure of agreement between thermocouple-based conductivity, K_{TC} and IR thermometer-based conductivity, K_{IRM} and between K_{TC} and IR camera-based conductivity K_{IRC} was conducted by producing Bland-Altman plots displaying 95% limits of agreement as well as an intraclass correlation coefficient (ICC). An ICC of 0 indicates no agreement and of 1 indicates perfect agreement (Ranganathan, Pramesh & Aggarwal, 2017).

3 Results

3.1 Demographic and biometric data of the trapped arctic foxes

A comprehensive study was conducted on lice infestation in arctic foxes from Svalbard, based on animals trapped during the 2022-2023 trapping season. A total of 36 foxes were trapped and delivered to the Norwegian Polar Institute of which 17 were included in this study. During the initial evaluation prior to skinning, 15 of these were found to be clear positive samples with lice, one with uncertain status (one egg seen). These 16 foxes, plus one non-infested sample, which was collected to be used as a control. These animals comprised of eight females and nine males.

From the 17 animals, 23 fur samples were obtained. One from the front section of each animal pelt, giving 17 samples, and six more from the back sections of six of the male fox pelts. These individuals were larger, and it was possible to extract both a front and a back pelt sample from them. One of these front/back pairs was from the lice-free control animal.

The front pelt from one of the animals (no-9) was excluded from conductivity analyses as there were discrepancies in the recording of the temperature measurements. The depth at which the in-fur thermocouples were mounted in this pelt was not clearly recorded. Without this information, it was not possible to reliably calculate fur conductivity. Fur conductance (C) is, however, reported, as this value depends only on the temperature difference between the skin and the ambient air, which was reliably measured and recorded.

Table 1 provides an overview of all the data collected and available about the arctic foxes. The ages of the 17 selected arctic foxes covered a range spanning from 1-2 years old to over 8 years old. There was a notable prevalence of young individuals, within the age of 1-2 years old (n=9).

Table 1 Summary of all demographic data collected for each individual arctic fox (named by animal ID) including measured and calculated parameters, K_{TC} (thermocouple-based conductivity), K_{IRM} (IR-thermometer-based conductivity), K_{IRC} (IR-camera-based conductivity), C (conductance), egg, nymph and adult density (per cm^2) and total louse density (sum of eggs, nymphs and adults per cm^2), fur depth in cm and fur damage score (D-score). K_{TC} of animal 9F was excluded as is described in 3.1. The green square indicates the control animal pelts.

Animal ID	Position	Date of trapping	Sex	Esti. Age	Weight(Kg)	K_{Tc}	K_{irm}	K_{irc}	C	Egg/cm^2	Nymph/cm^2	Adult /cm^2	Total lice/cm	Furdepth(	D-score
4	Front	2023-02-20	M	1-2	3,30	0,0865	0,0978	0,1094	1,71	5,92	3,25	9,00	18,2	4,20	660
5	Front	2023-03-03	M	8	3,05	0,0474	0,0466	0,0464	1,00	12,0	31,4	21,2	64,6	5,86	114
9	Front	2023-03-17	M	2	4,80	NA	0,1511	0,1631	2,80	0,278	0,06	1,00	1,33	7,00	552
9	Back	2023-03-17	M	2	4,80	0,0699	0,0715	0,0724	1,50	0,0556	0,00	0,0556	0,111	5,53	118,9
10	Front	2023-03-03	M	4-5	4,15	0,0671	0,0688	0,0739	2,94	0,306	0,06	0,667	1,03	3,86	1450
10	Back	2023-03-03	M	4-5	4,15	0,0456	0,0466	0,0492	0,97	0,0	0,00	0,0556	0,0556	5,30	72,0
14	Front	2023-01-29	F	1-2	3,15	0,0870	0,0953	0,0986	1,77	11,0	9,25	24,0	44,3	5,27	1535
15	Front	2023-01-23	M	1-2	3,60	0,0847	0,0841	0,0907	1,73	2,22	1,53	3,19	6,94	5,26	672
15	Back	2023-01-23	M	1-2	3,60	0,0706	0,0671	0,0724	1,47	0,0	0,00	0,00	0,00	6,27	68,5
19	Front	2023-03-12	M	2	3,30	0,0624	0,0635	0,0652	1,36	33,3	46,9	53,5	134	5,49	514,2
20	Front	2023-01-26	M	4-5	4,20	0,0757	0,0730	0,0777	1,58	0,361	0,0833	0,750	1,19	5,93	316
20	Back	2023-01-26	M	4-5	4,20	0,0540	0,0543	0,0558	1,13	0,0	0,00	0,167	0,167	5,51	39,9
21	Front	2023-02-26	F	1-2	3,25	0,0384	0,0602	0,0695	2,37	0,389	0,0278	0,0833	0,500	1,73	1020
22	Front	2023-02-26	M	1-2	4,10	0,0626	0,0630	0,0624	1,29	11,2	10,2	11,6	33,0	5,99	861
22	Back	2023-02-26	M	1-2	4,10	0,0835	0,0831	0,0858	1,82	0,3	0,167	0,306	0,750	5,31	697
24	Front	2023-02-28	F	2	2,70	0,0546	0,0577	0,0587	1,17	18,0	26,6	38,6	83,2	5,04	466
25	Front	2023-03-15	F	1-2	2,90	0,0451	0,0368	0,0390	1,84	13,7	33,8	40,4	87,9	3,33	820
26	Front	2023-03-04	F	2	2,90	0,0304	0,0325	0,0327	1,77	12,3	10,7	5,17	28,1	3,90	363
28	Front	2023-02-19	F	1-2	3,00	0,0525	0,0581	0,0617	1,12	20,3	36,9	35,4	92,6	4,67	266
30	Front	2023-03-05	F	1-2	2,90	0,0603	0,0588	0,0621	1,23	0,0	0,00	0,00	0,00	6,44	7,900
32	Front	2023-03-14	M	3-4	4,60	0,0592	0,0565	0,0600	1,24	0,0	0,00	0,00	0,00	6,90	0
32	Back	2023-03-14	M	3-5	4,60	0,0736	0,0736	0,0738	1,53	0,0	0,00	0,00	0,00	5,46	0
34	Front	2023-03-13	F	1-2	3,35	0,0585	0,0619	0,0656	1,27	30,4	44,6	46,3	121,3	5,06	396

3.2 Lice infestation, fur depth and damage score

Thirty-six arctic foxes were trapped during the 2022-2023 trapping season, 16 of them (44.4%) were found to be infested with fur lice.

The abundance of lice in the pelts was estimated according to the method laid out in section 2.3. The total number of adults, nymphs and eggs found in the full 36cm^2, and the derived densities for each pelt are found in **Table 1**.

Despite the five infested pelt pairs having a higher mean lice density in the front pelt for all of the different stages of louse development than the back pelts, this difference was not significant (p = 0.261, Figure 37 in appendix 5.2). Nor were there any significant differences in damage score (p=0.0566, Figure 38 in appendix 5.2) or fur depth (Figure 39 appendix 5.2, p=0.972) between the paired front and back pelts. Further analyses were carried out combining the results from both the front and back pelts.

When comparing these metrics for all infested front pelts against all infested back pelts, however, a significant difference was found between lice density (**Table 2**) (**Figure 13**, p =0.00157) and D-score (**Figure 14**, p = 0.0261). No significant difference was found in this way for fur depth (**Figure 15**, p=0.0986)

Table 2 Summary of louse densities. Each lice stage mean for front and back pelts and total lice density for front and back pelts given to three significant figures. 95% confidence interval in brackets. Control animal 32 excluded from means.

Pelt position	Mean adult lice density /cm^2	Mean nymphal lice density /cm^2	Mean lice egg density /cm^2	Total lice density /cm^2
Front (n=16)	18.1 (± 10.1)	16.0 (± 9.3)	10.7 (± 5.6)	44.8 (±24.5)
Back(n=5)	0.117 (± 0.140)	0.0333 (± 0.0857)	0.0667 (± 0.1383)	0.217 (±0.350)

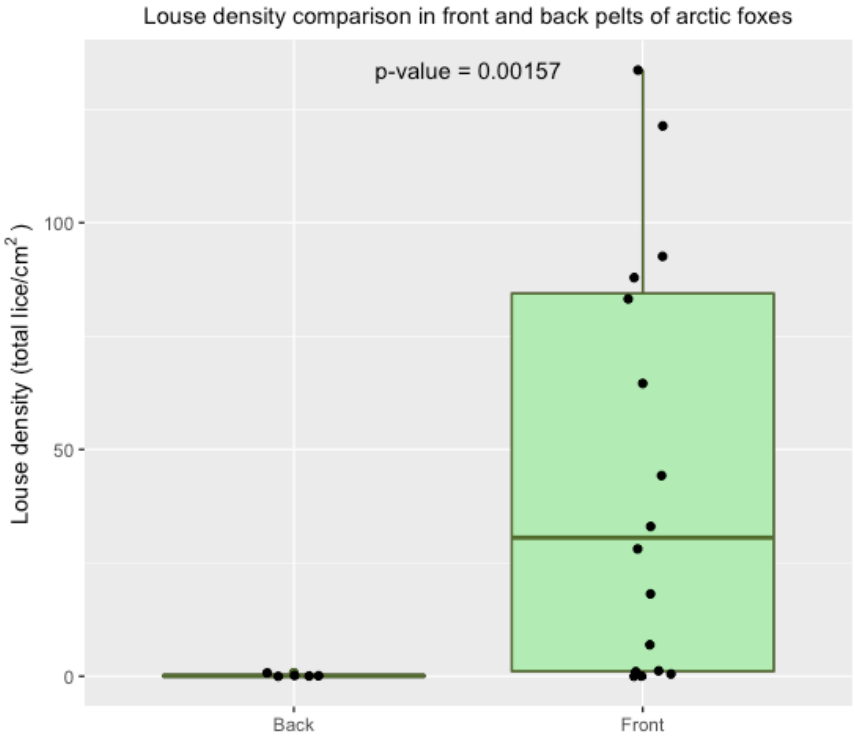

Figure 13 A box whisker plot showing the louse density (adults, nymphs and eggs combined per cm^2) of the front (n = 16) and back pelts (n = 5) from arctic foxed trapped on Svalbard during the 2022-2023 trapping season. The P-value indicates the statistical significance of the difference in total louse density between the front and back pelts, using Welch's two-sample t-test. Control animal 32 was excluded. The green box represents the interquartile range (IQR), encompassing the middle 50% of the data, the line dividing the box represents the median. Whiskers extend to data points within 1.5 times the IQR, which includes majority of the data, data points beyond are displayed as individual data points and are considered potential outliers.

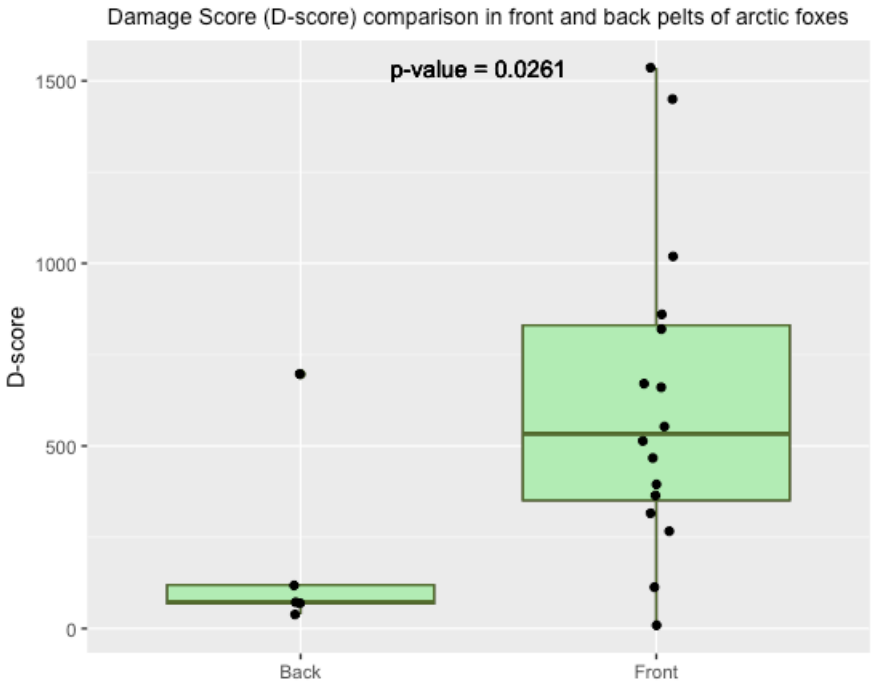

Figure 14 A box whisker plot showing the damage score (D-score) of the front (n = 16) and back pelts (n = 5) from arctic foxed trapped on Svalbard during the 2022-2023 trapping season. The P-value indicates the statistical significance of the difference in damage score between the front and back pelts, using Welch's two-sample t-test. Control animal 32 was excluded. The green box represents the interquartile range (IQR), encompassing the middle 50% of the data, the line dividing the box represents the median. Whiskers extend to data points within 1.5 times the IQR, which includes majority of the data, data points beyond are displayed as individual data points and are considered potential outliers.

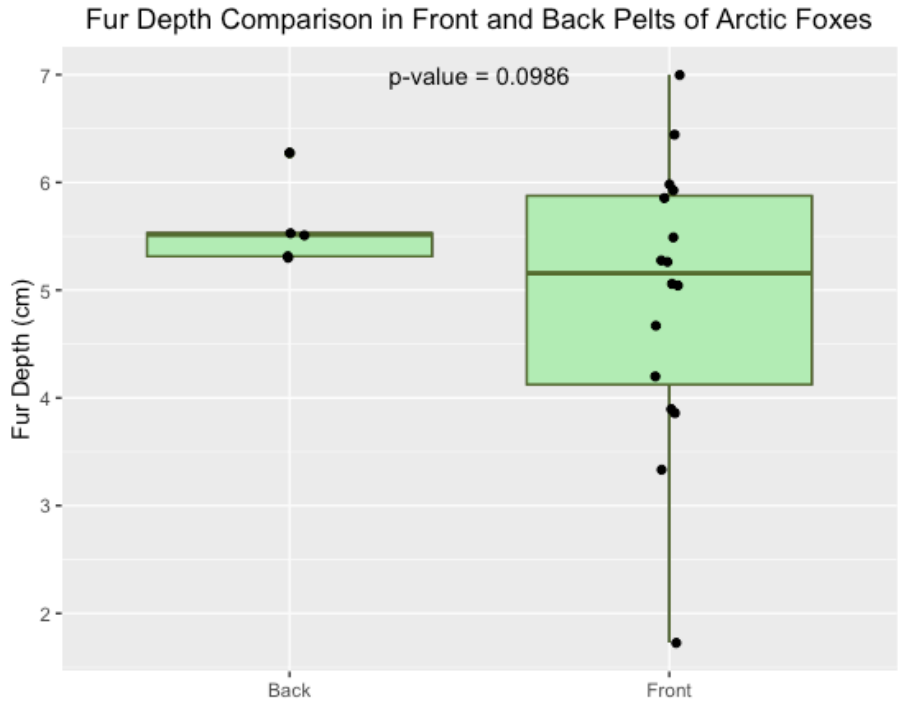

Figure 15 A box whisker plot showing fur depth (cm) of the front (n = 16) and back pelts (n = 5) from arctic foxed trapped on Svalbard during the 2022-2023 trapping season. The P-value indicates the statistical significance of the difference in fur depth between the front and back pelts, using Welch's two-sample t-test. Control animal 32 was excluded. The green box represents the interquartile range (IQR), encompassing the middle 50% of the data, the line dividing the box represents the median. Whiskers extend to data points within 1.5 times the IQR, which includes majority of the data, data points beyond are displayed as individual data points and are considered potential outliers.

3.2.1 Effect of trapping date on louse density, damage score and fur depth

The arctic foxes used in this study were trapped between the 23rd of January 2023 and 17 of March 2023. Linear regression analyses were conducted to examine the relationships between trapping date and louse density (total lice/cm^2), damage score (D-score) and fur depth. This was done as an aside from the main research questions in effort to establish any time dependency of louse density, fur damage or fur depth. For the sake of statistical rigour, and to prevent the same animal being included twice, the back pelts were excluded for these models.

3.2.1.1 Lice density and date of trapping

Individuals trapped later in the season exhibited a trend of higher louse density compared with those trapped earlier in the season. However, an ordinary least squares (OLS) regression analysis found no statistical significance with this trend (**Table 3**, **Figure 16**; p=0.880). The

louse density was log-transformed (**Figure 16**) to account for the wide variation in density values and to allow the representation of very low values on the y-axis.

Table 3 Summary of an ordinary least squares (OLS) regression analysis on log transformed total lice/cm^2, in the front pelts only, as a response variable and trapping date as a predictor variable.

Parameter	Predictor	Estimate	Std. Error	t value	P
Log(Total lice), (front)	Date of trapping	0.004535	0.029556	0.153	0.880
Intercept		-85.387773	573.800679	-0.149	0.884

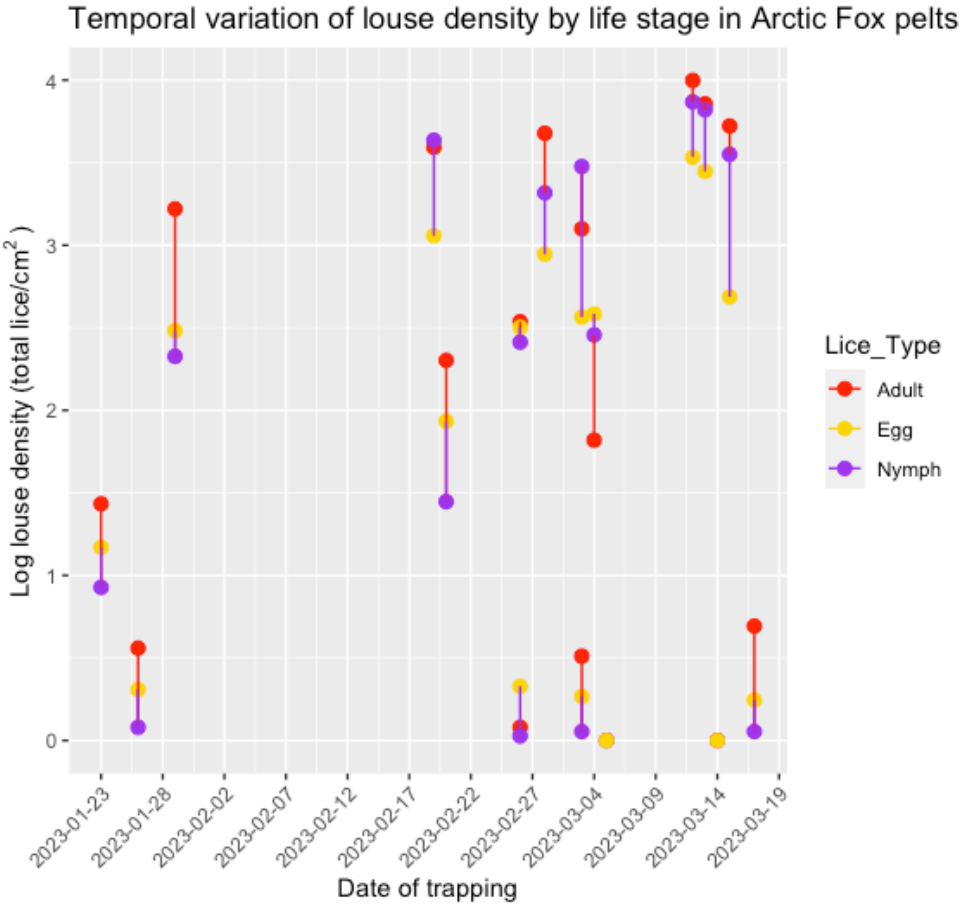

Figure 16 Illustration of temporal variation of louse density by life stage in arctic fox pelts, trapping dates of 17 arctic foxes during the trapping season. The x-axis displays the year, month, and day of trapping. The y-axis represents the log-transformed louse density for the front pelts (lice/cm²). Individual bars are colour-coded to distinguish between louse life stages (adults, nymphs, and eggs) whilst the lines between three coloured dots indicate that these are the louse density numbers from one individual.

3.2.1.2 Damage score and date of trapping

An ordinary least squares (OLS) regression analysis was performed to compare date of trapping and D-score. There was no visible linear pattern or significant relationship (**Table 4**, **Figure 17**; p=0.281).

Table 4 Summary of an ordinary least squares (OLS) regression analysis on damage score (D-score) as a response variable and trapping date as a predictor variable

Parameter	Predictor	Estimate	Std. Error	t value	P
D-score (front)	Trapping date	-7.389	6.610	-1.118	0.281
Intercept		144030.644	128326.035	1.122	0.279

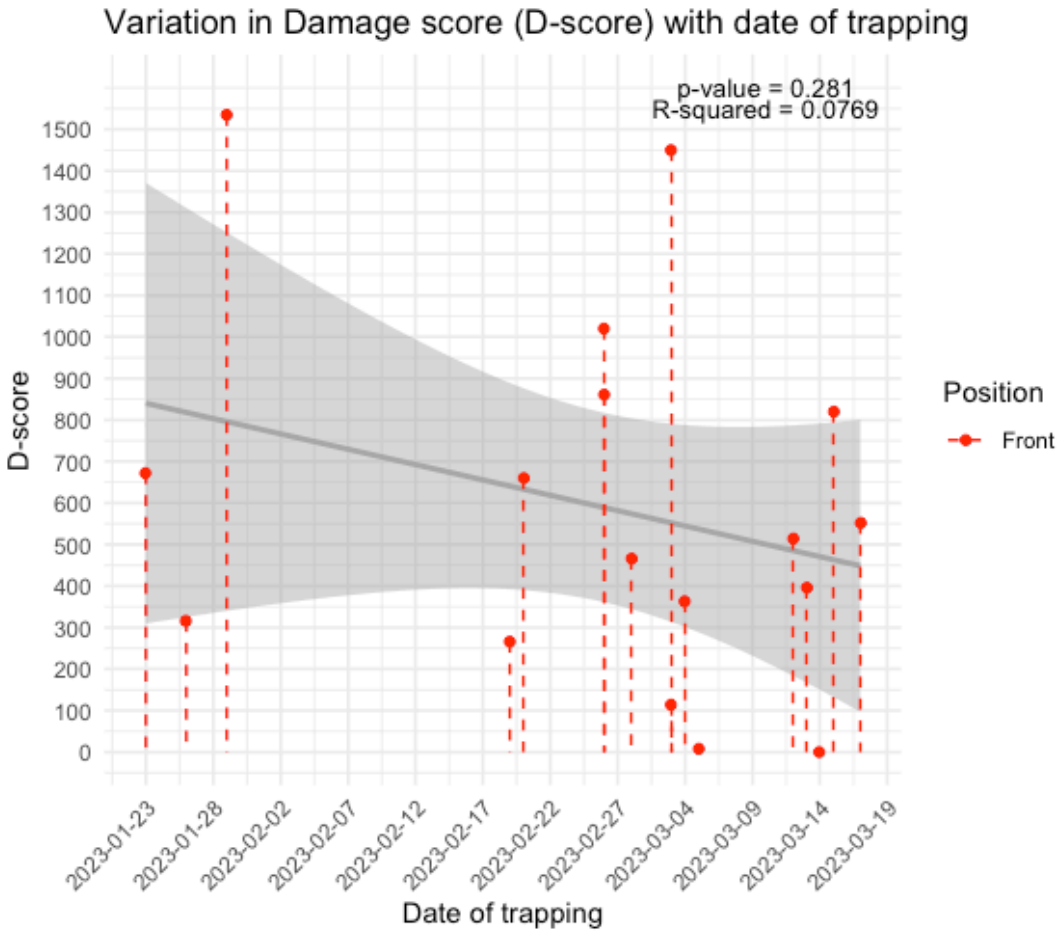

Figure 17 Trapping dates of the 17 arctic foxes plotted to damage score. The x-axis features the year, month, and day of trapping, while the damage score (D-score) of all front pelts is plotted on the y-axis. The model was fitted using an ordinary least squares (OLS) regression analysis, p-value and multiple R-squared values are displayed in the top right corner. The grey line represents the fitted line to the linear regression model. Grey shaded area represents the 95% confidence interval.

3.2.1.3 Fur depth and date of trapping

An ordinary least squares (OLS) regression analysis was performed to compare trapping date and fur depth. There was no visible linear pattern or significant relationship (**Table 5**, **Figure 18**; p=0.901) between trapping date and fur depth.

Table 5 Summary of the ordinary least squares (OLS) regression analysis fitted to fur depth of all front pelts as response variable and date of trapping as the predicting variable.

Parameter	Predictor	Estimate	Std. Error	t value	P
Fur depth (pooled)	Trapping date	0.00264	0.020954	0.126	0.901
Intercept		-46.278	406.800	0.114	0.911

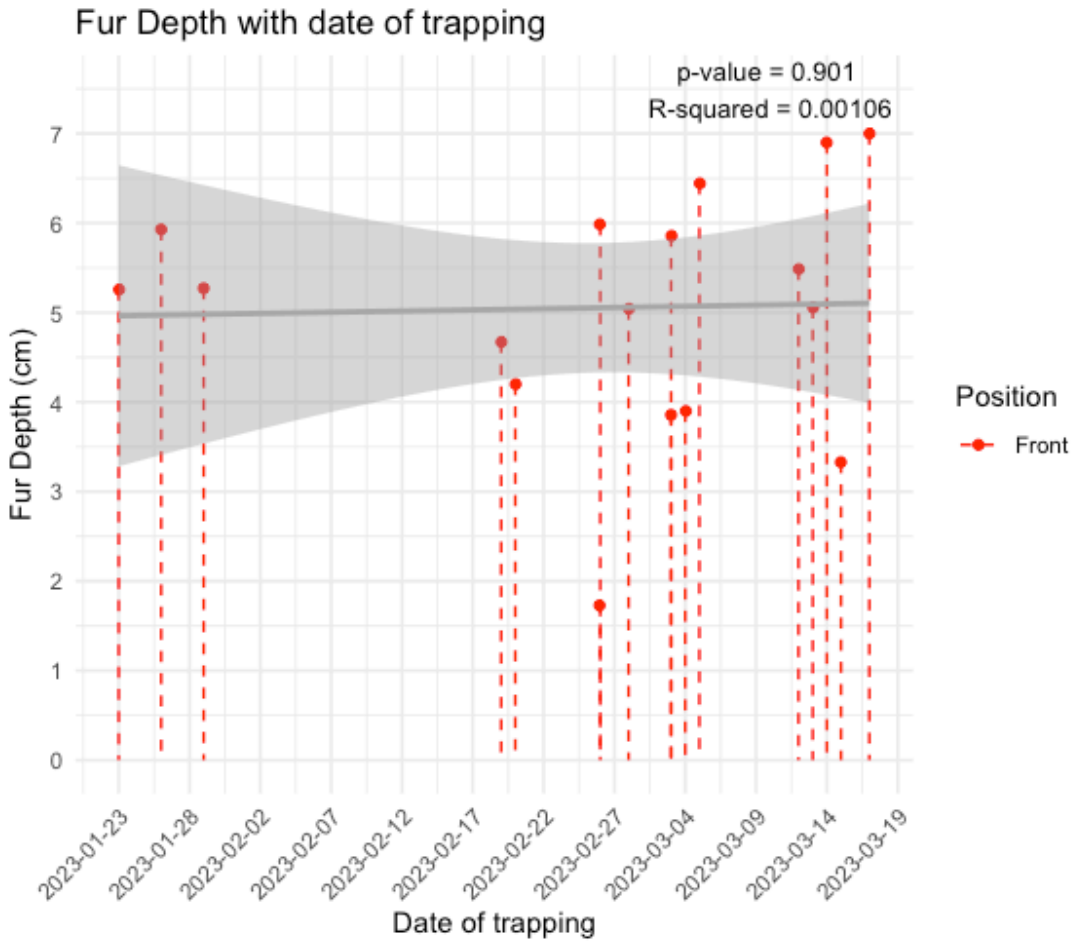

Figure 18 Trapping dates of the 17 arctic foxes plotted to fur depth. The x-axis features the year, month, and day of trapping, while the fur depth (cm) of all front pelts is plotted on the y-axis. The model was fitted using an ordinary least squares (OLS) regression analysis, p-value and multiple R-squared values are displayed in the top right corner. The grey line represents the fitted line to the linear regression model. Grey shaded area represents the 95% confidence interval.

3.2.2 Damage score and lice

A linear mixed model (LMM) (random effect applied to Animal ID) was used to assess the relationship between fur damage score (D-score), plotted as the response variable, and log-transformed louse density (log(total lice/cm^2)), plotted as the predictor (this data is given in **Table 1**). The model also accounted for the random effect between paired samples, as front and back pelts were included. The analysis indicated that there was no significant linear relationship (**Figure 19**; p-value=0.190) between log(total lice/cm^2) and D-score in the samples. (see Table 1).

Table 6 Summary of a linear mixed model (LMM) regression analysis fitted to damage score (D-score) as a response variable, and log transformed louse density (Log(total lice/cm^2 +1) as a predictor variable based on data from all arctic foxes included in the study (n=23 pelts).

Parameter	Predictor	Estimate	Std. Error	T value	P
D-score	Log(total lice/cm2 +1)	63.17	46.68	1.353	0.190
Intercept		352.60	129.86	2.715	0.013 *

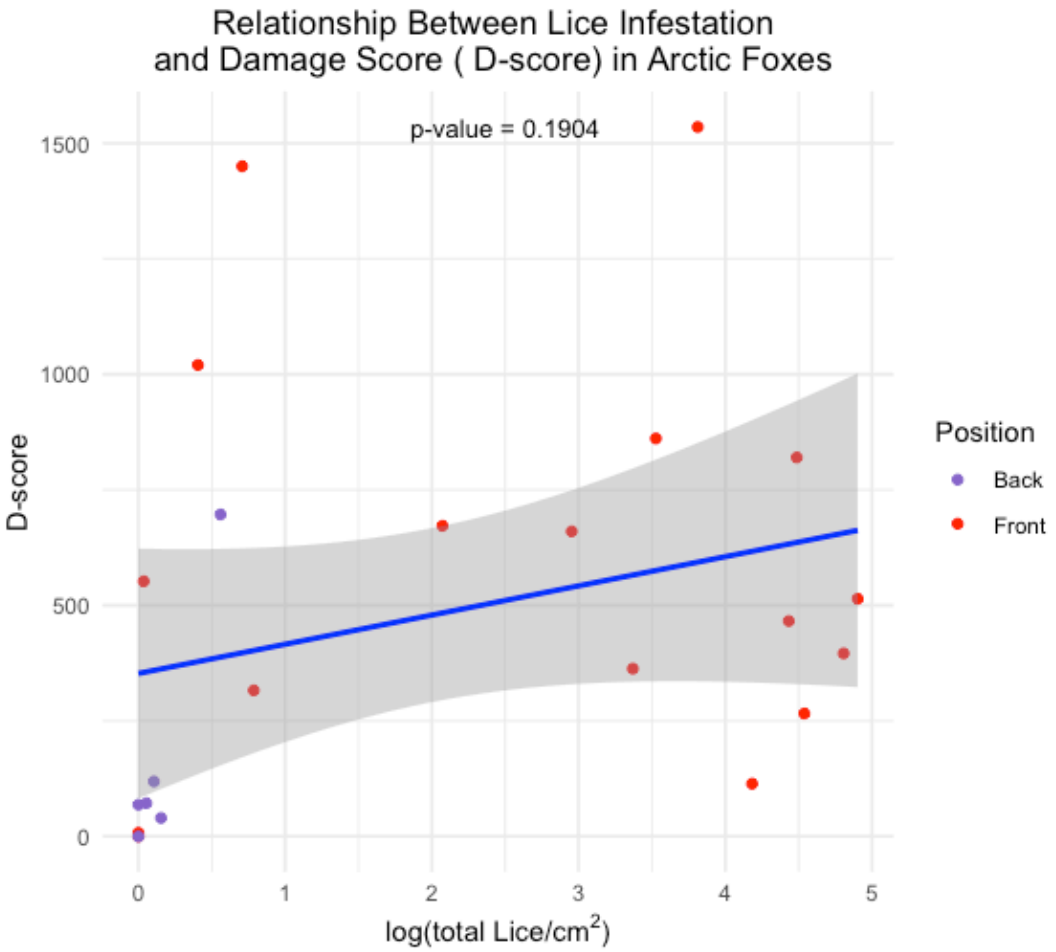

Figure 19 Damage score (D-score) and louse density plot. D-score on y-axis plotted against total lice/cm2 on the logarithmic scale (log(total lice/cm2)) on the x-axis. Points represent individual pelts from back (purple) and front (red). The blue line represents a linear regression model with a shaded region indicating the 95% confidence interval.

3.3 Conductivity and conductance results

Conductivity (K) and conductance (C) for both front and back pelts are summarised in Table 1.

The three sets of conductivity values were named for the method used to calculate them. Conductivity values calculated using surface temperatures measured by thermocouple are referred to as K_{TC} those calculated using surface temperatures obtained using an infrared (IR) thermometer as K_{IRM} and those calculated suing surface temperatures measured using the IR camera as K_{IRC}.

The highest value for a front pelt K_{TC} was 0.0869 W/m°C whereas the lowest was 0.0304 W/m°C. The highest K_{TC} of a back pelt was 0.0835 W/m°C and the lowest was 0.0455 W/m°C. Detailed averages separated by position and by conductivity calculation method (K_{TC} ,K_{IRM} and K_{IRC}) with corresponding 95% confidence intervals are presented in **Table 7**. There was no significant difference in K_{TC} between front and back pelts overall (**Figure 20**; p=0.646) or in pairs (meaning front and back pelts front of same individual) (Figure 40 in appendix; p= 0.436).

The highest value for thermal conductance (C) amongst front pelts was 2.94 W/m^2°C. The lowest was 1.00W/m^2°C (see **Figure 21**). The highest C measured in back pelts was 1.819 W/m^2°C and the lowest was 0.974 W/m^2°C. Detailed averages separated by position with corresponding 95% confidence intervals are presented in **Table 7**. There was no significant difference in conductance between front and back pelts overall (**Figure 21**; p=0.167) or in paired pelts (Figure 41 in appendix; p=0.444).

Since there were no significant difference between the K_{TC} or C for the front and back pelts, subsequent analyses used the pooled results from all the pelts (see sections below).

Table 7 Summary of averages, standard deviation, and 95% confidence intervals (CI, upper and lower limit) for the calculated conductivity (K_{TC}, K_{IRM} and K_{IRC} in W/m°C) and conductance (C in W/m^2°C) separated into the front pelts and back pelts. K_{TC} represents the conductivity estimates based on fur surface temperature measurements from the thermocouple (TC). K_{IRM} is based on fur surface temperatures measured by infrared thermometer. K_{IRC} is based on fur surface temperatures measured by infrared thermal imaging camera.

	K_{TC}	K_{IRM}	K_{IRC}	C
Average front(K_x;n=16, C; n=17)	0,062	0,064	0,067	1,66
St. dev	0,016	0,017	0,018	0,572
95% CI	0.055, 0.069	0.057, 0.071	0.059, 0.076	1.366 , 1.954
Average back (n=6)	0,066	0,066	0,068	1,40
St. dev	0,014	0,013	0,013	0,303
95% conf interval	0.052, 0.081	0.052, 0.080	0.054, 0.082	1.086 , 1.723

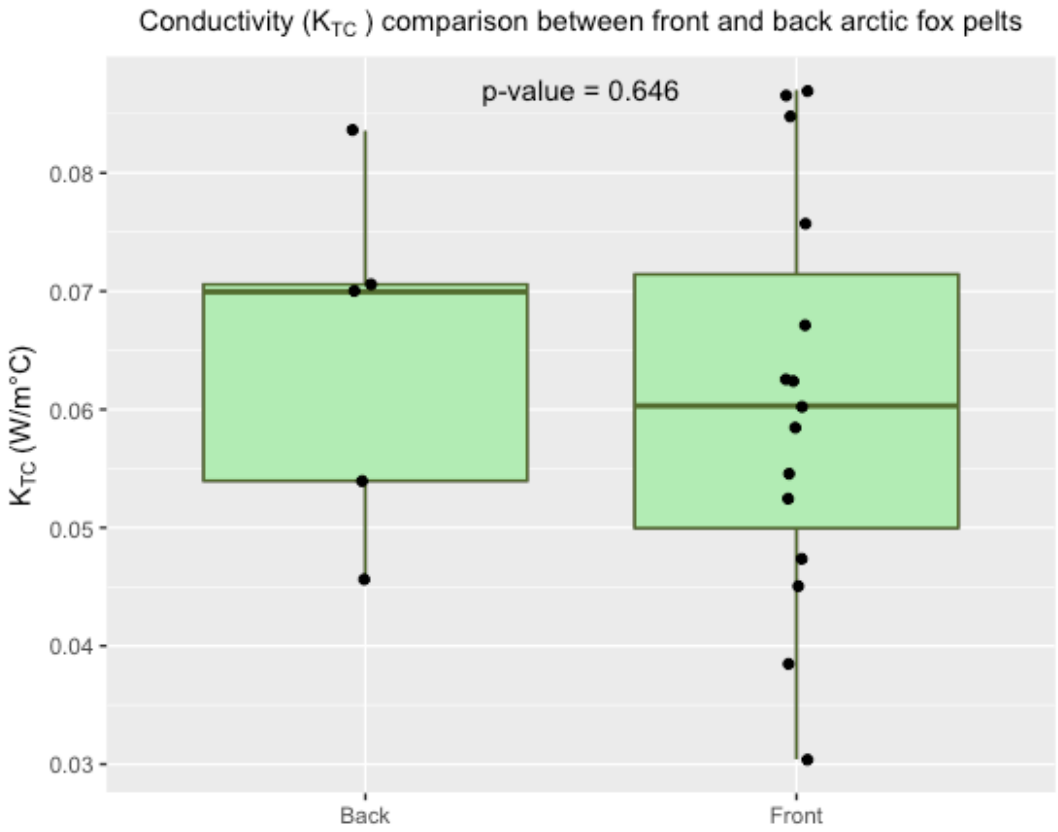

Figure 20 A box whisker plot showing conductivity (K_{TC}) of the front (n = 15) and back pelts (n = 5) from arctic foxed trapped on Svalbard during the 2022-2023 trapping season. The P-value indicates the statistical significance of the difference in K_{TC} between the front and back pelts, using Welch's two-sample t-test. Control animal 32 was excluded as well as front pelt from animal 9.

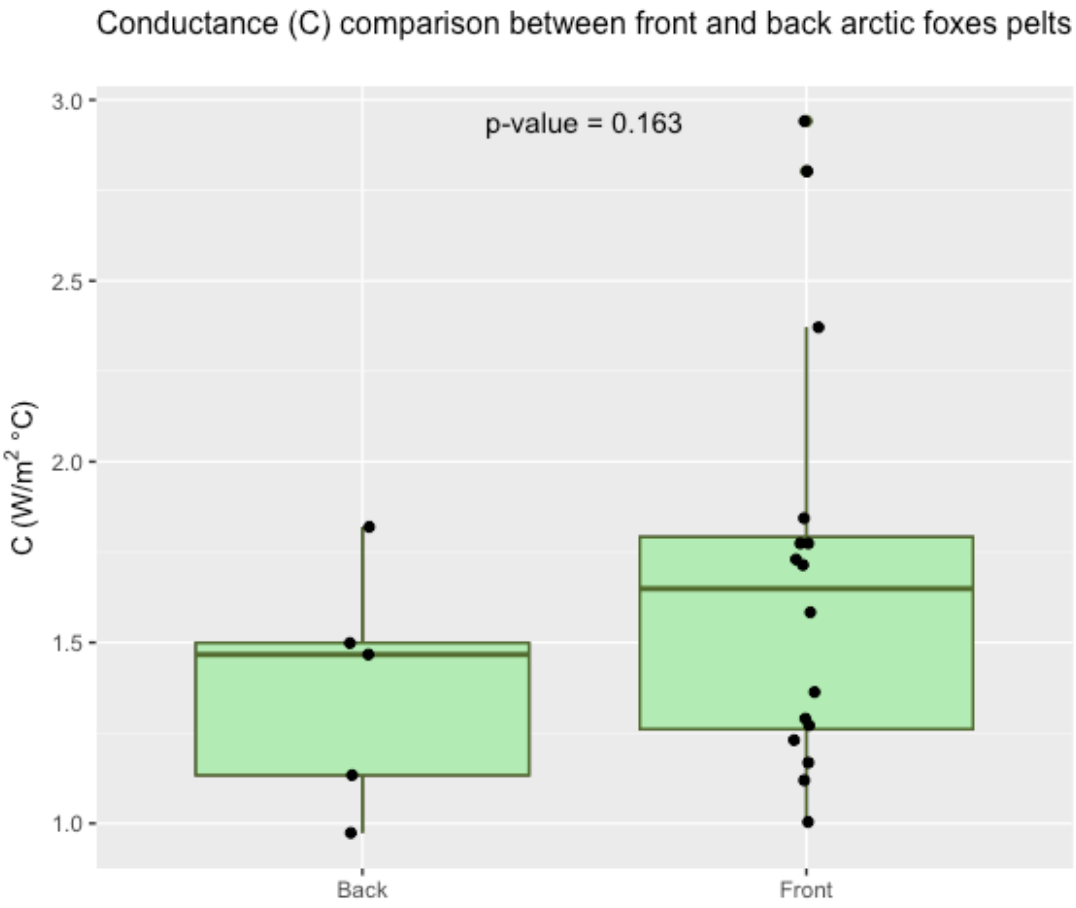

Figure 21. A box whisker plot showing conductance (*C*)of the front (n = 15) and back pelts (n = 5) from arctic foxed trapped on Svalbard during the 2022-2023 trapping season. The P-value indicates the statistical significance of the difference in *C* between the front and back pelts, using Welch's two-sample t-test. Control animal 32 was excluded as well as front pelt from animal 9.

3.3.1 Effect of trapping date on conductivity and conductance

Linear mixed model analyses (random effect applied to Animal ID) were conducted to examine the relationship between trapping date with K_{TC} and *C.* The K_{IRM} and K_{IRC} results were not used for these analyses.

3.3.1.1 Conductivity (K_{TC}) and date of trapping

Individuals trapped later in the season had significantly lower K_{TC} values compared to those trapped earlier in the season (**Table 8**, **Figure 22**; p=0.00713**).

Table 8 Summary of the ordinary least squares (OLS) regression analysis fitted to conductivity (K_{TC}) of all front pelts n=16 (except animal ID 9) as response variable and date of trapping as the predicting variable.

Parameter	Predictor	Estimate	Std. Error	t value	P
K_{TC}	Trapping date	-0.0006502	0.000207	-3.147	0.00713 **
Intercept		12.7	4.012	3.162	0.00692 **

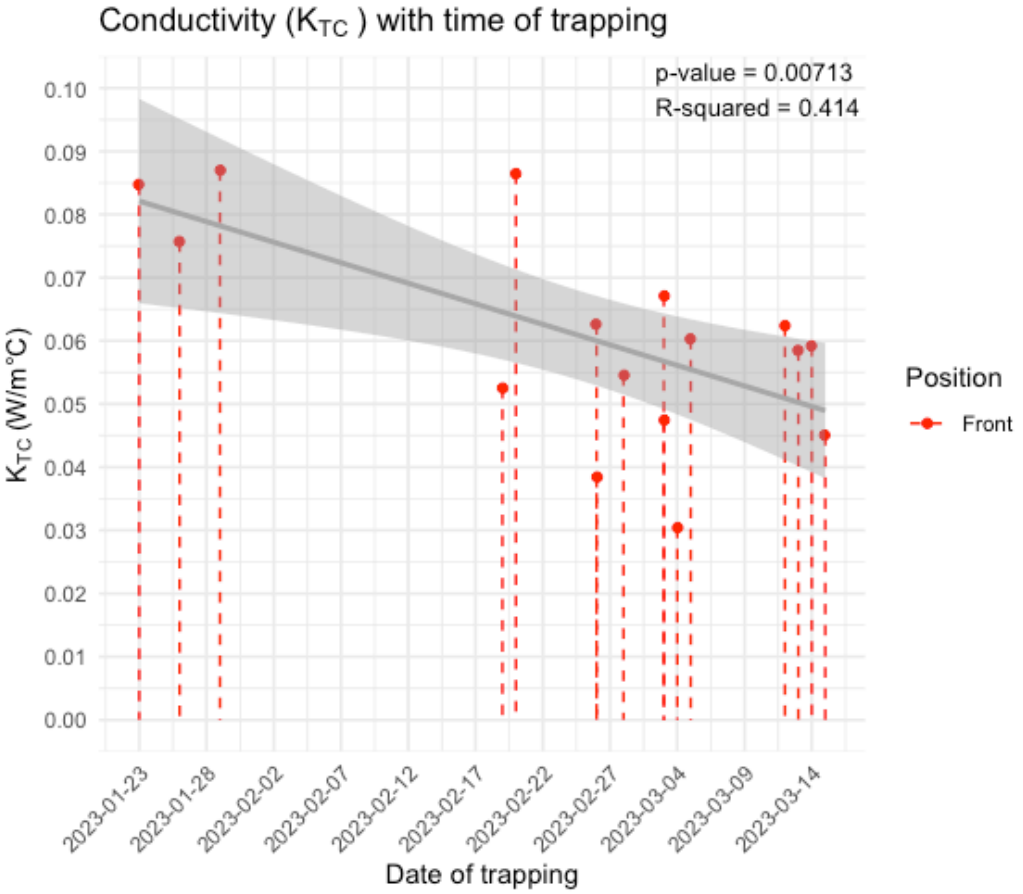

Figure 22 Thermocouple-based conductivity (K_{TC}) of the front pelts in relation to the trapping dates of 16 arctic foxes (x-axis featuring year, month, and day). Fox number 9 was excluded. The model was fitted using an ordinary least squares (OLS) regression analysis, p-value and multiple R-squared values is displayed in the top right corner, adjusted R squared= 0.373. The grey line represents the fitted line to the linear regression model.

3.3.1.2 Conductance (*C*) and date of trapping

Relationship between date of trapping and conductance *(C)* found a slight trend with *C* being higher in the later part of the trapping season than earlier in the season. But this trend was not significant evident (**Table 9**, **Figure 23**; p=0.839).

Table 9 Summary of the ordinary least squares (OLS) regression analysis fitted to conductance (*C*) of all front pelts as response variable and date of trapping as the predicting variable.

Parameter	Predictor	Estimate	Std. Error	t value	P
C	Trapping date	0.001832	0.008839	0.207	0.839
Intercept		-33.899568	171.598524	-0.198	0.846

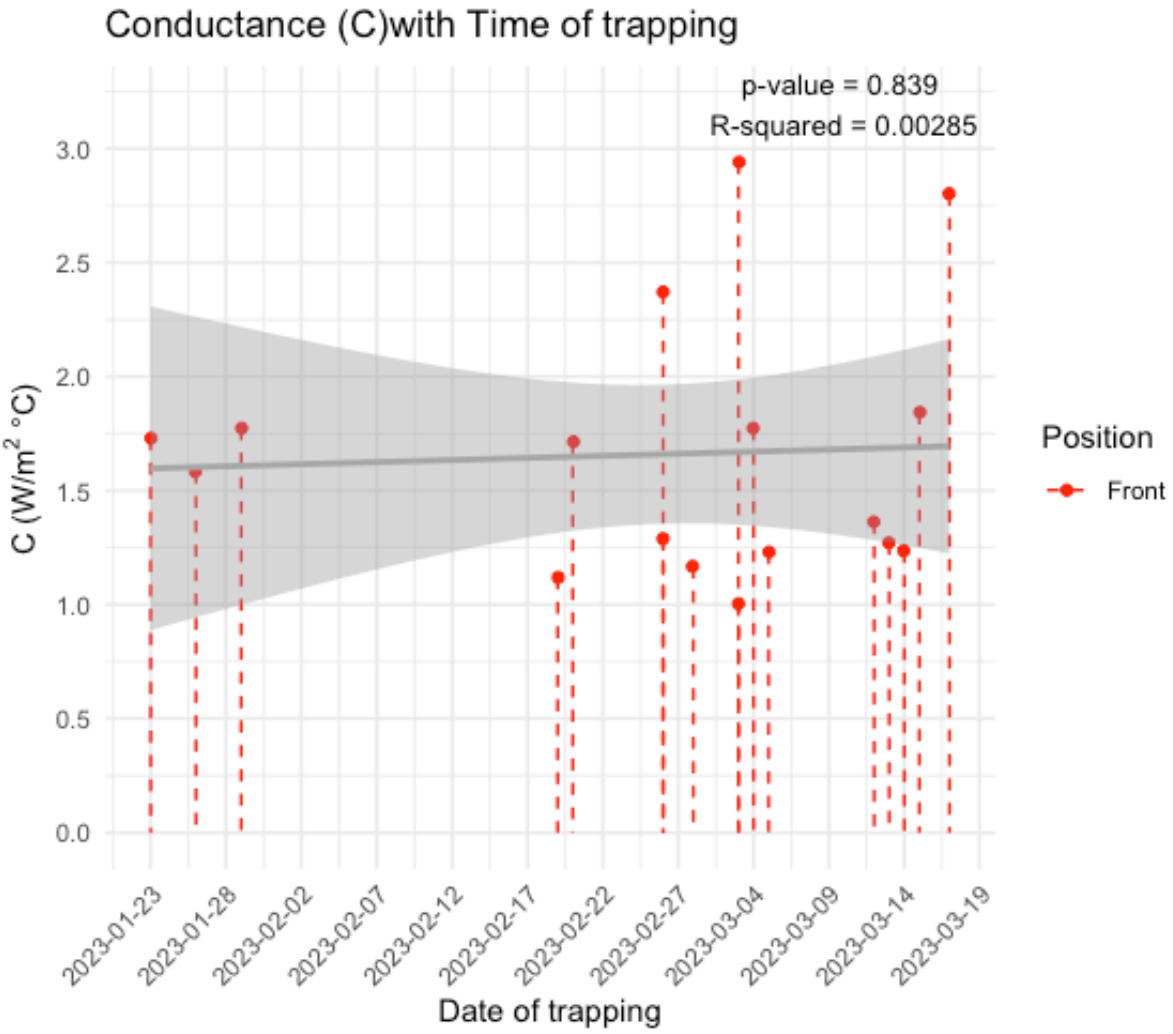

Figure 23 Conductance (C) of the front pelts in relation to the trapping dates of 17 arctic foxes (x-axis featuring year, month, and day). The model was fitted using an ordinary least squares (OLS) regression analysis, p-value and multiple R-squared values are displayed in the top right corner. The grey line represents the fitted line to the linear regression model.

3.3.2 Effect of the presence or absence of lice on thermal properties of pelts.

3.3.2.1 Conductivity (K_{TC}) and the effect of lice/no lice

There was no significant difference in conductivity between pelts infested with lice versus pelts without lice (Figure 24, p=0.701) using Welch's two-sample t-test. The spread in values of pelts infested was very wide compared to pelts not infested with lice, otherwise no trend was observed in plotted data of these metrics.

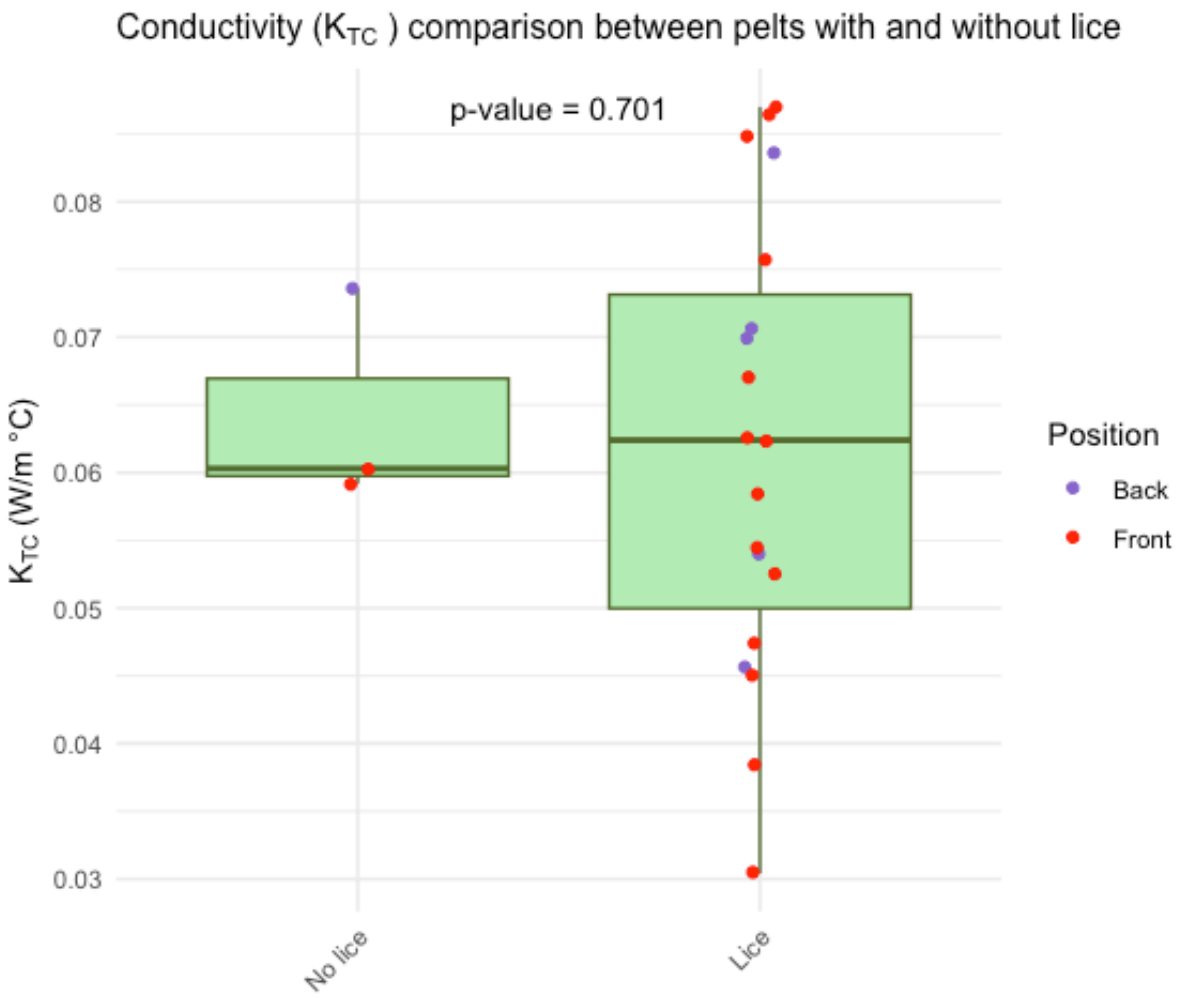

Figure 24 A box whisker plot showing the conductivity (K_{TC}) of non-infested pelts (*No lice*, n=3) and infested (*Lice, n*=19) from arctic foxed trapped on Svalbard during the 2022-2023 trapping season. Points represent individual pelts from back (purple) and front (red). The P-value indicates the statistical significance of the difference in K_{TC} between *No lice* and *Lice*, using Welch's two-sample t-test. Pelt from animal 9 from excluded. The green box represents the interquartile range (IQR), encompassing the middle 50% of the data, the line dividing the box represents the median. Whiskers extend to data points within 1.5 times the IQR, which includes majority of the data, data points beyond are displayed as individual data points and are considered potential outliers.

3.3.2.2 Conductance (*C*) and the effect of lice/no lice

There was no significant difference in conductance (*C*) between pelts infested with lice versus pelts not infested with lice (**Figure 25**, p=0.0872) when analysing the data using Welch's two-sample t-test. The spread in values of pelts infested was wider compared to pelts not infested with lice, with the *C* of uninfected pelts exhibiting lower values.

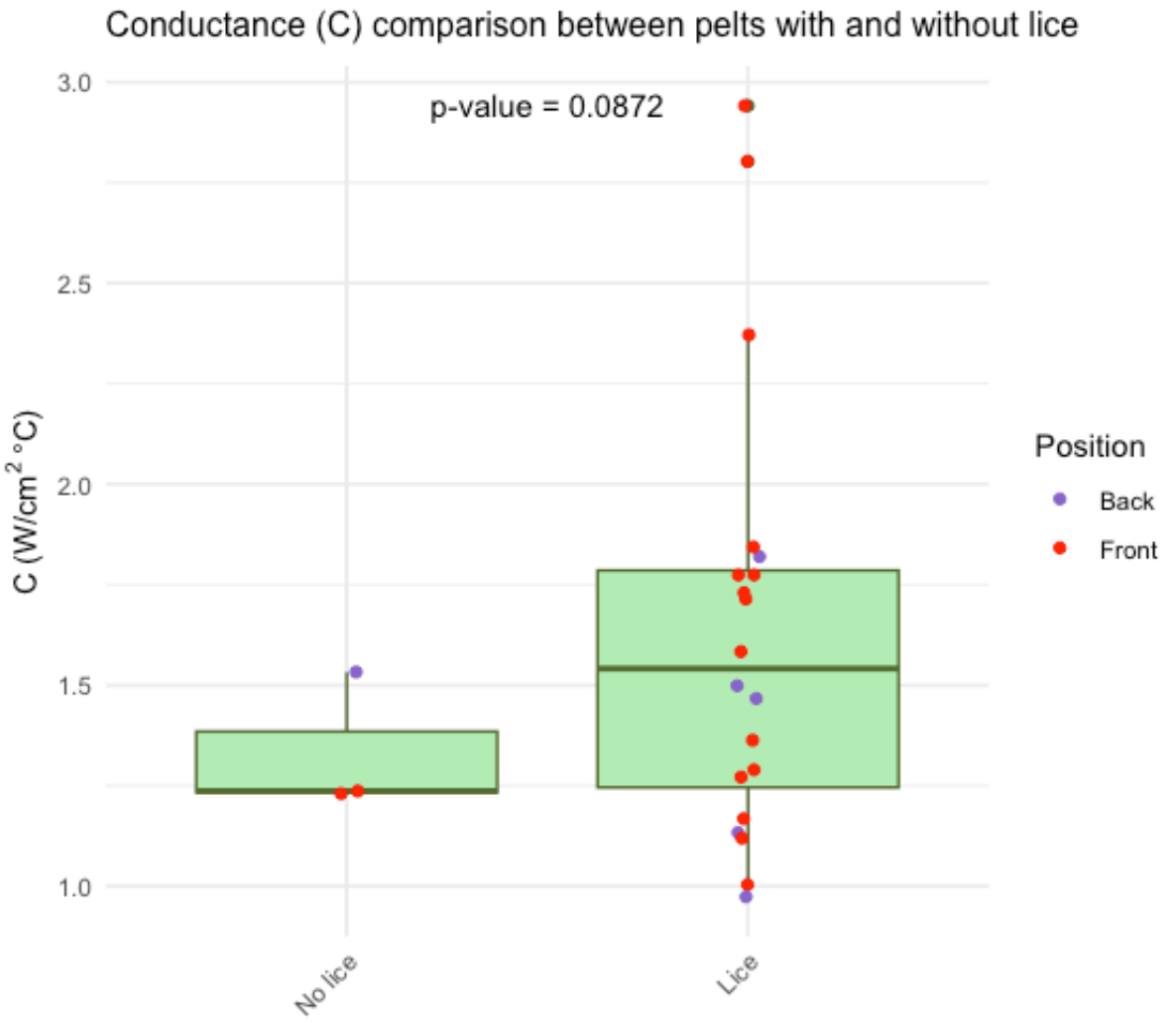

Figure 25 A box whisker plot showing the conductance (*C*) of non-infested pelts (*No lice*, n=3) and infested (*Lice, n* = 20) from arctic foxed trapped on Svalbard during the 2022-2023 trapping season. Points represent individual pelts from back (purple) and front (red). The P-value indicates the statistical significance of the difference in K_{TC} between *No lice* and *Lice* , using Welch's two-sample t-test. Pelt from animal 9 from excluded. The green box represents the interquartile range (IQR), encompassing the middle 50% of the data, the line dividing the box represents the median. Whiskers extend to data points within 1.5 times the IQR, which includes majority of the data, data points beyond are displayed as individual data points and are considered potential outliers.

3.3.3 Linear relationships of conductivity and conductance with predictors

Linear mixed models (LMM) (Table 9) were used to test for relationships between the different predictors and response variables. Both front and back pelts were included in this analysis. Animal ID was applied as a random effect to account for the pairing of front and back pelts.

3.3.3.1 Conductivity in relation to lice infestation, fur depth and damage score

Relationships between conductivity (K_{TC}) and louse density, K_{TC} and damage score (D-score) as well as K_{TC} and fur depth were investigated using linear mixed models (random effect applied to Animal ID), as well as linear regression plots and ordinary least squares (OLS) regression analysis.

K_{TC} plotted against louse density had a non-significant relationship, but did indicate a negative trend (Table 10a., model 4, Figure 26; p= 0.267)

K_{TC} plotted against D-score indicated had a non-significant relationship, but did indicate a positive relationship (Table 10 a., model 8, Figure 27; p=0.148.)

K_{TC} plotted against fur depth also indicated a positive relationship. This relationship was also not significant (Table 10 a., model 5, Figure 28; p=0.0907).

To account for the small sample size in the data set, the model was simplified to avoid overfitting. Overfitting occurs when models include an excessive number of predictor variables relative to the dataset size and may amplify noise and mask true patterns. Two of the predictor variables for fur conductivity (K_{TC}), namely D-score and fur depth, were found to be correlated. A Pearson's correlation test revealed a moderate-to-strong correlation of -0.5434 between these two predictor variables.

Table 10The final model (7) consisted of K_{TC} as a response variable and lice density (total lice/cm^2) and D-score as predictor variables, with fur depth excluded. No significant effects on K_{TC} were seen in this final model (Table 10 a.) model 7; total lice/cm^2 p=0.235, D-score p=0.114).

Because D-score and louse density each showed a significant difference between front and back pelts (Figure 13, Figure 14), to reduce the potential for polarity in the data Figure

13Figure 14the parameters used in model 7 were then tested using only the front pelts, by excluding the back pelts from the dataset. Using an ordinary least squares (OLS) to test this model (excluding back pelts) produced results that were not significant (table 7b; model 9 total lice/cm2 p=0.252, D-score p=0.646).

Table 10 Model parameters and regression comparison with conductivity as response.

Table a) shows parameters included in various combinations as predictor variables in models that were tested with conductivity (K_{TC})(W/m°C) as the response variable. These parameters are total lice/cm^2, fur depth (cm), fat index and damage score (D-score). All data sets included all pelts. Linear mixed model was used to fit the models.

The fixed effects coefficient summary of model 7 are displayed with marginal R-squared (mR-squared) and conditional R-squared (cR-squared).

Table b) shows the results from model 9, which used the same predictor variables as model 7, but excluded back pelts. The model was fitted using an ordinary least squares (OLS) regression analysis. The coefficient summary of model 9 is displayed with multiple and adjusted R-squared.

The Significance codes are: 0 '***' 0.001 '**' 0.01 '*' 0.05 '.' 0.1.

a) Linear mixed models (lmer)					
Model nr.	Predictor / Response	Louse density	Fur depth	Fat index	D-score
1	K_{TC}	p=0.303	p=0.0204 *	p=0.2577	p=0.0247 *
2	K_{TC}	p=0.457	p=0.258	p=0.0556 .	
3	K_{TC}	p=0.333	p=0.115		
4	K_{TC}	p=0.267			
5	K_{TC}		p=0.0907 .		
6	K_{TC}		p=0.00306 **		p=0.00745 **
7	K_{TC}	p=0.235			p=0.114
Fixed effects coefficients :		Estimate	Std. Error	t value	Pr(>|t|)
	(Intercept)	5.929e-02	5.693e-03	10.415	1.71e-08 ***
	Total lice/cm^2	-1.01e-04	8.12e-05	-1.237	0.235
	D-score	1.197e-05	7.079e-06	1.692	0.114
mR-squared: 0.149 , cR-squared: 0.548					
8	K_{TC}				0.148
b) Ordinary least squares model (lm) (front only)					
Model nr.	Predictor / Response	Louse density	Fur depth	Fat index	D-score
9	K_{TC}	p=0.252			p=0.646
Coefficients:		Estimate	Std. Error	t value.	Pr(>|t|)
	(Intercept)	5.767e-02	8.473e-03	6.807.	1.25e-05 ***
	Total lice/cm$^{2.}$	-6.766e-05	9.368e-05	-0.722	0.483
	D-score	1.038e-05	9.444e-06	1.099	0.292
mR-squared: 0.1304, cR-squared: -0.003436					

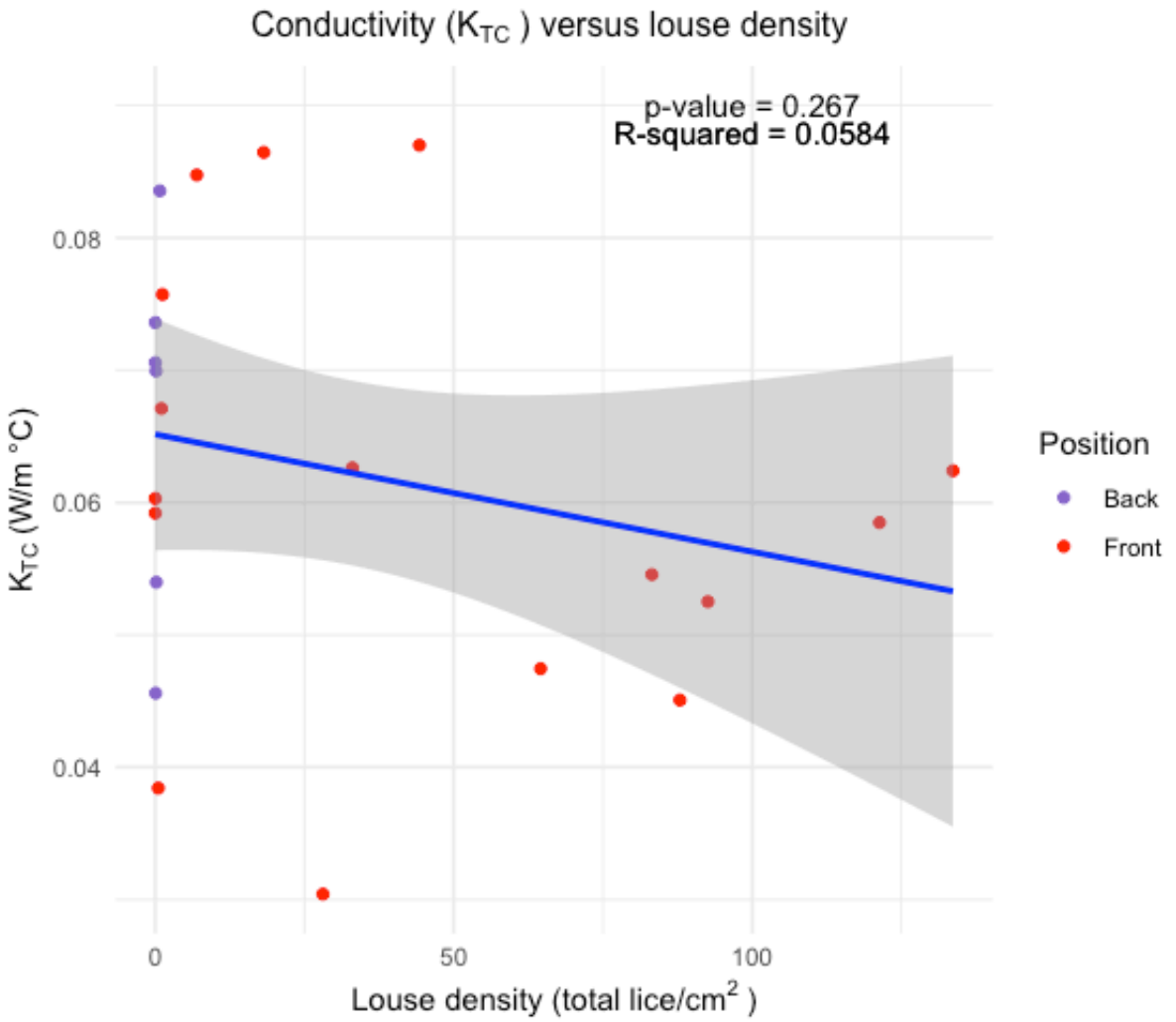

Figure 26 The relationship between conductivity (K_{TC}) and louse density. Red and purple points represent front and back positions of the pelts respectively. The y-axis represents K_{TC} in W/m°C, and the x-axis shows louse density (total lice/cm²). K_{TC} of front pelt animal nr.9 was excluded due to methodological issues. The blue line represents a linear regression model with the grey shaded area indicating the 95% confidence interval. One pelt's K_{TC} measurement was excluded due to methodological issues. A linear mixed model was used to fit the model. P-value and R-squared (marginal R-squared presented, conditional R-squared = 0.0584) are presented in the top right corner.

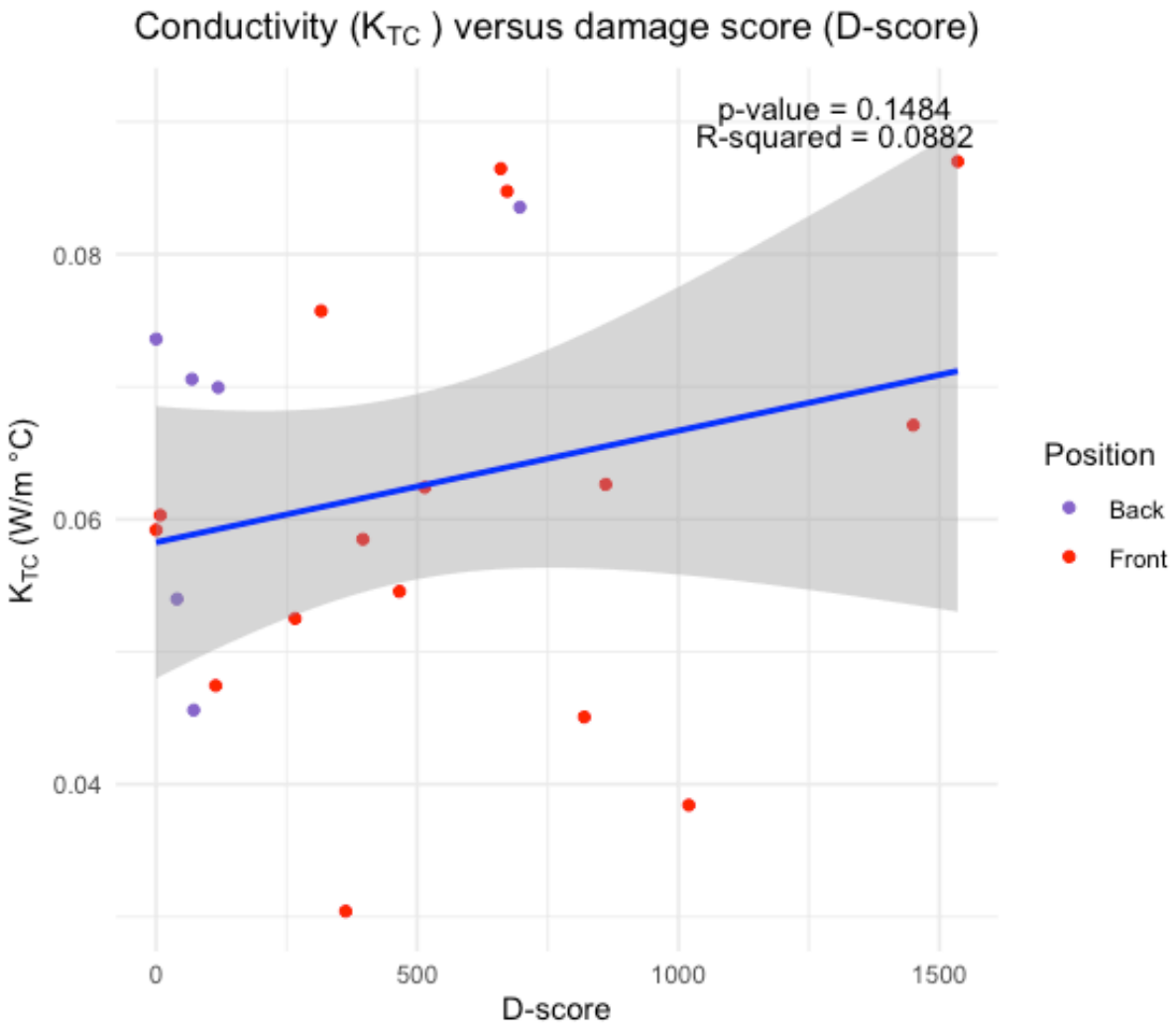

Figure 27 The relationship between conductivity (K_{TC}) and damage score (D-score). Red and purple points represent front and back positions of the pelts respectively. The y-axis represents K_{TC} in W/m°C, and the x-axis shows D-score. The blue line represents a linear regression model with the grey shaded area indicating the 95% confidence interval. K_{TC} of front pelt animal nr.9 was excluded due to methodological issues. A linear mixed model was used to fit the model. P-value and R-squared (marginal R-squared presented, conditional R-squared = 0.4849) are presented in the top right corner.

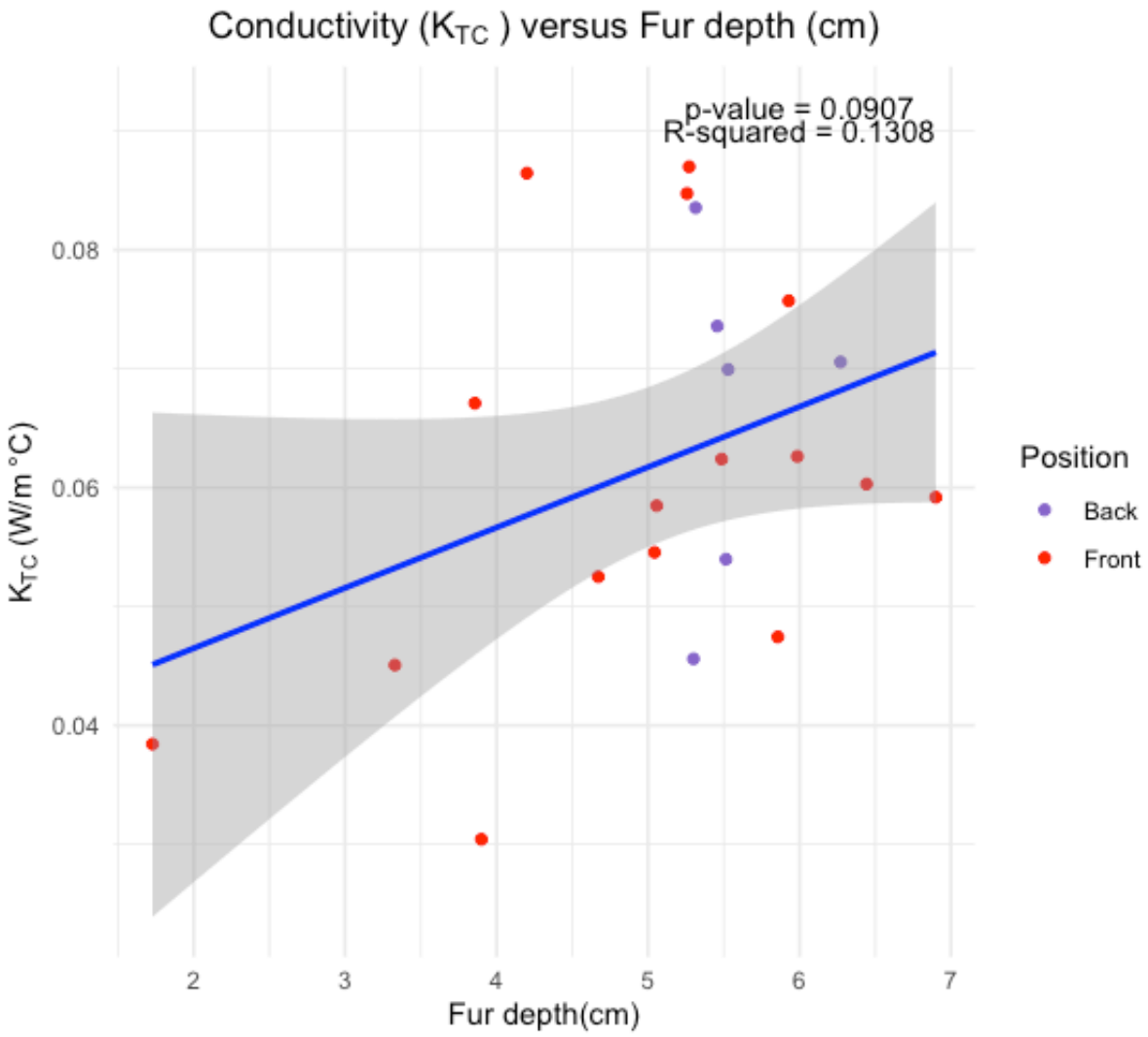

Figure 28 The relationship between conductivity (K_{TC}) and fur depth. Red and purple points represent front and back positions of the pelts respectively. The y-axis represents K_{TC} in W/m°C, and the x-axis shows fur depth (cm). The blue line represents a linear regression model with the grey shaded area indicating the 95% confidence interval. K_{TC} of front pelt animal nr.9 was excluded due to methodological issues. A linear mixed model was used to fit the model. P-value and R-squared (marginal R-squared presented, conditional R-squared = 0.1308) are presented in the top right corner.

3.3.3.2 Conductance in relation to lice infestation, fur depth and damage score

Relationships between conductance (C) and louse density, C and damage score (D-score) as well as C and fur depth were investigated using linear mixed models (random effect applied to Animal ID), as well as linear regression plots and ordinary least squares (OLS) regression analysis.

Conductance plotted against louse density had a non-significant relationship but did indicate a negative trend (**Table 11**a., model 4, **Figure 29**; p=0.145).

Conductance plotted against D-score had a significant relationship indicating a positive trend (**Table 11** a., model 8, **Figure 30**; p=0.000709).

Conductance plotted against fur depth had a non-significant relationship but did indicate a negative trend (**Table 11** a., model 5,**Figure 31**; p=0.0907)

To account for the small sample size in the data set, models were simplified to avoid overfitting. Overfitting occurs when models include an excessive number of predictor variables to the dataset size and may amplify noise and mask true patterns. Two of the predictor variables for fur conductance (*C*), namely D-score and fur depth, were found to be correlated. A Pearson's correlation test revealed a moderate-to-strong correlation of -0.5434 between these two predictor variables.

The final model (7) consisted of *C as* a response variable and lice density (total lice/cm^2) and D-score as predictor variables, with fur depth excluded. A significant relationship between C and the predictors was found in this final model (**Table 11**a. model 7; total lice/cm_2 p=0.0171*, D-score p= 0.000142***)

Because D-score and louse density each showed a significant difference between front and back pelts (**Figure 13**, **Figure 14**, to reduce the potential for polarity in the data the parameters used in model 7 were then tested using only the front pelts, by excluding the back pelts from the data set. Using an ordinary least square (OLS) to test this model (excluding back pelts) produced results that were significant (**Table 11** b.: model 9; total lice/cm^2 p=0.0316*, D-score p= 0.00509**).

Diagnostic plots of this model 9 (**Table 11** b.) showed two residuals with high statistical leverage on the model (i.e., with a substantial impact on the regression line). The two residuals were excluded, and analysis repeated. The exclusion of these residuals improved the fit of the model but did not alter the overall significance or the direction of the relationships between the C; D-score; louse density. Model 9's (**Table 11** b.)) had a R-squared value of 0.572 indicating that 57.2% of the variability in the response variables could be explained by

the combination of the two predictors, lice density and damage score. The adjusted R-squared, which considers the models complexity value, was 0.511.

Table 11 Model parameters and regression comparison with conductance (C) as a response.

a) shows parameters included in various combinations as predictor variables in models that were tested with conductance (C)($W/m^2°C$) as the response variable. These parameters are total lice/cm^2, fur depth (cm), fat index and damage score (D-score). All data sets included all pelts. Linear mixed model was used to fit the models.

The fixed effects coefficient summary of model 7 are displayed with marginal R-squared (mR-squared) and conditional R-squared (cR-squared).

b) shows the results from model 9, which used the same predictor variables as model 7, but excluded back pelts. The model was fitted using an ordinary least squares (OLS) regression analysis. The coefficient summary of model 9 is displayed with multiple and adjusted R-squared. The Significance codes are: 0 '***' 0.001 '**' 0.01 '*' 0.05 '.' 0.1.

	a) Linear mixed models ("lmer" in R studio)				
Model nr.	Predictor / Response	Louse density	Fur depth	Fat index	D-score
1	C	0.00797 **	0.0271 *	0.975	0.00205 **
2	C	0.0527 .	0.000318 ***	0.237	
3	C	0.0635 .	0.0428 *		
4	C	0.145			
5	C		0.0931 .		
6	C		0.828		0.00413 **
7	C	0.0171 *			0.000142 ***
Fixed effects coefficients :		Estimate	Std. Error	t value	Pr(>|t|)
	(Intercept)	1.35.	0.121.	11.14	5.03e-10 ***
	Total lice/cm^2	-0.00458	0.00176.	-2.599	0.0172 *
	D-score	0.000814	0.0001738.	24.686	0.000142 ***
	mR-squared: 0.547 ,		cR-squared: 0.547		
8	x				0.000709 ***
	b) Linear regression model ("lm" in R studio) (front only)				
Model nr.	Predictor / Response	Louse density	Fur depth	Fat index	D-score
9	C	0.03158 *			0.00509 **
Coefficients:		Estimate	Std. Error	t value.	Pr(>|t|)
	(Intercept)	1.43	0.196	7.335	3.71e-06 ***
	Total lice/cm^2	-0.00521	0.00218	-2.388	0.0316 *
	D-score	0.000751	0.000226	3.317	0.00509 **
	Multiple R-squared: 0.570,		Adjusted R-squared: 0.511		

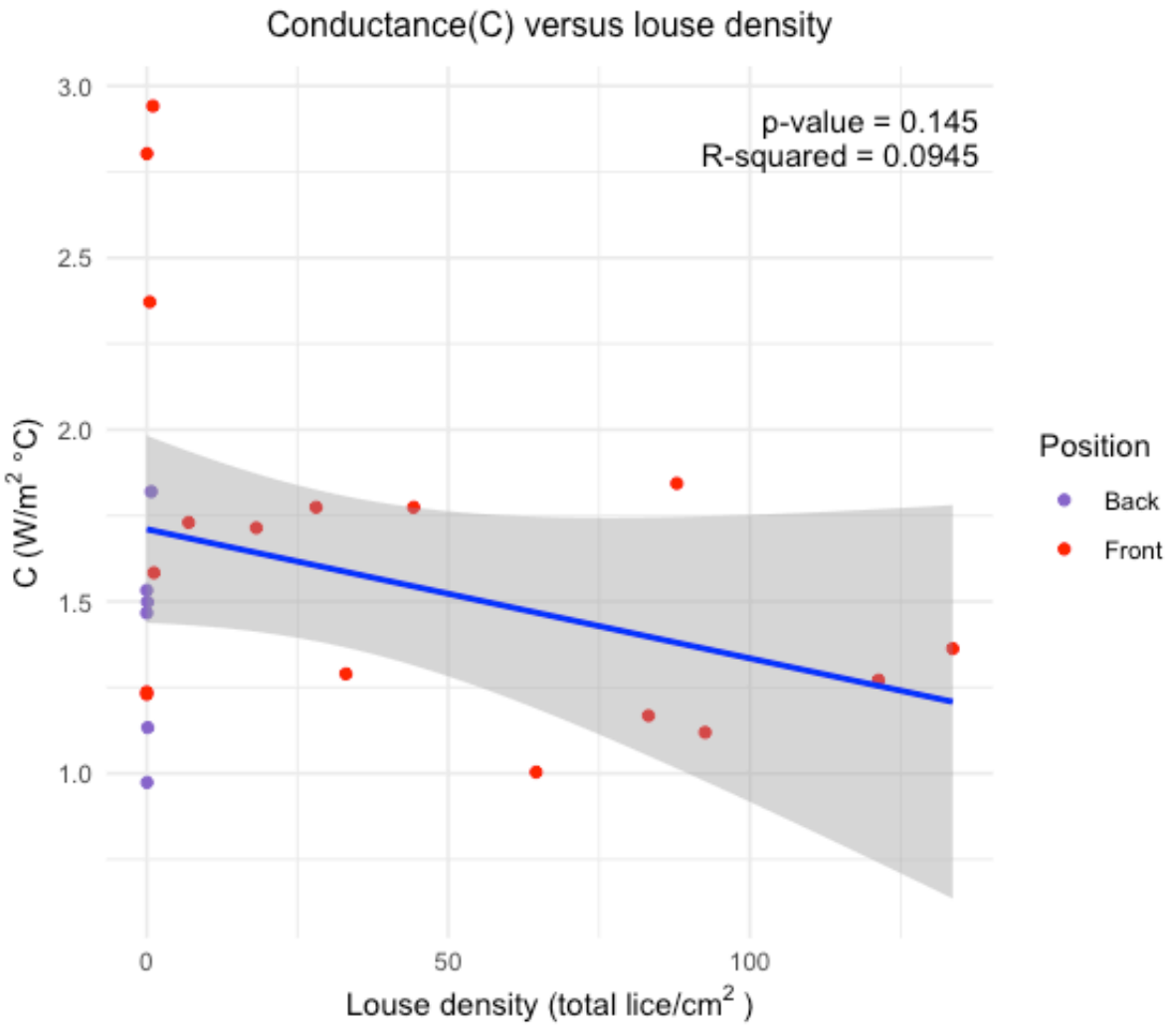

Figure 29 The relationship between conductance (*C)* louse density. Red and purple points represent front and back positions of the pelts respectively. The y-axis represents *C* in W/m^2°C, and the x-axis shows louse density(total lice/cm^2). The blue line represents a linear regression model with the grey shaded area indicating the 95% confidence interval. A linear mixed model was used to fit the model. P-value and R-squared (marginal R-squared presented, conditional R-squared = 0.0945) are presented in the top right corner. P-value and R-squared (marginal R-squared presented, however it was equal to conditional R-squared) are presented in the top right corner.

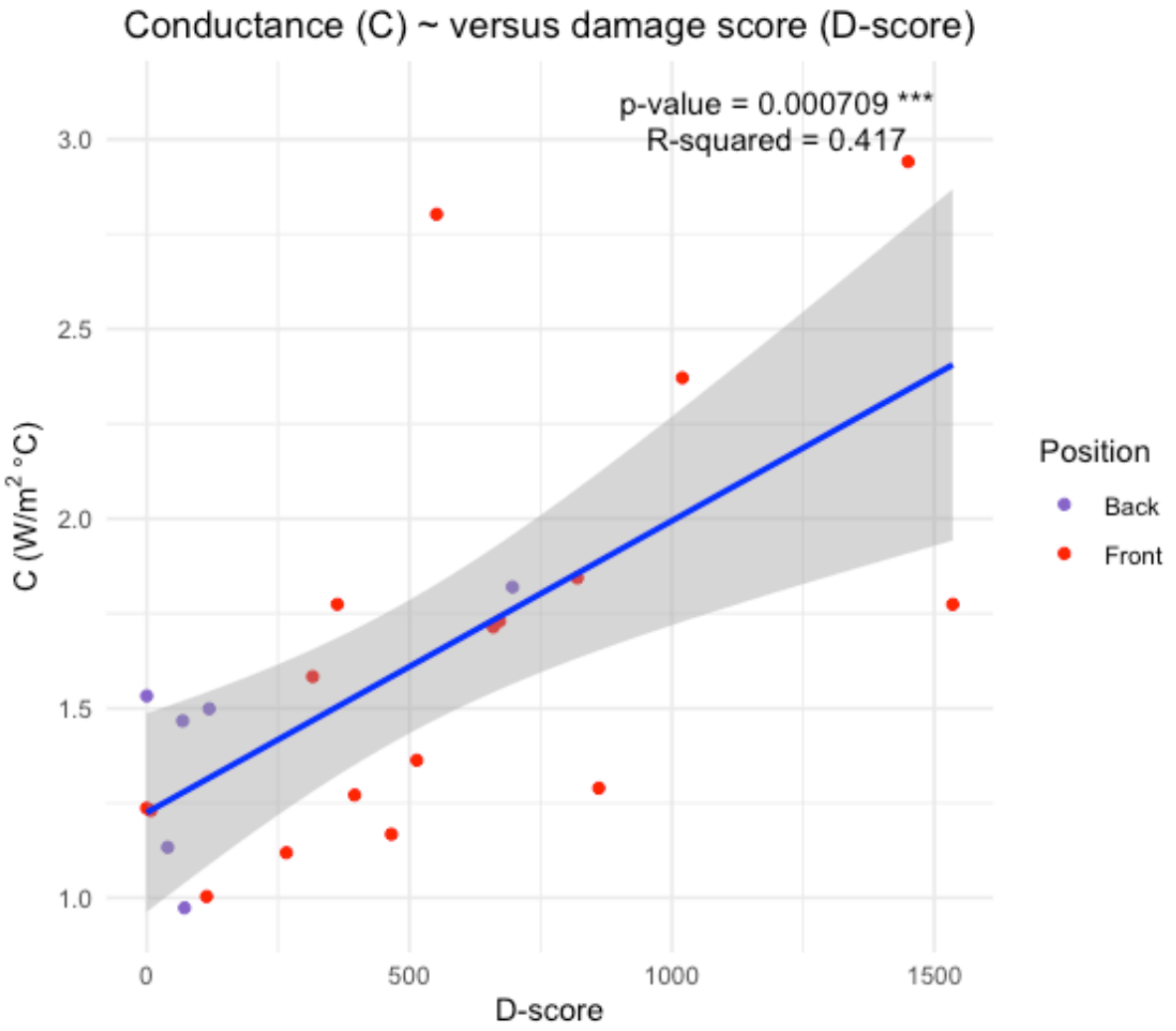

Figure 30 Relationship between conductance (*C*) and damage score (D-score). Red and purple points represent front and back positions of the pelts respectively. The y-axis represents *C* in W/m^2°C, and the x-axis shows D-score. The blue line represents a linear regression model with the grey shaded area indicating the 95% confidence interval. A linear mixed model was used to fit the model. P-value and R-squared (marginal R-squared presented, conditional R-squared= 0.425) are presented in the top right corner.

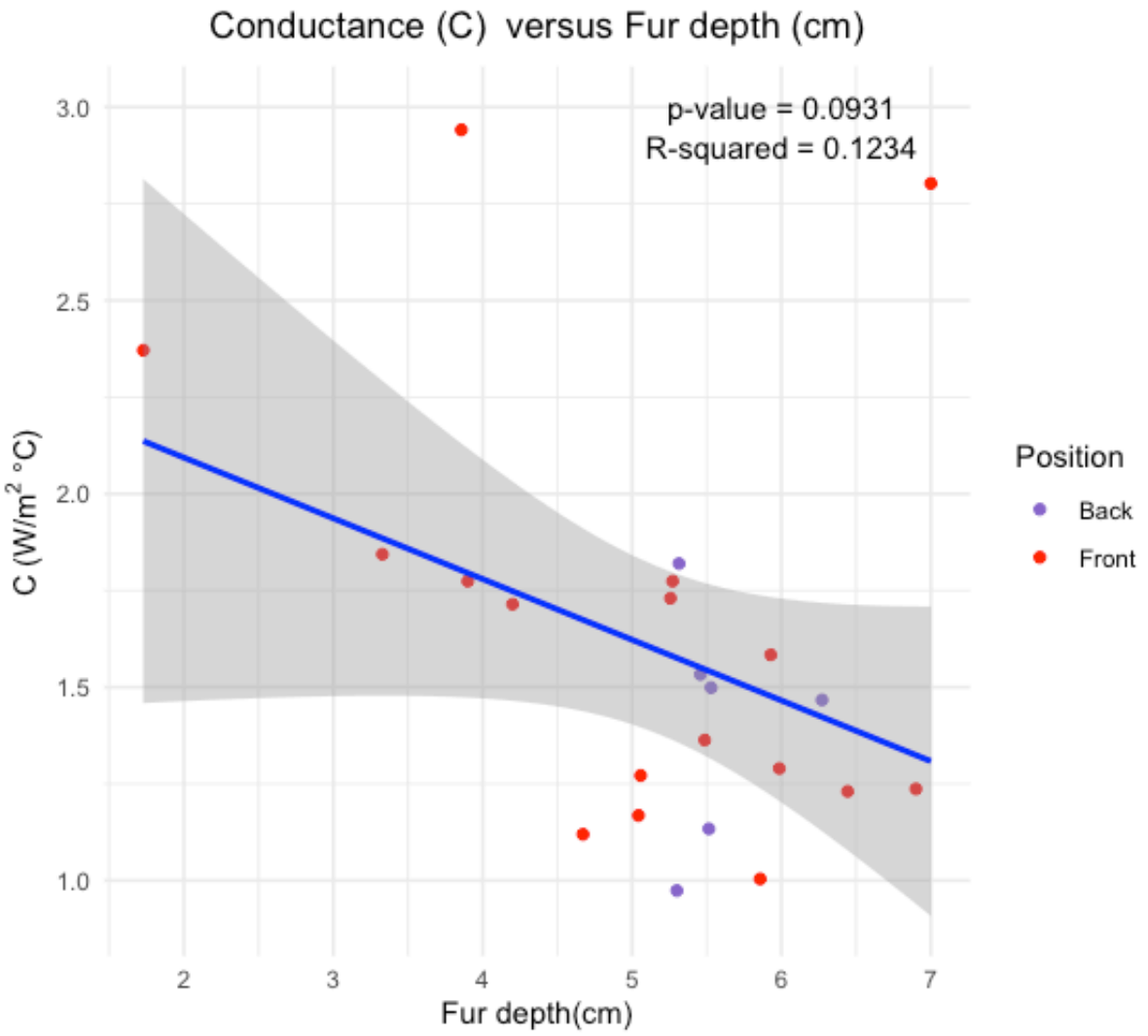

Figure 31 Relationship between conductance (*C*) and fur depth (cm). Red and purple points represent front and back positions of the pelts respectively. The y-axis represents *C* in W/m^2°C, and the x-axis shows fur depth (cm). The blue line represents a linear regression model with the grey shaded area indicating the 95% confidence interval. A linear mixed model was used to fit the model. P-value and R-squared (marginal R-squared presented, however it was equal to conditional R-squared) are presented in the top right corner.

3.3.4 Thermocouple data vs IR measurements in assessing conductivity

In this study, three different techniques were employed to assess fur surface temperatures for conductivity calculations:

1) Thermocouples inserted into the fur, with resulting conductivity value $K_{TC.}$

2) IR thermometer, giving conductivity value K_{IRM},

3) IR camera, giving conductivity value K_{IRC}.

The results from all three techniques are displayed in **Figure 32**, and tests of their agreement are described in section (3.3.4.1).

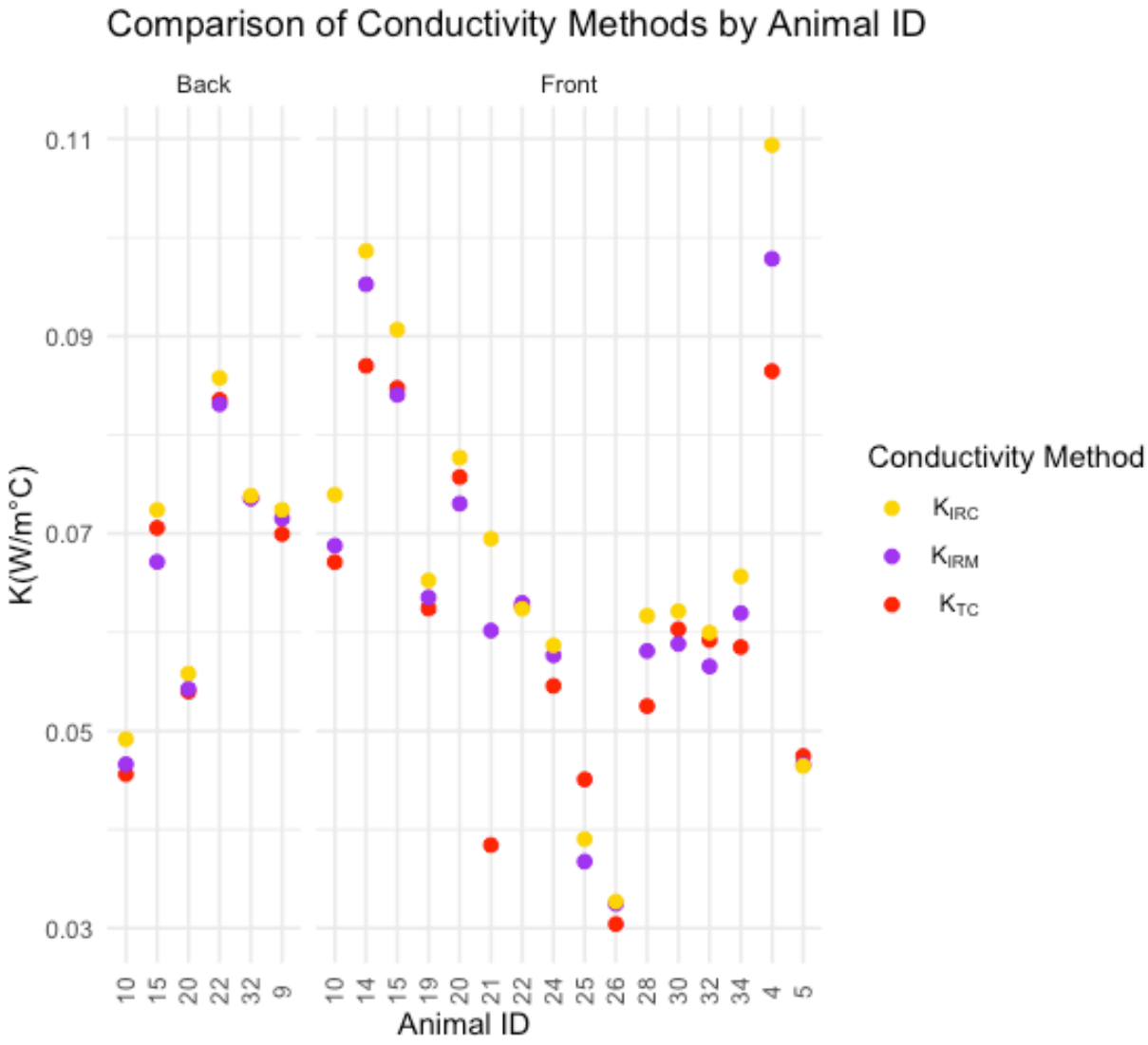

Figure 32 Comparison of methods measuring conductivity in arctic fox pelts. The plot provides a visual comparison of conductivity measurements obtained using 3 different techniques to measure in-fur temperatures: thermocouples (K_{TC}) as the standard method, infrared thermometer readings (K_{IRM}, based on surface temperatures), and infrared thermographic camera data (K_{IRC}, also based on surface temperatures) as alternative methods. The x-axis is divided into back and front furs, and displays the unique animal ID for individual foxes, while the y-axis represents conductivity in W/m°C. Each data point is coloured according to the conductivity method shown in the colour legend to the right of the figure. A large spread of the three points indicates a large discrepancy in the calculated values for conductivity, and a tight grouping of the three points indicates consistency between the three methods.

3.3.4.1 Measure of agreement between conductivity techniques

The level of agreement between the three conductivity techniques, K_{TC} with K_{IRM} and K_{IRC}, was assessed using Bland-Altman plots with 95% limit of agreement and calculating the intra-class coefficient (ICC)(**Figure 33**, **Figure 34**). The mean difference between K_{TC} and K_{IRM} is -0.00186 (± 0.0118, the 95% limit of agreement) and the mean difference between K_{TC} and K_{IRC} is -0.00515 (± 0.0158, the 95% limit of agreement).

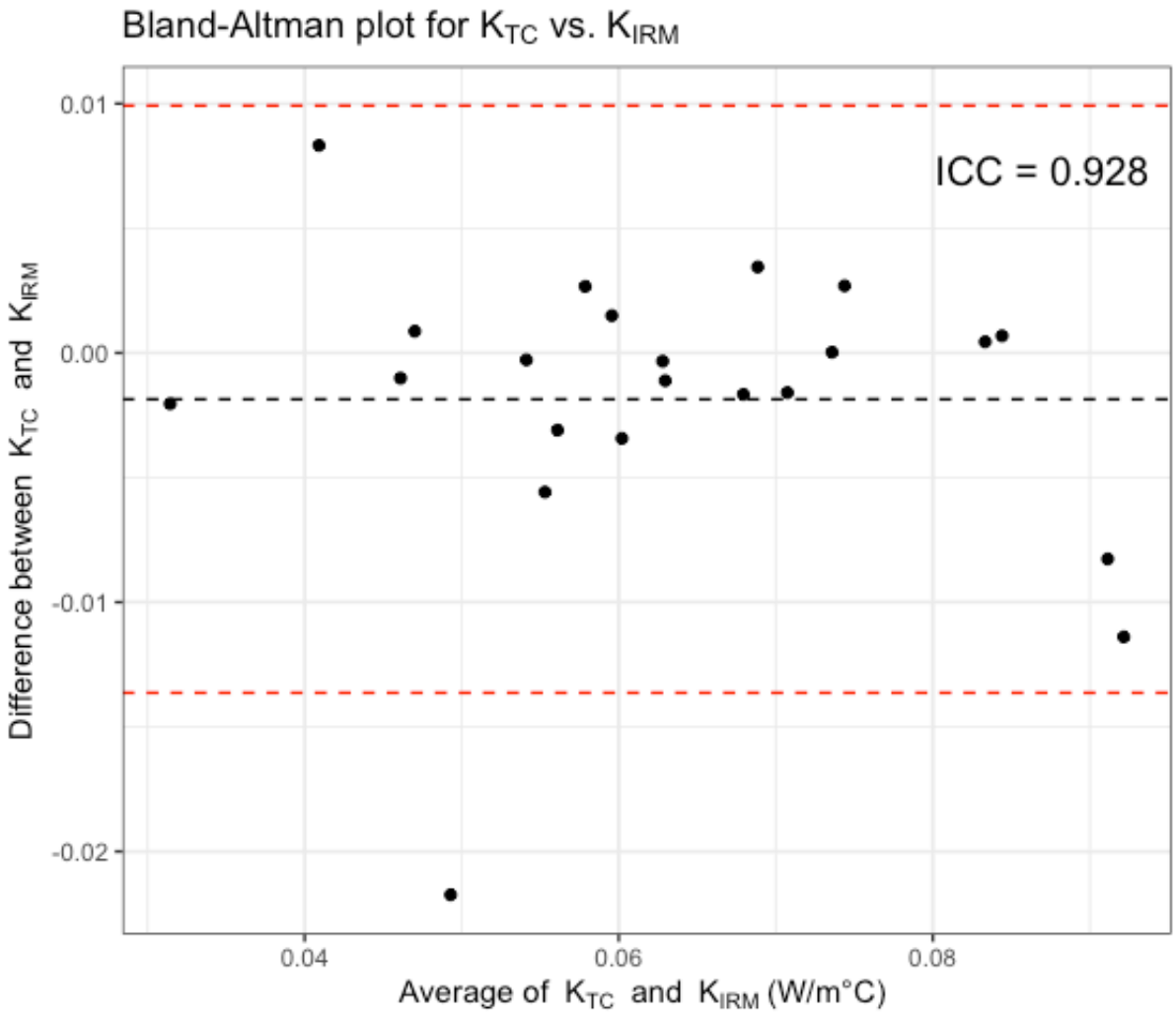

Figure 33 Evaluation of agreement between K_{TC} and K_{IRM} using a Bland-Altman plot with intra-class coefficient (ICC) displayed in the upper right corner. The y-axis shows the difference between each pair of K_{TC} and K_{IRM} values and the x-axis show the mean of each pair of K_{TC} and K_{IRM}. The black horizontal dashed lines show the mean difference in K_{TC} and K_{IRM} values, and the red lines show the upper and lower limits of agreement.

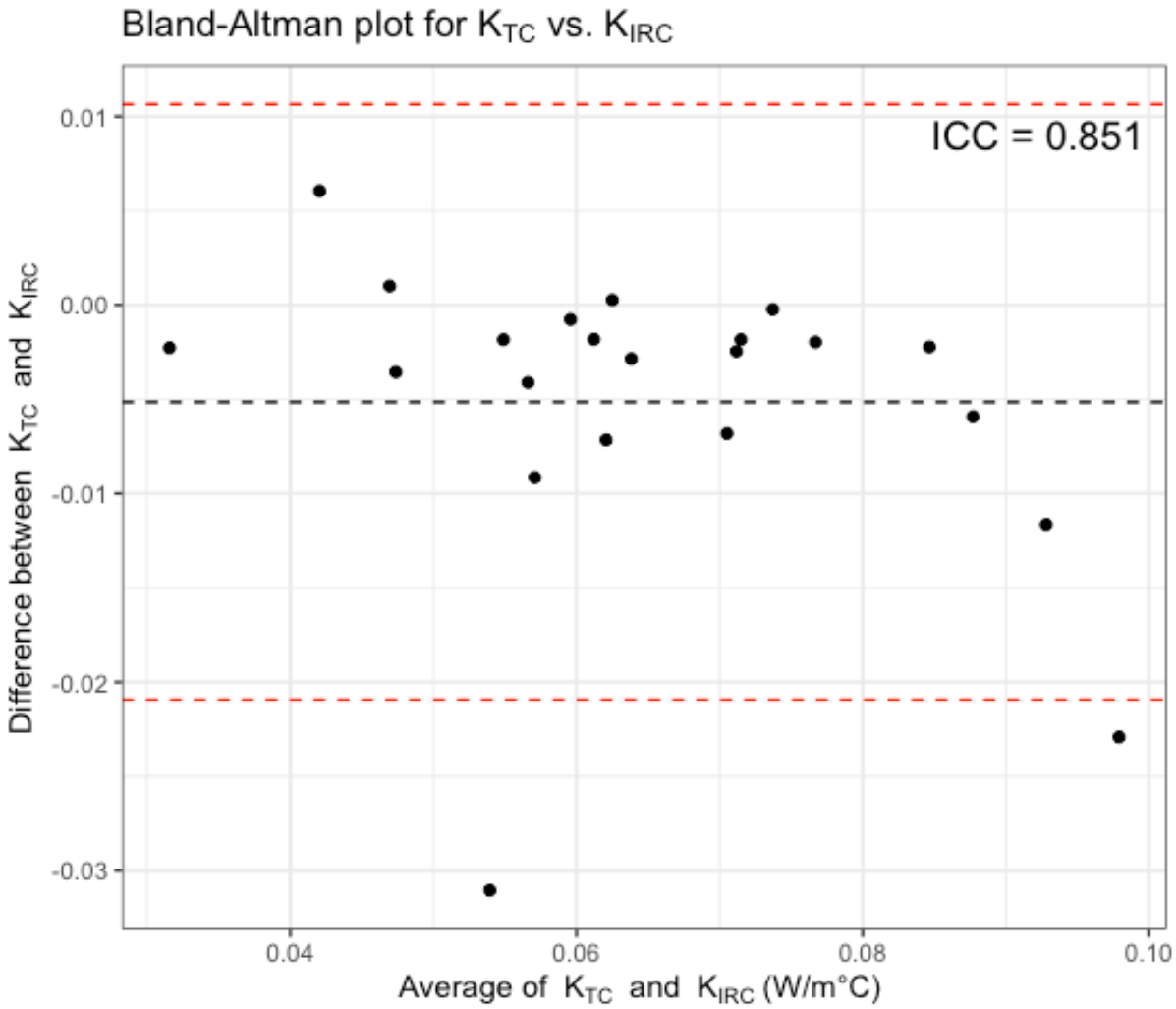

Figure 34 Evaluation of agreement between K_{TC} and K_{IRC} using a Bland-Altman plot with intra-class coefficient (ICC) displayed in the upper right corner. The y-axis shows the difference between each pair of K_{TC} and K_{IRC} values and the x-axis show the mean of each pair of K_{TC} and K_{IRC}. The black horizontal dashed lines show the mean difference in K_{TC} and K_{IRC} values, and the red lines show the upper and lower limits of agreement.

4 Discussion

4.1 Hypotheses and findings

The primary objective of this study was to assess the potential impact of lice infestation on arctic foxes and to address three fundamental research questions and one pilot study.

Research question 1:

The first research question sought to assess the prevalence of lice infestations in the Svalbard arctic fox population, and the areal density of lice in infected fox fur. Based on data from recent trapping seasons it was hypothesised that the prevalence would be high (above 60%) and that infested foxes would show a range of lice densities. The results are discussed in section 4.1.1.

Research question 2:

Research question 2 investigated the relationship between lice density and fur condition. It was hypothesised that the two would be closely related, with higher lice density corresponding to worse fur condition (quantified as a higher damage score). The results are discussed in section 4.1.2

Research question 3: How do observed fur damages and lice infestation affect the insulative properties of the fur?

The third research question posed how, or whether, lice density and fur damage influence the thermal properties of the fur. It was hypothesised that fur lice infestation would cause fur damage which would lead to a reduction in the insulative properties, primarily by altering the furs physical structure and thereby increasing thermal conductivity and/or conductance. This would be visible as a relationship between lice density and thermal conductivity or conductance, and between damage score and thermal conductivity or conductance. The results are discussed in section 4.1.3.

4.1.1 Research question 1 – Prevalence and abundance of lice infestations.

In the trapping season of 2022-2023, a total of 36 arctic foxes were trapped and delivered to the Norwegian Polar Institute. Of these, 44% were found to be infested with lice, a clear decrease in infestation compared to the previous trapping season of 2021-2022, when 76% of trapped arctic foxes were infested with lice (n=208) (Unpublished data by Fuglei E. 2022). Despite the small catch size of the 2022-2023 season, the prevalence appears to have decreased while remaining higher than the 2019-2020 (10%) and 2020-2021 (12.5%) seasons. This did not strictly agree with the hypothesis that the prevalence would increase or remain comparable to the previous year. The reason behind this is unclear, but could indicate an immunological response in infested foxes, perhaps even leading to a herd immunity following the high prevalence of the previous season. This is speculation, but Baron & Weintraub (1987) have noted a development of immunity to lice in mice, and sucking lice are known to trigger an immunological response in some host animals due to the direct mixing of salivary antigens with host blood (European Centre for Disease Prevention and Control, 2022). To my knowledge, there are no existing reports of such immunity in dogs, but most research describing canid louse infestation is in relation to medical treatment, and infestations are not allowed to develop naturally.

The detection and quantification of lice infestation in arctic foxes followed the recommended procedure for the detection of arthropodal skin parasites and is laid out in detail in 2.2 and 2.3. The results showed infested foxes to exhibit a large variation in abundance of lice at various developmental stages and ranging in numbers from a few lice to over a hundred lice per square centimetre (Table 1). This broadly agrees with the hypothesis.

4.1.2 Research question 2- Lice abundance and fur condition

A fur damage score procedure was developed to systematically investigate the level of damage seen in the fur. This is described in detail in section 2.4.

Plotting the damage score vs louse density, no coherent patterns or significant linear relationship was found (Figure 19), seeming to reject the hypothesis. The absence of a significant linear relationship suggest that the possibility of other mechanisms and patterns could exist.

That regions with high levels of fur damage, but no proportionally large louse densities were found, stands as a contradiction to the hypothesis, but may be related to the following scenario: The foxes trapped and included in this study were trapped at different times of the year, some in late January and others in March. When these individuals were infested with lice and how far along the infestation was is unknown and is hard to evaluate as there is currently no knowledge about how the stages of infestation unfold. As mentioned in 4.1.1, immunity to sucking lice has been observed in other animals. It is not impossible that a similar response is present in arctic foxes.

It is also possible, for example, that after some period of heavy infestation, the fur becomes inhospitable to lice due to fur damage and the lice move to another part of the fox, which was not investigated as closely. Additionally, it is possible that the loss of insulative fur prevents successful egg hatching, and the lice population naturally decreases. Although no studies on hatching temperatures have been conducted for the arctic fox lice or the dog lice (*L. setosus*), Saari, Näreaho & Nikander (2018) state that the human head louse (*Pediculus humanus capitis)* has an optimal temperature range of 29-32°C for eggs to hatch, and suggest a similar prerequisite of temperatures apply for dog lice as well. This could perhaps be extrapolated to arctic fox lice, but no explicit study of this nature exists.

In summary, it is possible there is a standard louse population dynamic which shows a peak in lice count followed by a decrease after excessive fur damage has been incurred, leaving fur regions with severe fur damage and few lice.

4.1.3 Research question 3- Thermal properties of fur and effect of lice and fur damage

4.1.3.1 Comparison to previous studies

The conductivity results in section 3.3 were in good overall agreement with previously published study of healthy, louse-free arctic foxes by Fuglesteg et al. (2006) who reported values between 0.059 to 0.080 W/m°C in arctic fox fur in winter. Further, while the results of Fuglesteg et al. (2006) were somewhat higher than the values reported by Scholander et al. (1950a)(between 0.038-0.051 W/m°C in winter fur of healthy arctic foxes, free of lice), the results of this study bridge these two sets of results, with results lying in the stated ranges of both Fuglesteg et al. (2006) and Scholander et al. (1950a), as well as between them.

The results of my study, along with the findings of previous studies imply that arctic fox fur may show a large variation in conductivity. These variations could be related to many factors, including but not necessarily limited to body region, the health of individual animals, the time of year (this mechanism is in fact noted in section 3.3.1.1) and indeed louse infestation.

The results for conductance in section 3.3 were also in broad agreement with Fuglesteg et al. (2006) who reported conductance values between 1.00 and 1.43 $W/m^2°C$ in the winter fur of louse-free, captive arctic foxes. The results of this study produced values that sit within this range, but the infested fur included in this study also produced conductance values which were much higher (as high as 2.94 $W/m^2°C$, which is higher even than the values of louse-free summer fur reported by Fugelsteg et al. (2006)).

4.1.3.2 Relationships and trends

After investigating the hypothesis that louse density would correlate to an increase in thermal conductivity and conductance, it was found that there was no significant relationship between louse density and either conductivity or conductance (section 3.3.3). Further, no significant difference in conductivity or conductance between infested and non-infested pelts was found (section 3.3.2). This lack of significant relationship could be explained by the discussion on louse population dynamics given in section 4.1.2.

It is notable that conductivity shows no significant relationship with any of the measured metrics, except with trapping date, discussed below, but that conductance did show significant relationships with both damage score, and with the combined effects of louse density and damage score. This suggests that conductivity is an inherent property of arctic fox fur and is unaffected by louse infestations or by damage to the fur, whereas conductance (an overall property of the coat) is significantly affected. This shows that it is the loss of fur rather than a change in the internal insulative properties of the fur itself that would negatively affect the thermal balance of a lice-infested arctic fox.

The relationship between conductance and the combined effects of louse density and D-score was further scrutinised by the method laid out in section 3.3.3.2, namely that high leverage residuals as indicated by diagnostic plotting, were removed to check their effect on the model. While this analysis did improve the fit, it did not change the significance, and importantly it

did not change the overall nature of the model. This shows the model to be robust and further supports the conclusion above.

4.1.3.3 Possible physiological and ecological implications

As a lice infestation leads to an increase in fur damage, which in turn leads to an increase in fur conductance (which corresponds to reduced insulation), this could have consequences for an individual fox's physiology, for the dynamics of the fox population, and potentially even the function of the Svalbard ecosystem.

An increase in heat loss would increase the lower critical temperature shift or narrow the thermoneutral zone (TNZ) and lead to an increased energy demand. The study by Cross et al. (2016), reporting increased energy demand in wolves infested with sarcoptic mange, causing fur loss, would support this speculation.

A higher energy demand caused by increased heat loss due to compromised fur will mean the arctic foxes need to compensate with increased food intake and/or rely to a larger extent on energy stored in the body. The winter being already scarce of food (reindeer carcasses being the main food in winter) increased heat loss may cause a decreased survival of arctic foxes, leading to a decrease in population density. Being an important apex predator of the local ecosystem of Svalbard (Fuglei & Ims, 2008), a significant decrease in the Svalbard arctic fox population could have a significant impact on the Svalbard food web - an impact that would ultimately be caused by fur lice.

The annual monitoring of the occupancy rate of arctic fox dens on Svalbard conducted by NPI provides valuable management advice about the population dynamics that can be used by the Governor of Svalbard. If the monitoring indicates a large reduction in the arctic fox population, this advice can be used by the Governor of Svalbard to make the decisions on the trapping regulations for the next season. The allowed bag size would be managed, and it could be reduced until monitoring showed an increase or stabilisation in the population. It should be noted that den monitoring by the Norwegian Polar Institute has so far shown no evidence of a change in arctic fox population size in connection to the discovery of the new fur lice (Fuglei, 2022).

4.2 Other emerging relationships

Aside from the three primary research questions, two more relationships emerged from the study. These are discussed here.

4.2.1 Body location

Following the investigation between all front pelts and all back pelts (section 3.2), a significant trend emerged, suggesting that front pelts exhibit more intense lice infestation levels compared to back pelts (Figure 11), as would be expected (Buhler et al, 2023): The main predilection site of these lice and the corresponding fur loss pattern have been noted in other research as being across the dorsum of the neck and shoulders (rereferred to as "front pelt" in this study), however, patches of less intense fur loss on the back and rump are not unheard of as reported by Buhler et al. (2023).

The comparison in louse density between only front and back pelts from the same individual revealed no significant difference between the two positions (Figure 37). However, the sample size was relatively small (n=5), and the related front pelts were not from the most heavily infested individuals. Hence, more data is needed to state a cohesive conclusion. Nonetheless, a noticeable trend emerged, suggesting that front pelts tend to have slightly higher lice infestation levels compared to back pelts.

4.2.2 Conductivity and time of trapping

A significant relationship was uncovered between conductivity and trapping date, showing conductivity to decrease throughout the trapping season. This could be a result of the dense insulative layer of fur continuing to grow until the spring moult in March, thereby causing a decrease in conductivity with time. (Underwood, 1971) reported that the growth of winter fur is complete by December and maintains an approximately constant fur depth until the beginning of the spring moult but did not investigate whether the internal structures of the fur change with time. This would require dedicated research to properly investigate.

4.3 Methodological considerations and possible limitations

4.3.1 Implicit assumption in modelling fur conductivity

In Fourier's equation (equation 4) conductivity k is given as a constant. When applied to model the thermal balance of an arctic fox, this assumes a uniform conductivity throughout

the fur. This assumption is also made in other studies, such as Fuglesteg et al. (2006), which compared the conductivities of summer and winter furs, stating one overall conductivity for each. This assumption can be called into question. Measurements of temperature profiles through furs do not show a linear relationship between temperature and fur depth (Scholander et al., 1950c; Underwood, 1971). From thermal physics and the Laplace equation (Bergman et al., 2011), this implies that conductivity is not perfectly uniform throughout the fur and in fact depends at least somewhat on fur depth. The Laplace equation (a generalised form of the heat equation) is a second-order differential equation that describes any diffusive flow through a medium, including heat through a conductor. The assumption that fur conductivity is uniform with depth should, therefore, be investigated in the future. Indeed, the Laplace equation would provide one very mathematical method of doing this.

The use of Fourier's equation does not invalidate the standard method of measuring conductivity, as used in Fuglesteg et al. (2006); Kvadsheim, Folkow & Blix (1994); Kvadsheim & Aarseth (2002); Scholander et al. (1950c), it merely limits the quoted value of conductivity to an averaged overall value for the fur. This is true so long as a consistent distance between the skin and the thermocouple is used when measuring temperatures. As is discussed in section 4.3.4, however, because of the varying degrees of fur damage in the pelts used in this study, the fur depth at which temperatures were measured had to be adjusted depending on the state of the fur. If conductivity varies with fur depth, this method could mask higher conductivities in severely damaged fur, thereby masking a relationship between conductance and fur damage.

To be significant, the difference in conductivity would have to vary considerably between the depths of measurement. For this reason, and because only four of the 22 skins used in the calculations of conductance had their depth adjusted, this effect is likely minimal but should nonetheless be considered in future work of the same nature.

4.3.2 K-meter

One possible drawback to the K-meter system is its susceptibility to potential escape of heat from the system. Ideally, the heat generated by the bronze block heat source should travel in a single direction, vertically- through both the standard material and the fur sample. In reality, as described by Kvadsheim, Folkow & Blix (1994), who used the exact same K-meter, some

heat will leak from the edges. Heat escaping from the small space between the insulative frame and Pehd-1000 with the sample mounted on it was detected using the infrared thermal camera, thus as described in section 2.5.1, an additional insulative strip was glued onto all edges of the standard material as well on the insulative frame to reduce this error. While the addition of the insulative strip enhanced the insulation of the setup, resulting in less heat leakage, this effect can never be totally negated. It is for this reason that temperature measurements used in calculations are all taken from close to the centre of the system, where this effect will be minimised, and almost all heat flow will indeed be vertical.

The conductivity of the Pehd-1000 standard material utilized in this study was presumed to be consistent with the value of 0.365 W/m°C determined by Kvadsheim, Folkow & Blix (1994), who measured the conductivity of the same material in the accuracy measurements of that study. It is highly unlikely that the conductivity of the material has changed since it was used by Kvadsheim, Folkow & Blix (1994), and Kvadsheim & Aarseth (2002) accepted the quoted value without verifying it. The consistency of my measurements with other studies using different equipment (Scholander et al., 1950c) suggests that this is not a problem.

4.3.3 Sample size and collection

The sample size was dictated by the number of arctic foxes successfully trapped by the recreational and professional trappers on Svalbard and by the prevalence of lice infestations within these arctic foxes. Although a higher number of arctic foxes was anticipated, only 36 were trapped, of which only 16 were found to be infested with lice.

This smaller-than-expected sample size imposed limits on the conclusions that could be drawn from statistical models, perhaps masking relationships that would have become statistically significant with more data.

While this was largely beyond the control of the study, one aspect where the sample size could be improved is the number of non-infested control animals. Only one control animal was deliberately included, plus one animal in which only one egg was found. This caused a possible limitation in the analysis of the comparison between infested and non-infested pelts, as the non-infested dataset had n=3 (two pelts from the control animal, plus one from the individual with one egg). As this particular analysis was not used directly in the drawing of any conclusions, this limitation has a minimal effect on the overall findings of this thesis.

Additionally, all of the foxes included in this study were trapped during the legal trapping season, which ends in mid-March. Anecdotal reports from Svalbard residents revealed that there were a high number of arctic foxes spotted showing abnormal fur loss after this date. The inclusion of foxes sampled after the end of the trapping season may improve the reliability of the results, but would be hard to justify, as it is during this period that the female arctic foxes are pregnant. It is for this reason that the trapping season ends before this period.

4.3.4 Thermocouples vs infrared

In the calculation of conductivity values, temperatures were measured using thermocouples. This is a well-established method in healthy fur, but in damaged fur, it runs into limitations. When determining the conductivity of a solid object, a surface temperature is recorded. Fur has no obvious surface, so instead the standard procedure is to take the in-fur temperature at a constant depth – taken to be deep enough that the air surrounding the thermocouple is sufficiently insulated from the ambient temperature as to provide a reliable result. In this study, however, the fur under investigation was often damaged, sometimes severely. In some cases, it was difficult to have the thermocouple fully enclosed in fur, even at lower depths than the standard of 0.04m. Even in the less damaged fur, there is an implicit assumption that the fur under investigation is sufficiently undamaged as to insulate the thermocouple from the ambient air temperature. This is problematic when fur damage is part of what is being investigated.

To explore the extent of this limitation, infrared thermometer and infrared camera measurements of the fur surface temperature were taken alongside the thermocouples and used to calculate conductivity. The two sets of infrared conductivity values were assessed for agreement with the thermocouple-based values as laid out in section 3.3.4.1.

In general, these comparisons showed a good agreement, with most data lying inside the limits of agreement and with intraclass correlation coefficients close to 1. This implies that the thermocouples and the infrared techniques generally provided an accurate means of calculating conductivity. A few notable outliers were present, however, and were identified as being those skins with high damage score, confirming the suspicion that temperature measurements become less reliable in highly damaged fur.

It is tempting to suggest that infrared measurements of surface temperature should replace thermocouples in studies of damaged fur, but this has its own limitations. Whereas thermocouples have a clearly defined position, and therefore the calculation of conductivity has a clearly defined value of thickness, infrared measurements are remote and have no easy definition of depth. Other studies have suggested an equivalent depth that the recorded temperature implies as a few millimetres below the surface (McCafferty et al., 2011), but this is intended for undamaged fur (or feathers) with a well-defined surface, which severely damaged fur often does not have.

Instead, it is concluded that the investigation of conductivity in damaged fur should use a composite approach of thermocouples and infrared technology, with each used as a check on the other and with a healthy awareness of the limitations of each method.

4.4 Future work

4.4.1 Lice population dynamics

As is noted in section 4.1.2, no study has been made of the dynamics of a natural louse infestation in arctic foxes (nor in any other canid). An investigation into how the total population of lice on a host change with time, and how its distribution across the body in response to fur damage could be very useful in explaining the lack of a relationship between louse density and fur damage, as well as becoming a useful resource for other future research in the field of parasitology.

4.4.2 Winter fur structure changes

It was noted in section that thermal conductivity of winter arctic fox fur was seen to decrease with time throughout the winter. While previous studies (Underwood, 1971) have investigated the changes in fur depth throughout the year, no study of the changes to the internal structure of an arctic fox winter coat have been made. My results could be a result of the small dataset that would be easily dismissed, or they could be the first suggestion that there may be some ongoing growth of the undercoat or an increase in fur density until the beginning of the spring moult. This could easily form the basis for a future study.

4.4.3 Assessment of the assumption of uniform conductivity

Section 4.3.1 called into question the assumption that conductivity is uniform throughout the depth of an arctic fox fur. This assumption is implicit in the use of Fourier's equation and underpins much of the research made in the thermal properties of arctic fox fur, as well as that of other animal furs and biological materials, for example blubber (Fuglesteg et al., 2006; Kvadsheim, Folkow & Blix, 1994; Kvadsheim & Aarseth, 2002; Scholander et al., 1950c). The non-linearity of temperature gradients in fur as recorded by (Scholander et al., 1950c); Underwood (1971) imply that this assumption is not entirely true. A dedicated investigation into how conductivity varies throughout the depth of an animal fur could determine whether this assumption is close to the truth, or whether it is invalid. This could be investigated by measuring temperatures at a series of fur depths and calculating the conductivity between each pair of measurements. Alternatively, a function of temperature against fur depth could be found by statistical analysis and tested as a solution in the one-dimensional Laplace equation, deriving conductivity as a function of fur depth.

4.4.4 Physiological and ecological effects of heat loss

While this study considers how louse infestations lead to reduced fur quality and higher heat loss in arctic foxes, no exploration is made into the effect this has on the fox population and ecosystem. There is potential here for a more ecosystem-based study, including large-scale, long-term monitoring of arctic fox populations and behaviours in relation to an unfolding louse epidemic and its effect.

4.5 Conclusion

In conclusion, this master's thesis has explored and contextualised the effects of a new species of fur louse in the Svalbard arctic fox population, investigating its prevalence and its effects on fur quality and on the thermal properties of arctic fox fur.

The prevalence of lice in the Svalbard arctic fox populations in the winter of 2022-2023 was given as 44% - a marked decrease compared to the 70% reported in the 2021-2022 season, but higher than the 10% and 12.5% prevalence reported from the 2019-2020 and 2020-2021 seasons respectively.

A method for inspecting fox fur and for quantifying a louse infestation was presented, and a purpose built "damage score" system was described for quantifying the degree of damage in

an arctic fox fur sample. These two methods were used to investigate the relationship between the severity of a louse infestation and the degree of fur damage exhibited in a fur sample. Intriguingly, no significant relationship was found between louse burden (measured as areal louse density in lice/cm^2) and fur damage. This contradicts the hypothesis that a high louse density would lead to a high degree of fur damage and that the two would therefore be correlated. It is nevertheless quite clear that the fur damages observed are linked to lice. This hints at a possible standard population dynamic in a lice infestation that represents a well-defined area for potential future study.

A method for measuring the thermal conductivity and thermal conductance of a fur sample was described, and the results were used to analyse how fur damage may affect the insulative value of fur. Data on fur thermal properties were compared to the louse density and damage score. Here, no significant relationship was uncovered between these parameters and conductivity, while a significant relationship did emerge when comparing these parameters to conductance, showing that conductance was positively correlated to louse density and fur damage. From this, it was concluded that any negative effect on the thermal physiology of an infested arctic fox arises from a reduction in the amount of fur, and not from a change to the internal structure or properties - including the thermal conductivity - of the coat.

5 Appendix

5.1 Infrared thermography pilot study

5.1.1 Method: Infrared thermographic camera

A pilot study was conducted to test the viability of detecting wild arctic foxes by infrared camera trap, and of diagnosing abnormal fur loss patterns in these images.

5.1.1.1 Field setup

The infrared (IR) camera used was an Optris Xi 80 with a 50° lens having a sensor with a spectral range of 8-14µm (corresponding to a temperature range of approximately -65°C to 90°C) with the resolution of 80x80 pixels. This range is suitable for detecting long-wave infrared (LWIR) radiation as is emitted by biological materials, as discussed by Tattersall (2016). This was mounted alongside an automatic, motion triggered, digital camera (Reconyx PC800; Reconyx, Holmen, Wisconsin, USA)

The IR camera was connected to a Lattepanda V1 computer (Windows 10) with a Samsung Evo plus 512GB micro-SD memory card used for imagery storage. A weatherproof polycarbonate enclosure box (Fibox Piccolo) was used to mount the camera and the Lattepanda V1 computer. A 25mm circular hole was drilled using a standard hand drill to make a hole for the camera lens. In the hole, a circular piece of GE (germanium) glass (diameter = 25mm) was glued in place and sealed with silicon, creating a weather-proof window. Subsequently the box, containing the camera, was attached to a rectangular plywood sheet (approximately 15cm by 25cm). On the back of the plywood, two aluminium pole tunnel attachments were fixed. 10 small bags (1g, 27x16mm) of WiseMini® Humidity Control Sachet (with silica gel) were placed within the weatherproof camera box for moisture protection.

Two car batteries (Starter battery AMG, 12V, 80Ah, Biltema) were used to power the IR camera system. A PWM (pulse width modulation) charging regulator (Solar panel controller, 20A) functioned as the hub connecting the camera, via a 1.5 m rubber cable, to the regulator. In the other sockets of the regulator a 100 W Polycrystalline solar panel (72 cells, max current 5.79A, max voltage 17,3V) was connected, used to maintain the car battery charge. On the back of the solar panel, two 25mm aluminium poles were attached along the short side at the top and bottom, serving as attachment points for field purposes. Batteries, charging regulator

and majority of cables were stored inside an aluminium Zarges © box. The whole final setup is illustrated in **Figure 35**.

5.1.1.2 Field equipment trial

Before deploying the equipment in field, a trial run was conducted at the Norwegian Polar Institute headquarters at Svalbard Research Park in Longyearbyen. The thermal camera, solar panel and batteries were installed, and the program configurated to simulate field conditions set up. The aim was to optimize the accuracy of the camera's trigger temperature setting. To achieve this, preliminary tests were done on an Alaskan husky (7 years old Freke, female). During the test, the husky was encouraged to stand at varying distances (1m, 2m and 3m) from the camera while being offered treats. Infrared thermal images from the test were reviewed and a threshold trigger temperature of 23°C was determined to be appropriate in ambient temperatures below -10°C. This decision was based on the observation that the eye temperature of the dog remained above 22.5 degrees across the various distances from the camera and was also in agreement with previous studies done on arctic fox surface temperatures (Klir & Heath (1992).The field trial was conducted, wherein the camera was exposed to outdoor conditions for a period of 2.5 days. During this time there were planned visits by the husky to validate the system and to check that the trigger temperature functioned as intended.

5.1.1.3 IR camera mounting in field.

The field IR camera site was located at a non-disclosed arctic fox den in Adventdalen, outside Longyearbyen (see **Figure 2**). The camera was mounted during the first week of May 2022. It was programmed to have a trigger threshold temperature of 23°C, and to take tree image per second for ten seconds, every time the threshold temperature was detected. The camera would not trigger again until the item holding the threshold temperature leaves the camera field of view or is shielded from the camera.

Five aluminium poles of 25mm diameter were placed into holes drilled into the sloping frozen ground with a depth of more than 1m, to account for the spring thawing of the soil. Four of the poles were arranged in a rectangular manner, the uphill poles 20 cm longer than the downhill ones. The 5th pole was placed next to the top right pole, aligning with the top line, 20 cm away. Socket attachments were attached on the top of the 4 aluminium poles functioning as the attachment site for the solar panel (**Figure 35** a.).

Between the 4 aluminium poles, the Zarges © box containing the batteries, cables and charging regulator, was affixed to the ground using two 0.75m copper probes with one end bent 180°. The poles were hammered into the frozen soil using a plastic mallet with the bent ends threading though the handles of the Zarges © box, to prevent it from moving, see **Figure 35**a.

The two cross aluminium bars on the back of the solar panel functioned as attachment points for the 4 aluminium poles. The power cable from the solar panel was pulled through a plastic tube to protect it from animals and attached to the frame using cable ties before entering the Zarges © box. The camera box was mounted on the 5th pole and top right pole of the solar panel rig by threading the aluminium attachment tunnels over the two aluminium poles and securing its placement by tightening the accompanying screws.

An automatic, motion triggered, digital camera (Reconyx PC800; Reconyx, Holmen, Wisconsin, USA) was mounted on an additional aluminium pole (See **Figure 35**a; G). This was part of the annual arctic fox den monitoring program run by The Norwegian Polar Institute, but images from this camera were also used in the analysis of thermal images.

Figure 35 Infrared thermographic camera field set up. a.) Illustrated the finished mounting on Svalbard. A. The weatherproof box with the camera. B. The GE (germanium) glass window for the camera with protective cap. C. Aluminium rig consisting of 25mm aluminium poles and attachment joints in aluminium. D. 100 W Polycrystalline solar panel. E. Aluminium Zarges© box, holding the power supply and regulator connected to the camera. F. Copper probe threaded through the handles, securing the placement of the Zarges © box. G.

b.) A photo of the content of the Zarges© box. H. Bar battery (Starter battery AMG, 12V, 80Ah, Biltema). I. The PWM (pulse width modulation) charging regulator.

5.1.1.4 IR field image processing

IR images captured from field were analysed in conjunction with the motion triggered digital images from the Reconyx camera. Simultaneous trigger in both the IR camera and Reconyx camera in time were considered to be successful triggers of IR images and used as a marker for when arctic foxes were present in the field of view. Triggers of the IR camera that were not in conjunction with any Reconyx camera time of triggers were considered as non-animal induced trigger. Systematic manual investigation of a subset of both classifications (true and false triggers) confirmed this to be a valid approach.

5.1.2 Results

5.1.2.1 Infrared thermal imaging of arctic foxes in the wild

This aspect of the study was a pilot, the objective of which was to assess the feasibility of using thermal cameras in natural settings to identify heat loss in wild arctic foxes potentially infested by lice.

The cameras were set up on the 2nd of May and removed on the 4th of July. In total, the infrared camera was triggered 2769 times. It was triggered by arctic foxes 1567 times and by other animals (reindeer and snow bunting) six times, each trigger producing 30 images over ten seconds. The remaining IR images produced were triggered by the solar heating of rocks and show no arctic foxes or other animals.

The infrared camera collected no images at all in the period 22nd of May to 5th of June, due to some unknown fault.

Notably, one of the images captured on the cameras (both digital and thermal) showed an arctic fox exhibiting signs of potential lice infestation (**Figure 36**). This was the only trigger of an arctic fox in May, all of the remaining images of arctic foxes either showed puppies or foxes that were in moult after the 5th of June.

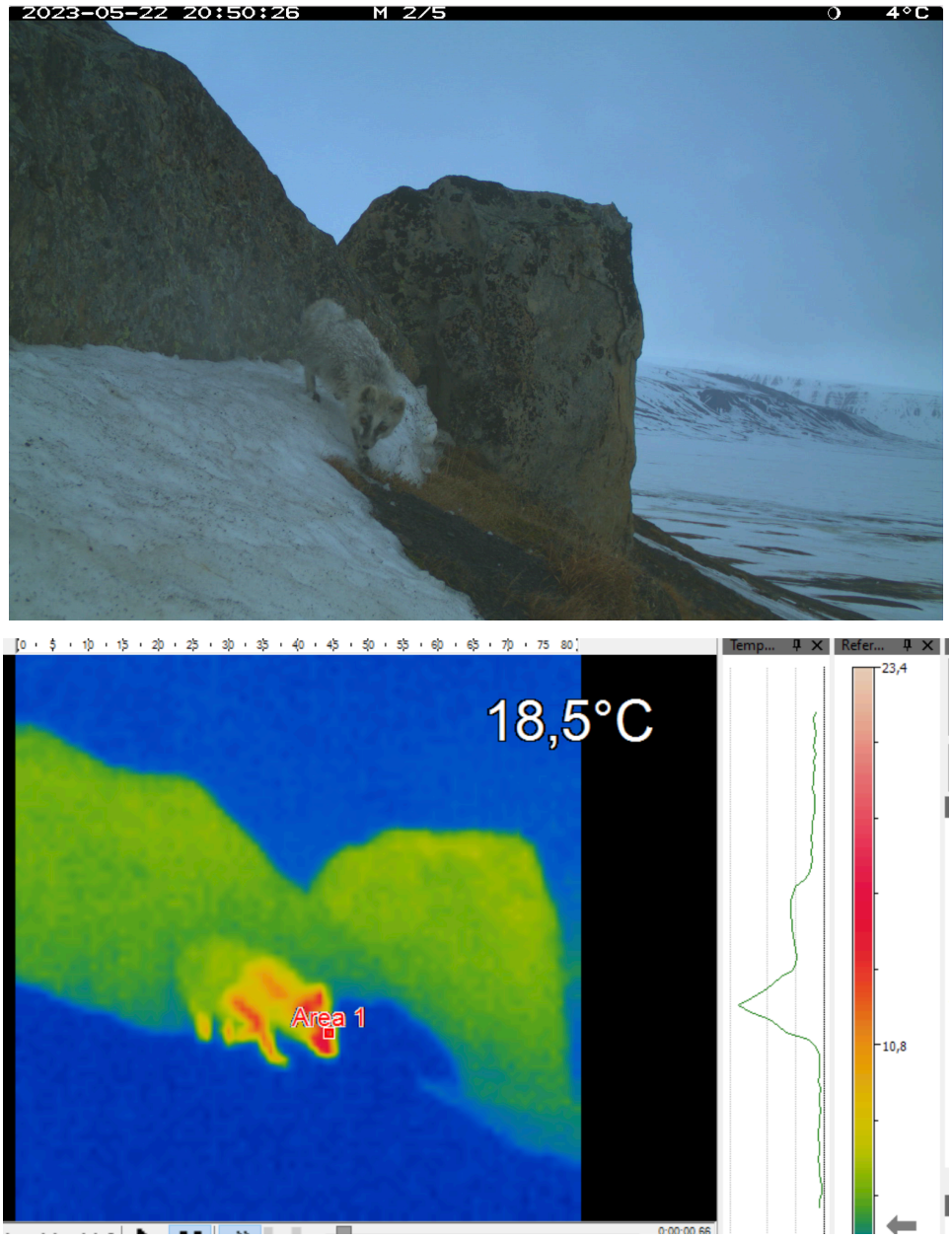

Figure 36 Comparison of digital and infrared thermal images of an arctic fox: the upper image is a digital photograph of an arctic fox showing abnormal fur loss, particularly on the dorsal neck and back region. The lower image is an infrared photograph of the same fox at the same point in time. A colour scale indicative of temperature is present to the right of the thermal image. Warmer temperatures are represented by shades of orange and red. The arctic fox in the image exhibits warmer temperatures in its face and legs (both of which are normal in a healthy fox) and higher temperatures behind the head on the neck and shoulders, indicating heat loss in the same region as the abnormal fur loss.

5.1.3 Discussion

A pilot study was conducted to assess the feasibility of using thermal cameras in natural settings to identify abnormal fur loss using the associated excess heat loss in wild arctic foxes, potentially infested by lice, with a view to this being developed into a diagnostic tool in future work. I hypothesised that abnormal fur loss in arctic foxes would cause higher heat loss, which would be identified as areas of higher temperature in the thermal images, as compared to a healthy fox of the same moulting stage.

One image pair (digital and thermal) was captured showing an adult fox with signs of abnormal fur loss in the digital image, which could be identified as an area of higher surface temperature in the thermal image. This supports the hypothesis.

5.1.3.1 Field application of Infrared thermal imaging

The pilot study sought to assess the use of infrared thermal imaging in the natural settings of the arctic fox, close to a den entrance, to see if it was possible to use heat loss to identify abnormal fur loss in arctic fox fur with potential lice infestation, and to lay the foundations for future investigations into heat loss in wild arctic foxes. It was hypothesised that abnormal fur loss in arctic foxes would exhibit higher heat loss, which would be identified as areas of higher temperature in the thermal images, as compared to a healthy fox of the same moulting stage.

The method employed achieved partially successful results. Notably, one of the several arctic foxes visiting the area and captured on the cameras (digital and thermal) exhibited signs of potential lice infestation (**Figure 36**).

Digital images of this arctic fox revealed signs of a compromised fur coat (**Figure 36**). These features included alternations in fur colour in combination with shorter and thinner fur with a patchy appearance, primarily visible in the dorsal neck and back region. These observations are coherent with previous observations of abnormal fur loss in arctic foxes (Buhler et al., 2021; Buhler et al., 2023). Thermal images of the same fox at the same point in time were compared to the digital images, this analysis showed that the areas corresponding to abnormal fur loss exhibited higher temperatures in the thermal images, identifying these areas as regions of higher heat loss.

A rigorous approach would be to compare this figure with an equivalent one of a healthy fox at the same time of year and same stage of moulting, unfortunately, while many images of healthy arctic foxes were captured, these were mostly from after the beginning of the spring moult, when the fur is very different in nature, and no comparable image was captured in this study.

5.1.3.2 Comparison to other research

As a pilot study, there is not a great deal of existing literature to which this research can be compared. Cross et al. (2016) used field based thermal imaging to estimate the energetic cost of fur loss caused by sarcoptic mange in wolves. This did, however, differ from this pilot study in its aims; it tried to quantify the extra energy expended through heat lost due to fur damage, while this pilot study merely sought to identify affected foxes. It does, though, identify some possible next steps.

A possible way forward in exploring the effects fur lice have on arctic foxes would be to employ a similar methodology as Cross et al. (2016) has, however this would require some important additional considerations. To accurately estimate heat loss from an animal, a reference temperature in view of the camera would be needed. This would function as a temperature calibration point in the subsequent analysis. Though employment of this technique this was initially considered for my study, it was quickly deemed unfeasible due to the power demand and cost of such a reference temperature system. A study of this nature would also be subject to solar effect in the 24h daylight of the Arctic summer.

5.1.3.3 Unknown technical fault

The pilot study captured many IR images of arctic foxes, but the majority were taken in the middle or late stages of the spring moult – too late to identify fur damage. There was a two-week period when no thermal images were captured, but the IR camera then resumed capturing images and functioned normally until it was removed in July. The digital camera continued to capture images during this time revealing there were arctic foxes present when the IR camera was not functioning.

This “blackout” implies that one or several aspects of the camera setup or system did not function as expected, raising questions as to where the error may lie.

A first plausible theory is that the camera's system experienced a malfunction that rendered it unable to trigger and capture images. The error cannot have been terminal, as the camera resumed functioning normally after two weeks of inactivity. It's plausible that the camera was unable to reinitiate functionality after scheduled rebooting (programmed to occur every six hours), however it is unlikely that such a long period of inactivity was caused by this.

The power supply to the camera was a possible explanation. The batteries had the capacity to sustain the camera for approximately 14 days before being depleted and were continually charged by a solar panel. The failure occurred 20 days into the study, so it is not impossible that this was the cause. When the set up was dismantled, however, the batteries were found to be charged beyond the rated voltage, indicating sufficient sunlight to keep the system charged.

5.1.3.4 Limitations of the infrared pilot study

The pilot study included one IR camera placed outside one den. More cameras would most likely have produced more data and increased the likelihood of capturing more IR images of foxes - both infested and non-infested.

The camera had a resolution of 80x80 pixels, which limits the level of detail. However, this was not one of the aims of this pilot study.

The camera used temperature as a trigger mechanism, but this caused issues with warm rocks and gravel triggering the camera for long periods of time, especially from mid-June and onwards. A better trigger mechanism would have been motion sensors, but time constraints prevented this from being included in the setup and testing.

The fault mentioned in section 5.1.3.3 meant that several visits by arctic foxes around the den were not recorded by the IR camera. This was a setback, as I had hoped to collect data during the first few weeks when foxes still exhibit winter fur and have not begun the moult.

5.1.4 Future work – development and implementation

The infrared field study described in this report was shown to have potential as a means of identifying abnormal fur loss as a result of lice infestation in the wild fox population, and Cross et al., (2016) lay out the means by which infrared thermography can be used to assess heat loss in animals suffering from fur damage. With more resources, laid out in section

5.1.3.2, these could be combined and developed towards a study of the energetic costs of louse infestations in wild arctic foxes. Such a study would be subject to limitations, particularly associated with the accurate measurement of heat loss, as radiation is only one of several mechanisms by which animals lose heat. Were captive foxes to be used for this purpose, the air temperature, wind, and moisture content could be controlled, and the other mechanisms of heat loss (conduction and convection) thereby estimated. This would also improve the problems associated with thermography in an environment with 24h sunlight.

5.1.5 Conclusion

This pilot study into the use of infrared imaging to identify fur loss in arctic foxes was presented. This was found to have limited success but show potential for development, particularly in conjunction with existing thermography-based research into energy loss due to fur damage in wolves.

5.2 Paired front and back pelt plots.

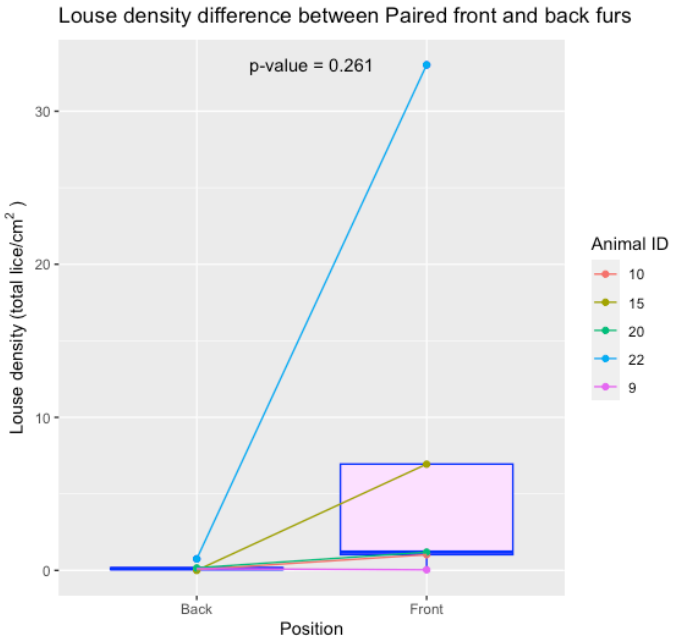

Figure 37 Difference in louse density between paired front and back pelts of arctic foxes. Coloured lines connect related pelts from the same animal. Plot does not include the control animal. The purple box represents the interquartile range (IQR), encompassing the middle 50% of the data, the blue line inside the box represents the median. Whiskers extend to data points within 1.5 times the IQR, which includes majority of the data, data points beyond are displayed as individual data points and are considered potential outliers. P-value indicate the statistical significance, analysis conducted using a paired t-test.

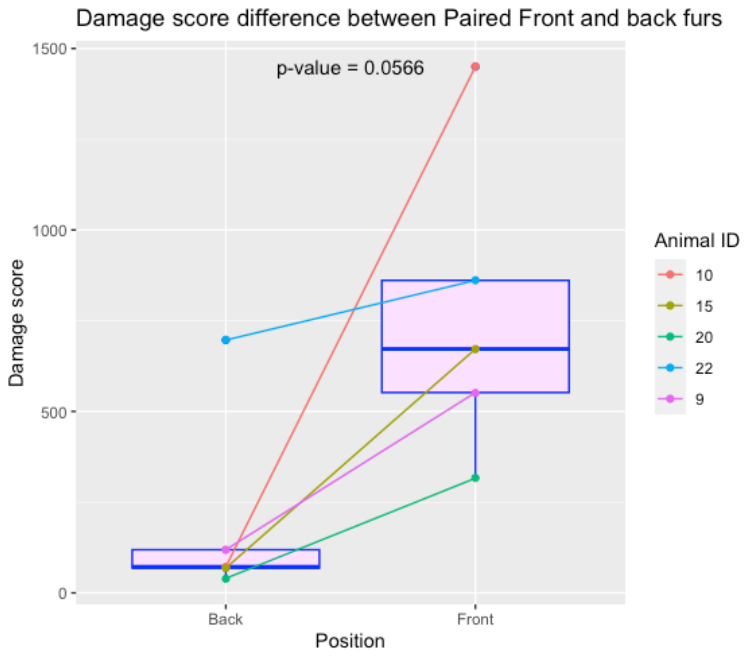

Figure 38 Difference in damage scores (D-score) between paired front and back pelts of arctic foxes. Coloured lines connect related pelts from the same animal. Plot does not include the control animal. The purple box represents the interquartile range (IQR), encompassing the middle 50% of the data, the blue line inside the box represents the median. Whiskers extend to data points within 1.5 times the IQR, which includes majority of the data, data points beyond are displayed as individual data points and are considered potential outliers. P-value indicate the statistical significance, analysis conducted using a paired t-test.

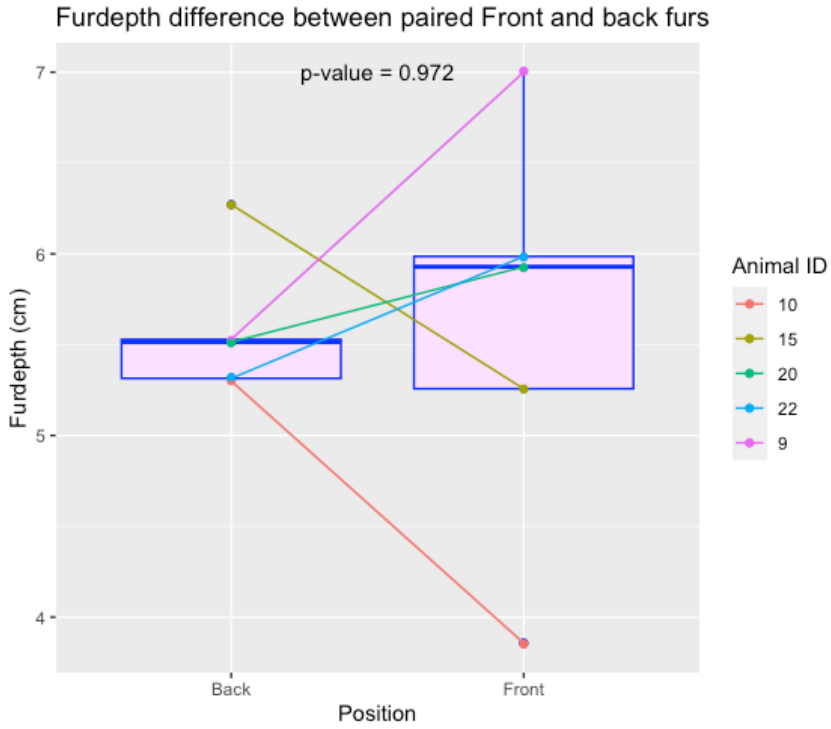

Figure 39 Difference in fur depth (cm) between paired front and back pelts of arctic foxes. Coloured lines connect related pelts from the same animal. Plot does not include the control animal. The purple box represents the interquartile range (IQR), encompassing the middle 50% of the data, the blue line inside the box represents the median. Whiskers extend to data points within 1.5 times the IQR, which includes majority of the data, data points beyond are displayed as individual data points and are considered potential outliers. P-value indicate the statistical significance, analysis conducted using a paired t-test.

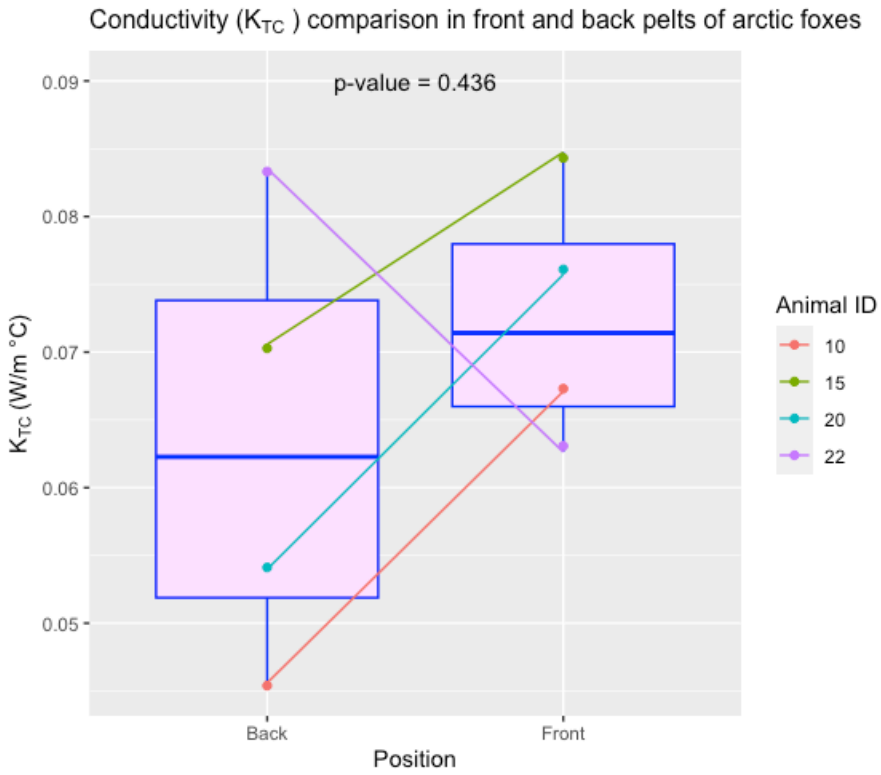

Figure 40 Difference in Conductivity (K_{TC}) between paired front and back pelts of arctic foxes. Coloured lines connect related pelts from the same animal. Plot does not include the control animal or animal number 9.The purple box represents the interquartile range (IQR), encompassing the middle 50% of the data, the blue line inside the box represents the median. Whiskers extend to data points within 1.5 times the IQR, which includes majority of the data, data points beyond are displayed as individual data points and are considered potential outliers. P-value indicate the statistical significance, analysis conducted using a paired t-test.

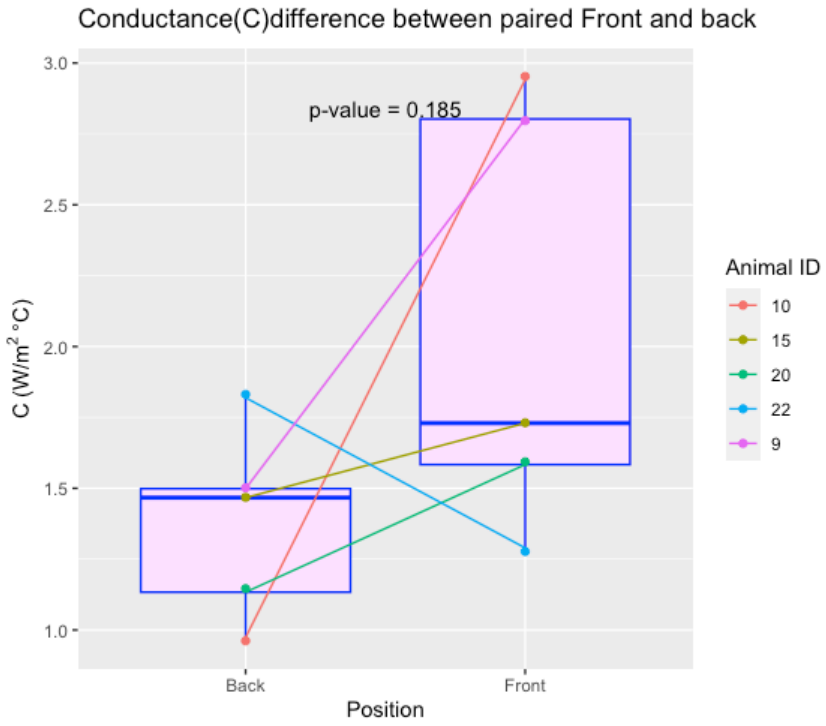

Figure 41 Difference in conductance (*C*) between paired front and back pelts of arctic foxes. Coloured lines connect related pelts from the same animal. Plot does not include the control animal. The purple box represents the interquartile range (IQR), encompassing the middle 50% of the data, the blue line inside the box represents the median. Whiskers extend to data points within 1.5 times the IQR, which includes majority of the data, data points beyond are displayed as individual data points and are considered potential outliers. P-value indicate the statistical significance, analysis conducted using a paired t-test.

5.3 R-studio codes used

Paired t-test

t.test(front_data, back_data, paired=TRUE)

Welch's t-test

t.test(front_data, back_data)

Linear mixed model

lmer(Response variable ~ parameter1 + parameter2+ …. + (1| Grouping variable), data = Data_set)

Calculate R-squared for linear mixed model

r.squaredGLMM(mixed_model_name)

Linear regression model- an ordinary least squares (OLS) regression analysis

lm(Response variable ~ parameter1 + parameter2+…+, data = Data_set)

Correlation

cor.test(parameter1, para

meter2) #parameter used in the test for correlation

6 Work cited

Andersen, M. S. et al. (2015). Levels and temporal trends of persistent organic pollutants (POPs) in arctic foxes (Vulpes lagopus) from Svalbard in relation to dietary habits and food availability. *Science of the Total Environment*, 511, 112-122.

Angerbjörn, A., Hersteinsson, P. & Tannerfeldt, M. (2004). Consequences of resource predictability in the arctic fox: two life history strategies. *The biology and conservation of canids. OUP, Oxford*, 163-172.

Angerbjörn, A. & Tannerfeldt, M. (2014). Vulpes lagopus. *The IUCN Red List of Threatened Species*, 2014.

Arenas, A. J. et al. (2002). An evaluation of the application of infrared thermal imaging to the tele-diagnosis of sarcoptic mange in the Spanish ibex (Capra pyrenaica). *Veterinary parasitology*, 109 (1-2), 111-117.

Arlov, T. B. (2003). *Svalbards historie*. Aschehoug.

Audet, A. M., Robbins, C. B. & Larivière, S. (2002). Alopex lagopus. *Mammalian species*, 2002 (713), 1-10.

Avni-Magen, N. et al. (2017). Use of infrared thermography in early diagnosis of pathologies in Asian elephants (Elephas maximus). *Israel Journal of Veterinary Medicine*, 72 (2), 22-27.

Baron, R. & Weintraub, J. (1987). Immunological responses to parasitic arthropods. *Parasitology Today*, 3 (3), 77-82.

Bates, D. et al. (2014). Fitting linear mixed-effects models using lme4. *arXiv preprint arXiv:1406.5823*.

Bergman, T. L. et al. (2011). *Introduction to heat transfer*. John Wiley & Sons.

Berteaux, D. et al. (2017). Foreword to Supplement 1: research on a polar species—the Arctic fox. *Polar Research*, 36 (sup1), 1.

Best, R. & Fowler, R. (1981). Infrared emissivity and radiant surface temperatures of Canada and snow geese. *The Journal of wildlife management*, 45 (4), 1026-1029.

Blix, A. S. (2005). *Arctic animals and their adaptations to life on the edge*. Tapir Academic Press.

Braestrup, F. W. (1941). *A study on the Arctic Fox in Greenland: immigrations, fluctuations in numbers, based mainly on trading statistics*. Reitzel.

Buhler, K. J. et al. (2021). Fur loss syndrome and lice infestations observed on Arctic foxes in central Nunavut, Canada. *Arctic Science*, 7 (4), 872-878.

Buhler, K. J. et al. (2023). A circumpolar parasite: Evidence of a cryptic undescribed species of sucking louse, Linognathus sp., collected from Arctic foxes, Vulpes lagopus, in Nunavut (Canada) and Svalbard (Norway). *Medical and Veterinary Entomology*.

Cortivo, P. D. et al. (2016). Use of thermographic images to detect external parasite load in cattle. *Computers and Electronics in Agriculture*, 127, 413-417.

Cross, P. C. et al. (2016). Energetic costs of mange in wolves estimated from infrared thermography. *Ecology*, 97 (8), 1938-1948.

Deplazes, P. et al. (2016). Parasitology in veterinary medicine. I: *Parasitology in Veterinary Medicine*: Wageningen Academic.

Dunbar, M. R. & MacCarthy, K. A. (2006). Use of infrared thermography to detect signs of rabies infection in raccoons (Procyon lotor). *Journal of Zoo and Wildlife Medicine*, 37 (4), 518-523.

Durden, L. A. (2019). Lice (Phthiraptera). I: *Medical and veterinary entomology* s. 79-106: Elsevier.

Eide, N. E. et al. (2012). Reproductive responses to spatial and temporal prey availability in a coastal Arctic fox population. *Journal of Animal Ecology*, 81 (3), 640-648.

Elmhagen, B. et al. (2000). The arctic fox (Alopex lagopus): an opportunistic specialist. *Journal of Zoology*, 251 (2), 139-149.
Englar, R. E. (2019). *Common clinical presentations in dogs and cats*. John Wiley & Sons.
Escobar, L. E. et al. (2022). Sarcoptic mange: An emerging panzootic in wildlife. *Transboundary and Emerging Diseases*, 69 (3), 927-942.
European Centre for Disease Prevention and Control. (2022). *Lice (Phthiraptera) - Factsheet for health professionals* Tilgjengelig fra: https://www.ecdc.europa.eu/en/all-topics-z/disease-vectors/facts/factsheet-lice-phthiraptera [Lest 2023.11.14].
Follmann, E. (1978). *Behavioral thermoregulation of arctic foxes in winter*. Biotelemetry: KARGER ALLSCHWILERSTRASSE 10, CH-4009 BASEL, SWITZERLAND. 36-36 s.
Fuglei, E. & Ims, R. A. (2008). Global warming and effects on the arctic fox. *Science progress*, 91 (2), 175-191.
Fuglei, E., Meldrum, E. A. & Ehrich, D. (2013). Effekt av fangst–fjellrev på Svalbard. *Sluttrapport til Svalbards Miljøvernfond*, 30.
Fuglei, E. (2022). *Arctic fox*: Environmental Monitoring of Svalbard and Jan Mayen (MOSJ). Tilgjengelig fra: https://mosj.no/en/indikator/fauna/terrestrial-fauna/arctic-fox/ [Lest 2023.11.12].
Fuglesteg, B. N. et al. (2006). Seasonal variations in basal metabolic rate, lower critical temperature and responses to temporary starvation in the arctic fox (Alopex lagopus) from Svalbard. *Polar Biology*, 29, 308-319.
Governor of Svalbard. (2023). *Revefangst*. Tilgjengelig fra: https://www.sysselmesteren.no/jakt-fangst-og-fiske/revefangst/ [Lest 2023.08.15].
Gunnarsson, L., Christensson, D. & Palmér, E. (2005). Clinical efficacy of selamectin in the treatment of naturally acquired infection of sucking lice (Linognathus setosus) in dogs. *Journal of the American Animal Hospital Association*, 41 (6), 388-394.
Hammel, H. T. (1956). Infrared emissivities of some arctic fauna. *Journal of Mammalogy*, 37 (3), 375-378.
Hanssen, I. et al. (1999). Field study on the insecticidal efficacy of Advantage against natural infestations of dogs with lice. *Parasitology research*, 85, 347-348.
Henshaw, R. E., Underwood, L. S. & Casey, T. M. (1972). Peripheral thermoregulation: foot temperature in two arctic canines. *Science*, 175 (4025), 988-990.
Hersteinsson, P. & Macdonald, D. W. (1992). Interspecific competition and the geographical distribution of red and arctic foxes Vulpes vulpes and Alopex lagopus. *Oikos*, 505-515.
Hill, R. W., Wyse, G. A. & Anderson, M. (2016). *Animal physiology*. Fourth edition. utg. Sunderland, Massachusetts: Sinauer Associates, Inc. Publishers.
Hopla, C. E., Durden, L. A. & Keirans, J. E. (1994). Ectoparasites and classification. *Revue scientifique et technique-Office international des epizooties*, 13 (4), 985-1034.
Irving, L. & Krog, J. (1955). Temperature of skin in the arctic as a regulator of heat. *Journal of Applied Physiology*, 7 (4), 355-364.
Klir, J. J. & Heath, J. E. (1992). An infrared thermographic study of surface temperature in relation to external thermal stress in three species of foxes: the red fox (Vulpes vulpes), arctic fox (Alopex lagopus), and kit fox (Vulpes macrotis). *Physiological zoology*, 65 (5), 1011-1021.
Kohler-Aanesen, H. et al. (2017). Efficacy of fluralaner (Bravecto™ chewable tablets) for the treatment of naturally acquired Linognathus setosus infestations on dogs. *Parasites & vectors*, 10 (1), 1-7.
Kvadsheim, P., Folkow, L. & Blix, A. (1994). A new device for measurement of the thermal conductivity of fur and blubber. *Journal of thermal Biology*, 19 (6), 431-435.

Kvadsheim, P. & Aarseth, J. (2002). Thermal function of phocid seal fur. *Marine Mammal Science*, 18 (4), 952-962.
Laporte‐Devylder, L. et al. (2023). A camera trap‐based assessment of climate‐driven phenotypic plasticity of seasonal moulting in an endangered carnivore. *Remote Sensing in Ecology and Conservation*, 9 (2), 210-221.
Macpherson, A. H. (1969). The dynamics of Canadian arctic fox populations.
McCafferty, D. et al. (2011). Estimating metabolic heat loss in birds and mammals by combining infrared thermography with biophysical modelling. *Comparative Biochemistry and Physiology Part A: Molecular & Integrative Physiology*, 158 (3), 337-345.
McCafferty, D. J. et al. (2021). Advances in thermal imaging. *Journal of Thermal Biology*, 102.
Miljødirektoratet. (2022). *Skabb på fjellrev*. Miljødirektoratet. Tilgjengelig fra: https://www.miljodirektoratet.no/aktuelt/nyheter/2022/juni-2022/skabb-oppdaget-pa-fjellrev-pa-hardangervidda/
Nakagawa, S. & Schielzeth, H. (2013). A general and simple method for obtaining R2 from generalized linear mixed‐effects models. *Methods in ecology and evolution*, 4 (2), 133-142.
Nansen, F. (1897). *Farthest north*. London: Gibson Square Books.
Nater, C. R. et al. (2021). Contributions from terrestrial and marine resources stabilize predator populations in a rapidly changing climate. *Ecosphere*, 12 (6), e03546.
Prestrud, P. (1991). Adaptations by the arctic fox (Alopex lagopus) to the polar winter. *Arctic*, 132-138.
Ranganathan, P., Pramesh, C. & Aggarwal, R. (2017). Common pitfalls in statistical analysis: Measures of agreement. *Perspectives in clinical research*, 8 (4), 187.
Saari, S., Näreaho, A. & Nikander, S. (2018). *Canine parasites and parasitic diseases*. Academic press.
Scholander, P. et al. (1950a). Adaptation to cold in arctic and tropical mammals and birds in relation to body temperature, insulation, and basal metabolic rate. *The Biological Bulletin*, 99 (2), 259-271.
Scholander, P. et al. (1950b). Heat regulation in some arctic and tropical mammals and birds. *The Biological Bulletin*, 99 (2), 237-258.
Scholander, P. et al. (1950c). Body insulation of some arctic and tropical mammals and birds. *The Biological Bulletin*, 99 (2), 225-236.
Stenseth, N. C. & Ims, R. A. (1993). The biology of lemmings. *(No Title)*.
Szafrańska, P. A. et al. (2020). Deep body and surface temperature responses to hot and cold environments in the zebra finch. *Journal of Thermal Biology*, 94, 102776.
Tannerfeldt, M. & Angerbjörn, A. (1996). Life history strategies in a fluctuating environment: establishment and reproductive success in the arctic fox. *Ecography*, 19 (3), 209-220.
Tattersall, G. J. (2016). Infrared thermography: A non-invasive window into thermal physiology. *Comparative Biochemistry and Physiology Part A: Molecular & Integrative Physiology*, 202, 78-98.
The Governor of Svalbard. (2022). *Bag of Arctic foxes in Svalbard. Environmental monitoring of Svalbard and Jan Mayen (MOSJ)*: Environmental Monitoring of Svalbard and Jan Mayen. Tilgjengelig fra: https://mosj.no/en/indikator/influence/hunting-and-trapping/arctic-fox-bag/ [Lest 2023.11.10].
Tiffin, H. S. et al. (2020). A Tissue Digestion Protocol for Measuring Sarcoptes scabiei (Astigmata: Sarcoptidae) Density in Skin Biopsies. *Journal of Insect Science*, 20 (6), 20.

Underwood, L. S. (1971). *THE BIOENERGETICS OF THE ARCTIC FOX (ALOPEX LAGOPUS L.)*. [Ph.D.] United States -- Pennsylvania: The Pennsylvania State University. 92 s

Underwood, L. S. & Reynolds, P. (1980). Photoperiod and fur lengths in the Arctic fox (Alopex lagopus L.). *International Journal of Biometeorology*, 24, 39-48.

Wall, R. L. & Shearer, D. (2001). *Veterinary Ectoparasites: Biology, Pathology and Control*. 2 utg. Newark: Newark: John Wiley & Sons, Incorporated.

Zimova, M. et al. (2018). Function and underlying mechanisms of seasonal colour moulting in mammals and birds: what keeps them changing in a warming world? *Biological Reviews*, 93 (3), 1478-1498.